8.1 Optical resonators

N. Hodgson

8.1.1 Introduction

The basic understanding of the properties of lasers and their radiation requires knowledge of the physics of optical resonators. The laser beam characteristics as well as efficiency and sensitivity against misalignment are determined mainly by the optical resonator. Without the resonator, light emitted by the active medium (solid-state material, gas, or liquid dye) differs insignificantly from the radiation emitted by thermal light sources. Characteristic properties of laser radiation, such as high brightness, high temporal and spatial coherence, and narrow bandwidth, are a result of the optical resonator feeding back the photons into the active medium.

The primary objective of laser resonator design is to create a specified beam quality and, at the same time, maximize output power and efficiency. Unfortunately, this design goal usually is accompanied by technical constraints such as limited space, low sensitivity to misalignment and pump power variations, small bandwidth, as well as by the practical challenge of low cost and reasonable manufacturability. Thus, it is critical to understand the physical properties of optical resonators in order to achieve a laser design that meets technical and commercial requirements.

Resonators currently used in commercial lasers can be divided into four categories: linear stable resonators, linear unstable resonators, ring resonators, and waveguide resonators.

8.1.1.1 Linear stable resonators

In linear stable resonators, light travels between an output coupling mirror and a high-reflecting end mirror. The resonator can be folded by additional high-reflecting mirrors. The main characteristic of stable resonators is the Gaussian beam being the fundamental mode, whereby the Gaussian beam diameter is determined by the geometrical dimensions of the resonator (length and mirror curvatures). Higher-order modes (Gauss–Laguerre modes or Gauss–Hermite modes) are power-orthogonal and their diameter as well as their beam-propagation factor increase as the mode order is increased. This implies that the beam quality of the stable resonator can be controlled by using intracavity apertures.

8.1.1.2 Linear unstable resonators

In linear unstable resonators, light travels between a confined high-reflecting mirror and a larger high-reflecting end mirror. The field is magnified with each roundtrip and the output coupling is produced by the consequent overfill of the confined high reflector. The annular near field generates side lobes in the far field due to hard-edge diffraction at the output coupler. The diffraction can be minimized by using Variable Reflectivity Mirrors (VRM) that exhibit maximum reflectance

at the center and a gradual decrease towards the perimeter. In contrast to stable resonators, the diameter of unstable resonator modes is determined by the size of the output coupling mirror. The mode diameter does not depend on the mode order and since all transverse modes share the same gain area, only the lowest-loss mode is oscillating. This enables one to fill large-diameter active media in fundamental-mode operation by adapting the size of the output coupler to the size of the active medium. Due to the relatively high output coupling, unstable resonators can only be used efficiently in medium-to-high-gain lasers, i.e. high-power CO_2 lasers, excimer lasers, pulsed solid-state lasers, and military chemical lasers generating output powers in the MW range.

8.1.1.3 Ring resonators

In ring resonators, the beam is not incident normal to the mirror surfaces, but propagates in a ring-like pattern. In general, the field propagates in two directions but unidirectional operation can be achieved through the use of polarization rotators (stable resonators) or apertures (unstable resonators), both of which induce additional loss to the field of one propagation direction. The unidirectionality prevents spatial hole burning of the gain which facilitates single-mode operation (e.g. in dye lasers and solid-state lasers). In monolithic solid-state ring lasers, unidirectional operation provides very high stability and narrow linewidths.

8.1.1.4 Waveguide resonators

In waveguide resonators, the beam is guided within the active medium through grazing-incidence reflections off the outer surfaces and the feedback is achieved by resonator mirrors on both waveguide ends. The beam properties of waveguide lasers are determined by the degree of mode matching between the waveguide modes and the modes of the external stable resonator. Fundamental-mode operation is attained by adapting the free-space Gaussian beam diameter to the diameter of the fundamental waveguide mode. Waveguide resonators are used in laser systems that exhibit a power limitation due to inefficient cooling of the active media if conventional geometries (tube, rod) are used (e.g. sealed-off gas lasers). In addition to the improved thermal properties, the maximum output power of planar waveguides is scaled by area rather than length as in conventional geometries. Planar waveguides are widely used in sealed-off kW CO_2 and CO lasers.

8.1.1.5 Reviewing the basic properties of all optical resonators

The basic properties of all optical resonators can be reviewed without taking nonlinear interaction in the active medium into account. Mode structure, diffraction losses, misalignment sensitivity, and beam quality can be evaluated by finding the eigenmodes and eigenvalues of Fresnel-integrals for the round trip inside the resonator. Leaving the active medium out of the treatment is the classical approach to the subject since the gain generally only perturbs the physical properties of the resonator rather than completely changing them. Despite its more subtle impact the active medium is, in fact, important to assess because it affects the mode properties due to gain saturation, thermal lensing, and birefringence. Incorporation of the active medium into the theory is also required to calculate output power, optimum output coupling, and power stability. In general, the amplification of the electric field inside the active medium is described by coupled rate equations for the field and the inversion density, and the field propagation is performed by diffraction integrals. The laser properties can then be calculated using numerical methods.

8.1.2 Classification of optical resonators

An optical resonator usually consists of two spherical mirrors with radius of curvatures ρ_1, ρ_2 separated by a distance L (Fig. 8.1.1). It is customary to replace each mirror by two lenses with focal length $f_i = \rho_i$ and locate the reference planes in between. The reference planes are the mirror surfaces, which means a plane wave in this representation is actually a spherical wave having the curvature of the mirror in real space. The ray-transfer matrix for the round trip inside an arbitrary optical resonator starting at mirror 1 is given by:

$$\mathsf{M}_{\mathrm{RES}} = \begin{pmatrix} 2g_1g_2 - 1 & 2Lg_2 \\ \dfrac{(2g_1g_2-1)^2 - 1}{2Lg_2} & 2g_1g_2 - 1 \end{pmatrix} \tag{8.1.1}$$

with

$$g_i = 1 - \frac{L}{\rho_i}\ ; \quad i = 1, 2\ .$$

The parameters g_1 and g_2 are called the g-parameters of the optical resonator. Note that the radius of curvature is positive for a concave mirror (focusing mirror) and negative for a convex mirror! According to (8.1.1), the imaging properties of two-mirror resonators are fully defined by the g-parameters and the mirror spacing L. We can further simplify the ray-transfer matrix $\mathsf{M}_{\mathrm{RES}}$ by introducing the *equivalent G-parameter* $G = 2g_1g_2 - 1$:

$$\mathsf{M}_{\mathrm{RES}} = \begin{pmatrix} G & 2Lg_2 \\ \dfrac{G^2 - 1}{2Lg_2} & G \end{pmatrix}\ . \tag{8.1.2}$$

This matrix can be used to find spherical wavefronts at mirror 1 whose radii of curvature reproduce themselves after one roundtrip. In general, two reproducing spherical waves exist which are defined by the eigenvectors of the round-trip ray-transfer matrix. The corresponding eigenvalue is the magnification by which the lateral dimension of the wave is increased per round trip. The

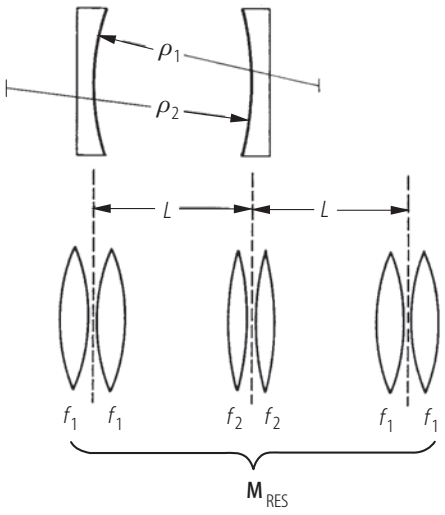

Fig. 8.1.1. A round trip in an optical resonator can be described as a transit in an equivalent lens waveguide. Each mirror has been replaced by a lens pair with focal length $f_i = \rho_i$.

eigenvalues and the corresponding self-reproducing wave curvatures for matrix (8.1.2) read (note that R_a and R_b refer to the dotted planes in Fig. 8.1.1):

$$\mu_a = G + \sqrt{G^2 - 1}\,, \tag{8.1.3}$$

$$R_a = \frac{+2Lg_2}{\sqrt{G^2 - 1}}\,, \tag{8.1.4}$$

$$\mu_b = G - \sqrt{G^2 - 1}\,, \tag{8.1.5}$$

$$R_b = \frac{-2Lg_2}{\sqrt{G^2 - 1}}\,. \tag{8.1.6}$$

According to these eigensolutions we can distinguish between three different types of optical resonators:

1. $|G| > 1$, *equivalent to* $|g_1 g_2| > 1$
   We can find two spherical waves with real values for the radii of curvature $R_{a,b}$ reproducing themselves inside the resonator. If the beam diameter on mirror 1 is d, the spherical wave with radius of curvature R_a increases its diameter by $|\mu_a|$ every round trip (Fig. 8.1.2a). This eigensolution is called the divergent wave. The second eigensolution, the convergent wave, leads to a decrease of the beam diameter by $|\mu_b|$ per round trip. These resonators are referred to as *unstable resonators*.
2. $|G| = 1$, *equivalent to* $|g_1 g_2| = 1$
   Both radii of curvature R_a and R_b are infinite and both eigenvalues are equal to 1, which means that a plane wavefront is coming back planar after the round trip without change in diameter. These resonators are referred to as the *resonators on the stability boundaries*. The plane-plane resonator in Fig. 8.1.2b is one example of such a resonator.
3. $|G| < 1$, *equivalent to* $|g_1 g_2| < 1$
   The radii of curvature and the eigenvalues are all complex numbers. This result can only be interpreted in such a way that in geometrical optics no eigensolutions can be found in this type of resonator. Eigensolutions exist, but they can only be calculated by applying diffraction theory. These resonators are called *stable resonators*.

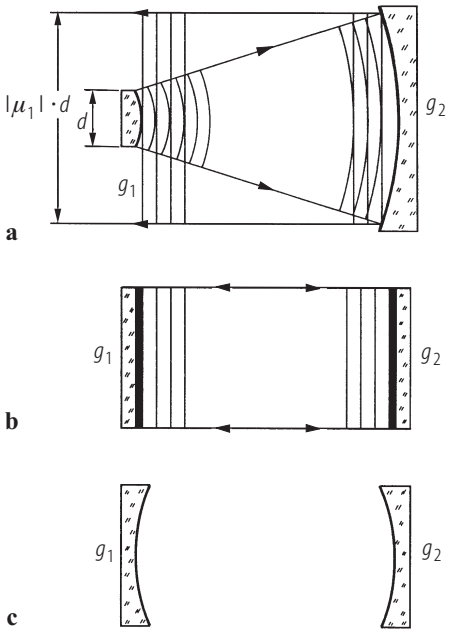

Fig. 8.1.2. The three types of optical resonators with spherical mirrors: (**a**) unstable resonator, (**b**) plane-plane resonator as an example of a resonator on the stability boundaries, (**c**) stable resonator having no eigensolutions in geometrical optics.

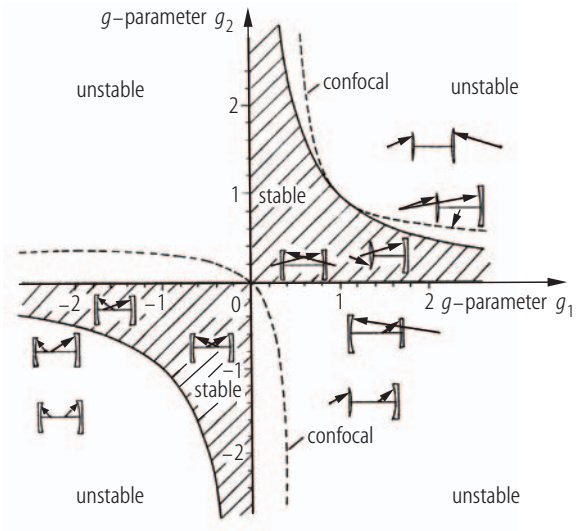

Fig. 8.1.3. The stability diagram of optical resonators with two spherical mirrors [97Hod].

Optical resonators with two mirrors can be visualized in a diagram where the g-parameters represent the coordinate axes (Fig. 8.1.3). This diagram is referred to as the g-diagram or, more often, as the stability diagram. A resonator defined by the g-parameters g_1 and g_2 is represented by a point in the stability diagram. Unfortunately, this representation is not unambiguous because the mirror spacing is not included. A special class of resonators are the confocal resonators with both mirrors having a common focal point. The confocal condition reads:

$$g_1 + g_2 = 2g_1g_2 \; . \tag{8.1.7}$$

8.1.3 Unconfined stable resonators

The goal of a theoretical resonator description is to find steady-state distributions of the electric field on the resonator mirrors. These so-called eigensolutions $E_i(x, y)$ on mirror i will reproduce itself after each round trip (Fig. 8.1.4). The round trip in the resonator is described mathematically by the Kirchhoff integral equation [61Boy, 63Fox, 65Sie, 69Bau, 70Col]:

$$\gamma E_i(x_2, y_2) = \mathrm{i}\,\frac{\exp[-\mathrm{i}kL]}{2Lg_j\lambda_0}\int\int E_i(x_1, y_1)\cdot\exp\Big[\,\frac{-\mathrm{i}\pi}{2Lg_j\lambda_0}\big(G(x_1^2+y_1^2+x_2^2+y_2^2) - 2(x_1x_2+y_1y_2)\big)\Big]\mathrm{d}x_1\mathrm{d}y_1 \tag{8.1.8}$$

with

$G = 2g_1g_2 - 1$; $i, j = 1, 2$; $i \neq j$,
$L = nL_0$: optical resonator length,
L_0 : geometrical length,
λ_0 : vacuum wavelength,
$k = 2\pi/\lambda_0$: wave number.

The solutions to this integral equation represent the eigenmodes of the optical resonator. In general an infinite number of eigenmodes exist. The field distributions of the eigenmodes do not change their shapes but they might experience a decrease in amplitude due to diffraction losses. This is taken into account by the complex eigenvalue γ. The loss factor $V = \gamma\gamma^*$ represents the

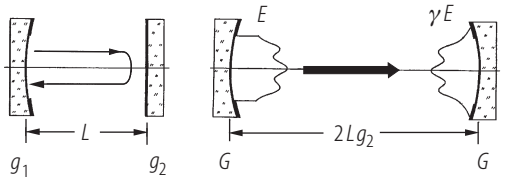

Fig. 8.1.4. A steady-state field distribution $E(x, y)$ must reproduce itself after each round trip. On the right side the round trip is presented as a transit in the equivalent resonator.

fraction of the initial power hitting the mirror after the round trip. The loss factor V is related to the loss ΔV via $\Delta V = 1 - V$. If both resonator mirrors are unconfined and perfectly reflecting, no power is lost during the round trip and the loss factor, therefore, is equal to 1.0. The condition $\gamma = 1.0$, referred to as the *resonance condition* of the optical resonator, yields the resonance frequencies.

8.1.3.1 Transverse mode structures

8.1.3.1.1 Gauss–Laguerre and Gauss–Hermite modes

Equation (8.1.8) can be solved analytically yielding an infinite number of eigensolutions. Which of these eigensolutions will actually be observed in the resonator depends on the geometry and the size of the mirrors. In reality, the mirrors will have a finite size with a shape that usually is round or rectangular. This boundary condition is taken into account by choosing those eigensolutions that exhibit circular or rectangular symmetry, respectively. The solutions to (8.1.8) for the two symmetries are described below (the index i denotes the mirror) [61Fox, 86Sie, 88Mil], see also Vol. VIII/1A1, Sect. 3.1.3.3:

(a) circular symmetry (Gauss–Laguerre modes):

$$E_{p\ell}^{(i)}(r, \Phi) = E_0 \left[\frac{\sqrt{2}\, r}{w_i}\right]^{\ell} L_{p\ell}\left(\frac{2r^2}{w_i^2}\right) \exp\left[\frac{-r^2}{w_i^2}\right] \cdot \begin{cases} \cos(\ell\Phi) \\ \sin(\ell\Phi) \end{cases}, \tag{8.1.9}$$

$$\gamma = \exp\left[ik\left(2L - \frac{\lambda_0}{\pi}(2p + \ell + 1)\,\mathrm{acos}\sqrt{g_1 g_2}\right)\right] \tag{8.1.10}$$

with

$L_{pl}(t)$: Laguerre polynomial of order p, l; p, l: integer,
r, Φ: radial and azimuthal coordinate,
$k = 2\pi/\lambda_0$: wave number; λ_0: wavelength in vacuum,
$L = nL_0$: optical mirror spacing.

The Laguerre polynomials can be found in mathematical handbooks [64Abr, 66Mag]. For low orders p, l they read:

$$L_{0\ell}(t) = 1\,,$$
$$L_{1\ell}(t) = \ell + 1 - t\,,$$
$$L_{2\ell}(t) = \frac{(\ell+1)(\ell+2)}{2} - (\ell+2)\,t + \frac{1}{2}\,t^2\,,$$
$$L_{3\ell}(t) = \frac{(\ell+1)(\ell+2)(\ell+3)}{6} - \frac{(\ell+2)(\ell+3)}{2}\,t + \frac{(\ell+3)}{2}\,t^2 - \frac{1}{6}\,t^3\,;$$

(b) rectangular symmetry (Gauss–Hermite modes):

$$E_{mn}^{(i)}(x,y) = E_0 \exp\left[\frac{-(x^2+y^2)}{(w_{00}^{(i)})^2}\right] H_m\left(\frac{\sqrt{2}\,x}{w_{00}^{(i)}}\right) H_n\left(\frac{\sqrt{2}\,y}{w_{00}^{(i)}}\right) , \tag{8.1.11}$$

$$\gamma = \exp\left[ik\left(2L - \frac{\lambda_0}{\pi}(m+n+1)\,\mathrm{acos}\sqrt{g_1 g_2}\right)\right] . \tag{8.1.12}$$

The Hermite polynomials H_m can also be looked up in mathematical handbooks. For low-order numbers m, n they read:

$H_0(t) = 1$,
$H_1(t) = 2\,t$,
$H_2(t) = 4\,t^2 - 2$,
$H_3(t) = 8\,t^3 - 12\,t$,
$H_4(t) = 16\,t^4 - 48\,t^2 + 12$,
$H_5(t) = 32\,t^5 - 160\,t^3 + 120\,t$.

In both symmetries the loss factor V is equal to 1.0 since the mirrors are not limited by an aperture and, consequently, no power can leak out of the resonator. Figures 3.1.6 and 3.1.7 in Vol. VIII/1A1 present intensity distributions as a function of the order numbers p, l and m, n, calculated with (8.1.9) and (8.1.11), respectively.

The steady-state electric field distribution is characterized by the indices plq and mnq. In rectangular symmetry the first two indices represent the number of nodal lines of the intensity distribution in the corresponding direction. In circular symmetry the intensity distributions exhibit p radial and l azimuthal nodes at which the intensity is equal to zero. The index q represents the number of half wavelengths fitting into the mirror spacing (longitudinal mode order).

A single-frequency steady-state field distribution oscillating inside the resonator is called an eigenmode of the resonator. The eigenmodes are characterized by the transverse mode structure (transverse mode index p, l or m, n) and the axial mode order q. The notations for the eigenmodes are TEM_{plq} and TEM_{mnq} where the abbreviation TEM represents the fact that the electric and the magnetic field vectors are perpendicular to each other and to the wave vector $\boldsymbol{k}$ (Transverse Electro Magnetic). This is not entirely true since the diffraction generates small field components in the direction of the wave propagation. Only in the limit of large beam radii (large Fresnel numbers) is the field truly transverse. The notation TEM was adopted from the modes of waveguides which in fact are transversal. Although not physically correct, it is customary to refer to the modes of open resonators as TEM modes as well. In general, the axial mode index q is not used and the mode structure is specified by the order numbers p, l and m, n (q is on the order of 10^6).

The lateral extent of the eigenmodes on mirror i is determined by the beam radius $w_{00}^{(i)}$ of the TEM_{00} mode. The beam radii on the two mirrors depend on the mirror spacing and the g-parameters of the resonator:

$$w_{00}^{(i)^2} = \frac{\lambda L}{\pi}\sqrt{\frac{g_j}{g_i(1-g_1 g_2)}} ; \quad i,j = 1,2 ; \quad i \neq j . \tag{8.1.13}$$

As can be seen in Fig. 8.1.5, the size of the intensity distributions increases as the mode order is increased. In both symmetries the TEM_{00} mode has the same shape (Figs. 3.1.6 and 3.1.7 in Vol. VIII/1A1); the intensity distribution is Gaussian. At a distance $r = w_i$ from the center of gravity, the intensity has decreased by a factor of $1/e^2$ and 86.5% of the beam power is contained within the corresponding circle. The lateral extent of the TEM_{00} mode is therefore defined by the beam radius w_i, also referred to as the Gaussian beam radius. The TEM_{00} mode is the mode with the smallest size that can oscillate in a stable resonator. It is generally referred to as the

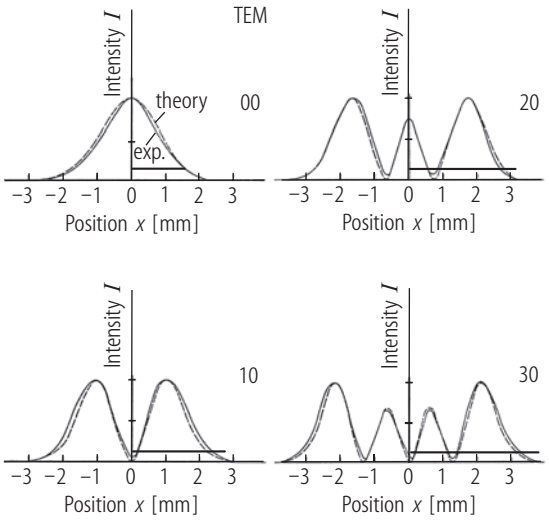

Fig. 8.1.5. Measured (solid line) and calculated (dashed line) one-dimensional intensity distributions of transverse modes TEM_{mn} in rectangular symmetry. The horizontal lines indicate the beam radii w_{m0} defined by the second intensity moments.

fundamental mode or the Gaussian beam. For transverse modes of higher order pl or mn, the beam radii are defined via the second-order intensity moments. This definition of the beam radii enables one to calculate the propagation of arbitrary field distributions through ABCD-type optics by applying the generalized ABCD law. The beam radii on mirror i read [79Nem, 80Car]:

circular symmetry:
$$w_{pl}^{(i)} = w_{pl}^{(i)} \sqrt{2p + l + 1} \,, \tag{8.1.14}$$

rectangular symmetry:
$$w_{mn}^{(i)} = w_{00}^{(i)} \sqrt{2m + 1} \quad (x\text{-direction}) \,, \tag{8.1.15}$$

$$w_{mn}^{(i)} = w_{00}^{(i)} \sqrt{2n + 1} \quad (y\text{-direction}) \,. \tag{8.1.16}$$

The cross-sectional area of the Gaussian beam radius scales linearly with the wavelength and the resonator length. It is for this reason that CO_2 lasers with their large emission wavelength of 10.6 μm exhibit relatively large fundamental mode diameters on the order of 10 mm. On the other hand, diode lasers have very small Gaussian beam radii on the order of μm due to their short mirror spacing in the sub-mm range. Furthermore, at a fixed wavelength and a fixed resonator length, the Gaussian beam radius will decrease as the resonator design is chosen closer to a stability limit in the g-diagram. This fact is visualized in Fig. 8.1.6 which presents curves of constant cross-sectional area of the Gaussian beam at mirror 1. The beam radius at mirror 2 can be obtained from this graph by switching g_1 and g_2.

The transverse modes that are actually observed in a laser resonator are mainly determined by the size of the mirrors. The resonator mirrors are generally limited either by apertures or by the active medium itself. Only those transverse modes whose beam radii are smaller than the radii of the mirror apertures can be observed. If the gain of the laser medium is increased, more transverse modes will, however, reach the laser threshold. As a rule of thumb, a higher-order transverse mode will oscillate if the radius of the aperture a is greater than 0.9 ... 1.0 times the beam radius. Fundamental-mode operation requires an aperture radius a of 1.0 ... 1.4 times the Gaussian beam radius. Upper values and lower values correspond to low-gain and to high-gain active media, respectively.

Lasers can be forced to oscillate only in the fundamental mode by inserting apertures into the resonator with a diameter close to the diameter of the Gaussian beam at the aperture plane. If the apertures are considerably larger than the Gaussian beam, all higher transverse modes fitting into the aperture will oscillate. It is for this reason that in multimode lasers one does generally not observe the characteristic intensity distributions of Fig. 8.1.7. Since all of these modes exhibit virtually no loss, they are oscillating simultaneously resulting in a more or less homogenous beam

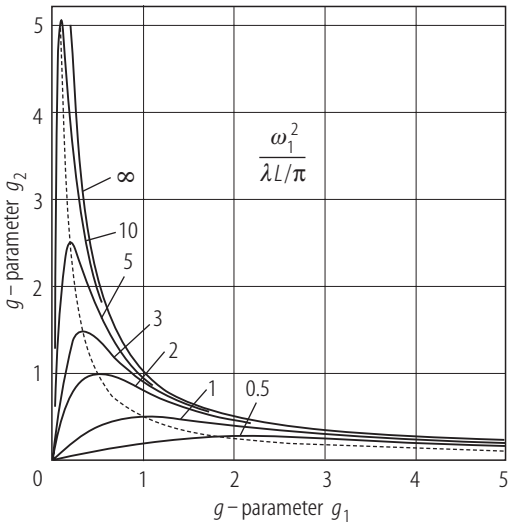

Fig. 8.1.6. Curves of constant cross-sectional area of the Gaussian beam at mirror 1 in the stability diagram. The cross-sectional area is normalized to $\lambda L/\pi$. The beam radius at mirror 2 can be obtained by switching g_1 and g_2.

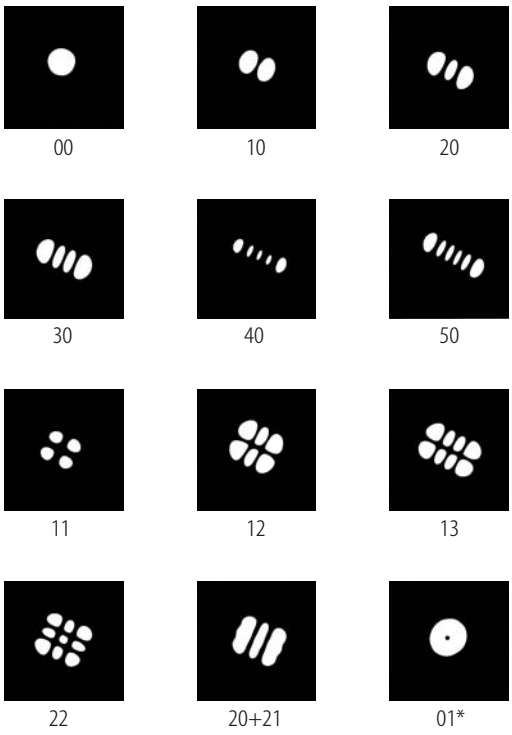

Fig. 8.1.7. Photographs of intensity distributions of different transverse modes at the output coupling mirror of a HeNe laser with a stable resonator. Moveable intracavity cross-wires were used to select modes with rectangular symmetry. The lower right photograph shows the lowest-order donut mode (without cross-wires) [97Hod].

profile. The more modes that participate in this process the more homogenous the laser beam becomes (Fig. 8.1.8). This multimode behavior is supported by the fact that different modes exhibit their intensity maxima in different areas of the active medium. The gain at the nodal lines of the intensity distribution is not depleted and can then be used by a different mode that has its intensity peaks in these vacant areas.

Fig. 8.1.8. Photograph of the beam profile of a Nd:YAG rod laser (λ = 1.064 μm) with a stable resonator in multimode operation (maximum of $2p+l+1$ is about 60) [97Hod].

8.1.3.1.2 Hybrid modes

In circularly symmetric laser resonators one can quite often observe intensity distributions of modes that exhibit an annular intensity profile with almost zero intensity in the center. These beam profiles are generated by a superposition of two circularly symmetric transverse modes of the same order pl which are both linearly polarized and oscillate rotated by an angle of 90° with respect to each other (Fig. 8.1.9). There are four different ways to combine two linearly polarized modes resulting in different polarization states of the sum mode. The superposition always yields the same annular intensity profile with $p+1$ rings with maximum intensity and a characteristic hole in the center. It is quite obvious why these modes are called donut modes. Sometimes they are also referred to as hybrid modes. Hybrid modes are marked by an asterisk next to the mode order numbers. Due to the different polarizations, the two transverse modes do not interfere and the intensity distribution of the sum is given by the sum of the individual mode intensity profiles. Application of (8.1.9) yields for the radial intensity distribution of hybrid modes at mirror i:

$$I_{p\ell^*}(t) = I_0\, t^{\ell} \exp[-t]\, [L_{p\ell}(t)]^2 \tag{8.1.17}$$

with

$$t = 2\left[r/w_{00}^{(i)}\right]^2 .$$

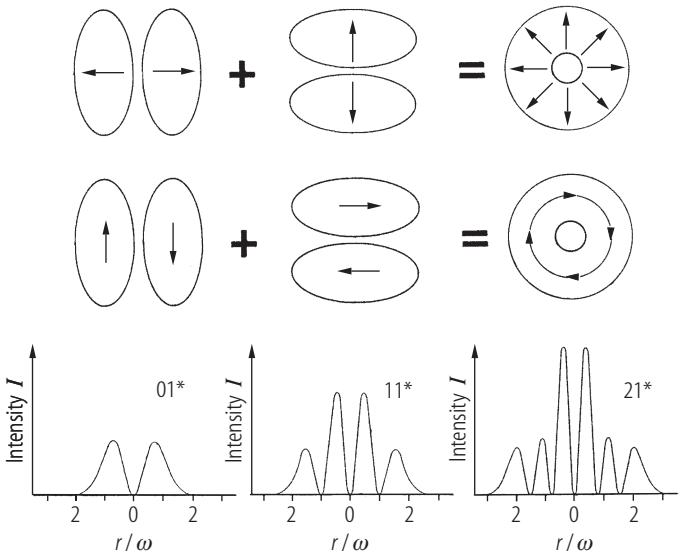

Fig. 8.1.9. Hybrid modes are generated by the superposition of two linearly polarized circularly symmetric transverse modes of the same order pl which oscillate rotated by 90° with respect to each other. The graph shows two of the four possible ways to superimpose the mode structures. The lower graphs present the radial intensity distributions of the three lowest-order hybrid modes TEM_{01^*}, TEM_{11^*}, and TEM_{21^*}.

8.1.3.2 Beam propagation of stable resonator modes

8.1.3.2.1 Fundamental mode

The Gaussian beam radius $w_{00}^{(i)}$ at mirror i determines the lateral dimension of the mode. For stable resonators, the intensity distributions at any plane inside or outside the resonator exhibit the same shape as the distributions on the mirrors; only the beam radius changes with the propagation.

For the fundamental mode, or Gaussian beam, the beam radius as a function of the distance can be calculated by using the ABCD law. If z denotes the distance along the optical axis from the position of the beam waist with radius w_0, the Gaussian beam radius $w_{00}(z)$ inside the resonator reads (Fig. 8.1.10):

$$w_{00}(z) = w_0 \sqrt{1 + \left(\frac{z}{z_0}\right)^2} \tag{8.1.18}$$

with

$$w_0^2 = \frac{\lambda L}{\pi} \frac{\sqrt{g_1 g_2 (1 - g_1 g_2)}}{|g_1 + g_2 - 2 g_1 g_2|} \quad (\textit{waist radius}) \,, \tag{8.1.19}$$

$$z_0 = \frac{\pi\, w_0^2}{\lambda} \quad (\textit{Rayleigh range}) \,, \tag{8.1.20}$$

$$L_{01} = L\, \frac{(1 - g_1) g_2}{|g_1 + g_2 - 2 g_1 g_2|} \quad (\textit{waist position}) \,. \tag{8.1.21}$$

At the distance of one Rayleigh range z_0 from the position of the beam waist the beam radius has increased by a factor of $\sqrt{2}$, which means that the cross-sectional area of the beam has doubled. The waist position L_{01} is the distance of the minimum beam radius (beam waist) from mirror 1. If L_{01} is positive the waist is located to the right of mirror 1 (as shown in Fig. 8.1.10), for a negative L_{01} the waist is found to the left of mirror 1.

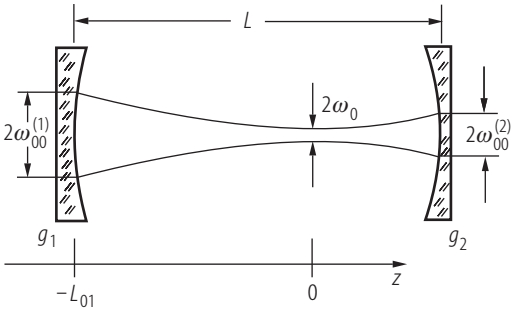

Fig. 8.1.10. Propagation of a Gaussian beam in a stable resonator.

The Gaussian beam is fully determined by the beam radius, the Rayleigh range, and the location of the beam waist. The divergence angle (half cone angle) θ_0 is obtained from these quantities by using the relation:

$$\theta_0 = \frac{\lambda}{\pi\, w_0} = \frac{w_0}{z_0} \,. \tag{8.1.22}$$

The beam parameter product $w_0 \theta_0$ is a constant of the Gaussian beam as long as the beam propagates through ABCD-type optical systems (aberration-free optics). By combining (8.1.19) and (8.1.22), the angle of divergence θ_0 for a general stable resonator is given by:

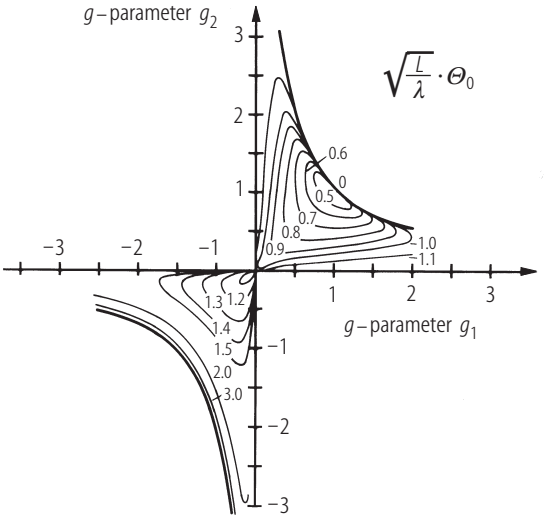

Fig. 8.1.11. Curves of constant angle of divergence θ_0 of the Gaussian beam in the g-diagram. The parameter is the normalized angle of divergence $\theta_0\sqrt{(L/\lambda)}$, which is 1.0 for the confocal resonator.

$$\theta_0^2 = \frac{\lambda}{\pi L}\,\frac{|g_1 + g_2 - 2g_1g_2|}{\sqrt{g_1g_2(1-g_1g_2)}}\,. \tag{8.1.23}$$

The normalized angle $\theta_0\sqrt{(L/\lambda)}$ depends only on the g-parameters of the resonator (Fig. 8.1.11). For a constant resonator length L, the angle of divergence becomes very small if the resonator is chosen close to the hyperbola in the first quadrant. The corresponding beam waist radius w_0 is, of course, very large for these resonators since the beam parameter product $w_0\theta_0$ is a constant. The largest angles of divergence are found for negative g-parameters at the stability limit $g_2 = 1/g_1$, where the concentric resonators are located. Since the large angles of divergence are generated by extremely small intracavity beam waists, these resonators have a small mode volume and have therefore found only limited application in laser systems.

The radius of curvature $R^{(i)}$ of the Gaussian beam at mirror i is always equal to the radius of curvature ρ_i of the mirror. The general expression for the radius of curvature R as a function of the propagation distance z reads:

$$R(z) = z_0\left[\frac{z}{z_0} + \frac{z_0}{z}\right]\,. \tag{8.1.24}$$

It can be easily verified that the mirror surfaces indeed represent surfaces of constant phase of the Gaussian beam by setting $z = L_{01}$ and $z = L - L_{01}$ in (8.1.24). The radius of curvature exhibits a minimum at the Rayleigh range z_0. The nonlinearity of $R(z)$ is the reason for the deviation of the imaging condition of Gaussian beams from Newton's law of geometrical optics. The general expression for the electric field of a Gaussian beam as a function of the distance z from the waist is given by:

$$E(x,y,z) = \frac{E_0}{\sqrt{1+(z/z_0)^2}}\,\exp\left[\frac{-(x^2+y^2)}{w_{00}^2(z)} - \frac{\mathrm{i}k(x^2+y^2)}{2R(z)}\right]\exp\left[-\mathrm{i}\,\mathrm{atan}\left(\frac{z}{z_0}\right)\right]\exp[\mathrm{i}kz]\,. \tag{8.1.25}$$

The last term is referred to as the Gouy phase shift. This additional phase is the reason why the resonance frequency has an additional term that depends on the g-parameters of the resonator. By introducing the q-parameter of the Gaussian beam:

$$\frac{1}{q(z)} = \frac{1}{R(z)} - \frac{\mathrm{i}\lambda}{\pi\, w_{00}^2(z)} \tag{8.1.26}$$

the field distribution of a Gaussian beam can be written as:

$$E(x,y,z) = \frac{E_0}{\sqrt{1+(z/z_0)^2}} \exp\left[-\frac{\mathrm{i}k(x^2+y^2)}{2q(z)}\right] \exp\left[-\mathrm{i}\,\mathrm{atan}\left(\frac{z}{z_0}\right)\right] \exp[\mathrm{i}kz] \,. \tag{8.1.27}$$

Propagation of the Gaussian beam through ABCD-type optics can be accomplished by using the ABCD-law for the q-parameter:

$$q_2 = \frac{Aq_1 + B}{Cq_1 + D} \,, \tag{8.1.28}$$

where the index 1 and 2 denote the two reference planes between which the propagation occurs. A transverse distribution of the form

$$E(x_1,y_1) = E_0 \exp\left[-\frac{\mathrm{i}k(x_1^2+y_1^2)}{2q_1}\right] \tag{8.1.29}$$

transforms into

$$E(x_2,y_2) = \frac{E_0}{A - B/q_1} \exp\left[-\frac{\mathrm{i}k(x_2^2+y_2^2)}{2q_2}\right] \,. \tag{8.1.30}$$

8.1.3.2.2 Higher-order modes

The treatment of the propagation of higher-order modes in the resonators becomes quite simple given the preceding detailed discussion of the propagation of Gaussian beams. In both circular and rectangular symmetries the propagation of the fundamental mode and of the higher-order modes is similar. If w_0 and θ_0 denote the waist radius and the angle of divergence (half angle) of the fundamental mode, the beam radius as a function of the propagation distance from the waist position reads as follows:

(a) circular symmetry:

$$w_{p\ell}(z) = w_0\sqrt{2p+\ell+1}\,\sqrt{1+\left(\frac{z}{z_0}\right)^2} \quad (\textit{beam radius at location } z) \,, \tag{8.1.31}$$

$$w_{p\ell} = w_0\sqrt{2p+\ell+1} \quad (\textit{waist radius}) \,, \tag{8.1.32}$$

$$\theta_{p\ell} = \theta_0\sqrt{2p+\ell+1} \quad (\textit{angle of divergence}) \,. \tag{8.1.33}$$

(b) rectangular symmetry:

$$w_m(z) = w_0\sqrt{2m+1}\,\sqrt{1+\left(\frac{z}{z_0}\right)^2} \quad (\textit{beam radius at location } z) \,, \tag{8.1.34}$$

$$w_m = w_0\sqrt{2m+1} \quad (\textit{waist radius}) \,, \tag{8.1.35}$$

$$\theta_m = \theta_0\sqrt{2m+1} \quad (\textit{angle of divergence}) \,. \tag{8.1.36}$$

The Rayleigh range is the same as for the Gaussian beam, see Fig. 8.1.12:

$$z_0 = \frac{w_m}{\theta_m} = \frac{w_0}{\theta_0} = \frac{\pi\, w_0^2}{\lambda} \,. \tag{8.1.37}$$

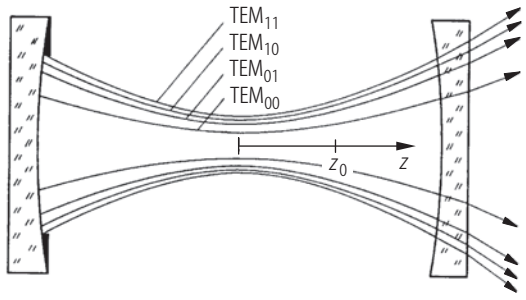

Fig. 8.1.12. Beam propagation of higher-order modes. All modes have the same Rayleigh range. At any plane the beam radii are $\sqrt{2p+\ell+1}$ larger than the Gaussian beam radius.

The beam parameter product $w\theta$ is a constant of the beam with

$$w_{p\ell}\theta_{p\ell} = (2p+\ell+1)\frac{\lambda}{\pi} = M^2\frac{\lambda}{\pi}\,, \tag{8.1.38}$$

$$w_m\theta_m = (2m+1)\frac{\lambda}{\pi} = M^2\frac{\lambda}{\pi}\,. \tag{8.1.39}$$

The term M^2 is referred to as the beam propagation factor of the mode. In a laser resonator, the maximum propagation factor corresponding to the highest-order transverse mode determines the beam quality of the laser beam. If N apertures with radii a_i are located inside the resonator at positions $z_1 \ldots z_N$ and $w_{00}(z_i)$ are the beam radii of the Gaussian beam at the apertures, the maximum propagation factor, to a good approximation, can be calculated using the relation

$$M^2_{\max} = \min\left(\left[\frac{a_1}{w_{00}(z_1)}\right]^2, \left[\frac{a_2}{w_{00}(z_2)}\right]^2, ..., \left[\frac{a_N}{w_{00}(z_N)}\right]^2\right)\,, \tag{8.1.40}$$

where "min" is the minimum term in the group.

The electric field distribution of individual transverse modes as a function of the propagation distance z reads:

(a) in circular symmetry:

$$E(r,\Phi,z) = \frac{E_0}{\sqrt{1+(z/z_0)^2}}\,\exp\left[\frac{-r^2}{w_{00}^2(z)} - \frac{\mathrm{i}kr^2}{2R(z)}\right]\left[\frac{\sqrt{2}\,r}{w_{00}(z)}\right]^\ell L_{p\ell}\left[\frac{2r^2}{w_{00}(z)^2}\right]\begin{Bmatrix}\cos(\ell\Phi)\\ \sin(\ell\Phi)\end{Bmatrix}$$
$$\times\exp\left[-\mathrm{i}(2p+\ell+1)\,\mathrm{atan}\left(\frac{z}{z_0}\right)\right]\,, \tag{8.1.41}$$

(b) in rectangular symmetry:

$$E(x,y,z) = \frac{E_0}{\sqrt{1+(z/z_0)^2}}\,\exp\left[\frac{-(x^2+y^2)}{w_{00}^2(z)} - \frac{\mathrm{i}k(x^2+y^2)}{2R(z)}\right]H_m\left[\frac{\sqrt{2}\,x}{w_{00}(z)}\right]H_n\left[\frac{\sqrt{2}\,y}{w_{00}(z)}\right]$$
$$\times\exp\left[-\mathrm{i}(m+n+1)\,\mathrm{atan}\left(\frac{z}{z_0}\right)\right]\,. \tag{8.1.42}$$

The beam radius $w_{00}(z)$ and the radius of curvature $R(z)$ are those of the Gaussian beam. The Gouy phase shift (last term) generates the frequency difference between modes of different transverse order.

By introducing the q-parameter

$$\frac{1}{q(z)} = \frac{1}{R(z)} - \frac{\mathrm{i}\lambda M^2}{\pi\, w_{p\ell}^2(z)} \tag{8.1.43}$$

the propagation of higher-order modes from a plane 1 to a plane 2 through ABCD-type optics can be calculated by using the ABCD-law for the q-parameter (8.1.28).

8.1.3.3 Beam quality and resonator parameters

The magnitude of the beam parameter product of a stable laser resonator depends on the number of transverse modes oscillating. The beam propagation factor M^2 is determined by the radius and the location of the smallest aperture (with respect to the Gaussian beam radius) inside the resonator. To a very good approximation, the beam propagation factor can be calculated by using (8.1.40). If b denotes the radius of the active medium with length l and the distances from the endfaces to the nearest mirror are l_1 and l_2 (Fig. 8.1.13), the beam propagation factor as a function of the resonator parameters reads:

$$M^2 = \frac{\pi b^2}{\lambda L} \frac{|g_1 + g_2 - 2g_1g_2|}{\sqrt{g_1g_2(1-g_1g_2)}} \times \left[1 + \frac{\left[[g_1 + g_2 - 2g_1g_2][X - Lg_2(1-g_1)/(g_1 + g_2 - 2g_1g_2)]\right]^2}{L^2(g_1g_2(1-g_1g_2))}\right]^{-1} \quad (8.1.44)$$

with

$X = l_1 + l$, if $L_{01} < l_1 + l/2$ (see Fig. 8.1.13 and (8.1.21)),
$X = l_1$ otherwise,
$L = l_1 + l_2 + l$.

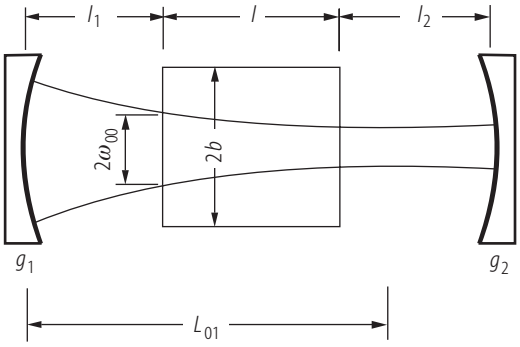

Fig. 8.1.13. The size of the active medium determines the number of transverse modes. The ratio of the radius b to the largest Gaussian beam radius inside the medium w_{00} determines the beam propagation factor. L_{01} is the distance of the beam waist from mirror 1, given by (8.1.21).

Figure 8.1.14 presents the beam parameter product as a function of the g-parameters for stable resonators of equal length $L = 1$ m and different locations of the active medium with radius $b = 5$ mm. The best beam quality is attained near the stability limits at positive g-parameters since the Gaussian beam radii go to infinity in this area. If the active medium is placed in the middle of the resonator, the concentric resonator generally exhibits the worst beam quality. Note that the beam parameter product in multimode operation does not depend on the wavelength! This means that the size of the focal spot does not depend on the type of laser material used. A smaller wavelength will generate a smaller-radius Gaussian beam which in turn increases the number of transverse modes fitting into the medium. Therefore, the product $M^2\lambda$ is a constant of the resonator.

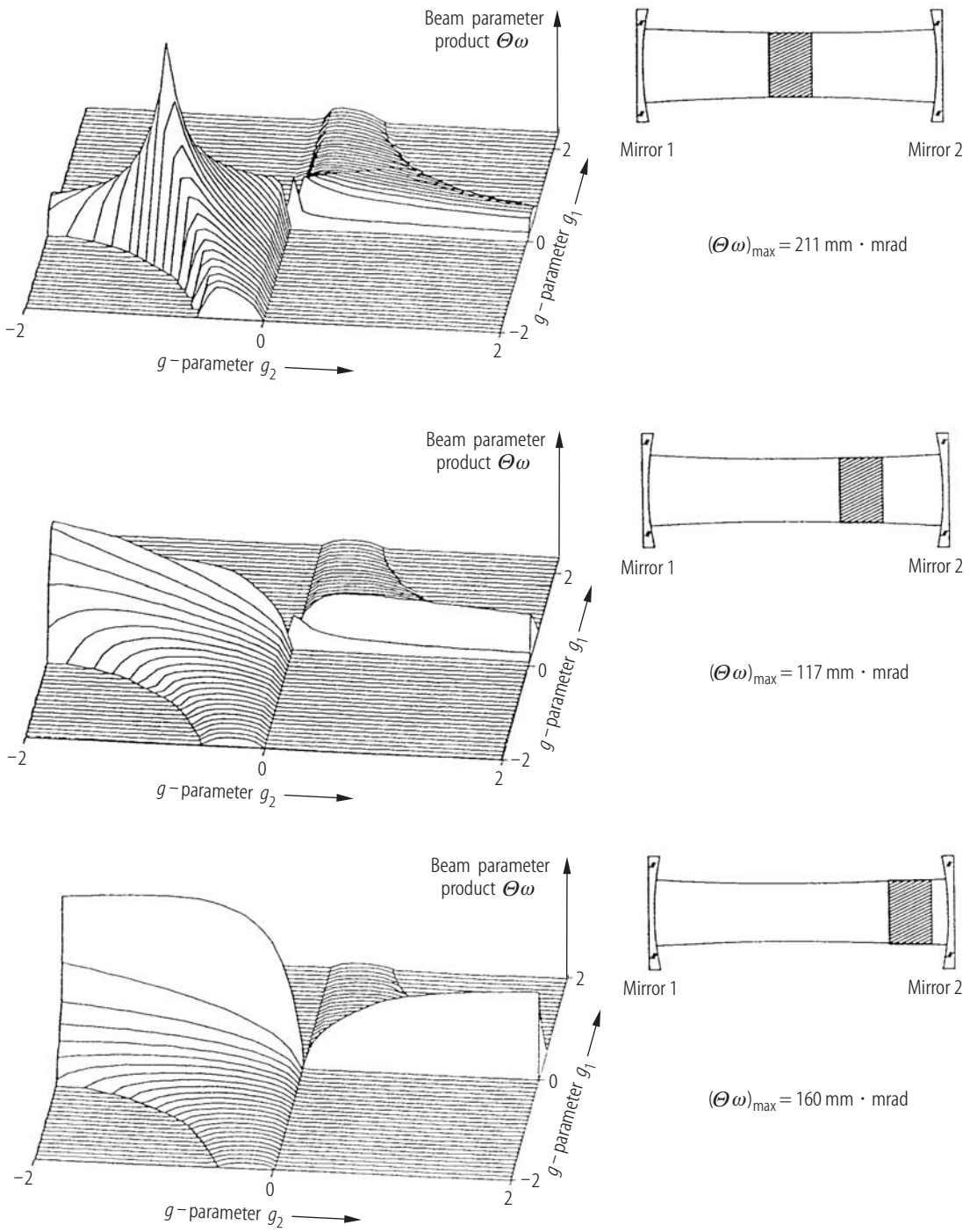

Fig. 8.1.14. Beam parameter products in the stability diagram for different positions of the active medium ($b = 5$ mm, $l = 100$ mm). The resonator length is always $L = 1$ m. For each graph the maximum beam parameter product is given [97Hod].

8.1.3.4 Resonance frequencies

The development of steady-state field distributions in an unconfined optical resonator requires that both the amplitude and the phase of the electric field $E(x, y)$ are reproduced after each round trip. According to (8.1.8) this requirement is met if the eigenvalue γ is equal to 1.0, which is referred to as the *resonance condition*. Together with (8.1.10) and (8.1.12), the resonance condition yields the resonance frequencies ν of the eigenmodes [61Fox]:

circular symmetry:

$$\nu_{plq} = \frac{c_0}{2L}\left[q + \frac{2p + \ell + 1}{\pi}\ \text{acos}\ \sqrt{g_1 g_2}\right] , \tag{8.1.45}$$

rectangular symmetry:

$$\nu_{mnq} = \frac{c_0}{2L}\left[q + \frac{m + n + 1}{\pi}\ \text{acos}\ \sqrt{g_1 g_2}\right] \tag{8.1.46}$$

with

c_0 : speed of light in vacuum,
$L = nL_0$: optical mirror spacing (L_0: geometrical spacing, n: index of refraction inside the resonator).

The resonance frequencies thus depend on both the axial and the transverse mode order. In contrast to the plane-plane resonator FPI ($g_1 = g_2 = 1$) whose resonance frequencies are only determined by the axial mode index, each axial mode of stable resonators is subdivided into a sequence of frequencies corresponding to different transverse modes. This separation is controlled by the g-parameters of the resonator mirrors (Fig. 8.1.15). As the origin of the g-diagram is approached, the frequency gap between different transverse modes having the same axial mode order becomes wider. In the limit of the stable confocal resonator ($g_1 = g_2 = 0$), the frequency gap equals $c_0/(4L)$ which is half the axial mode distance.

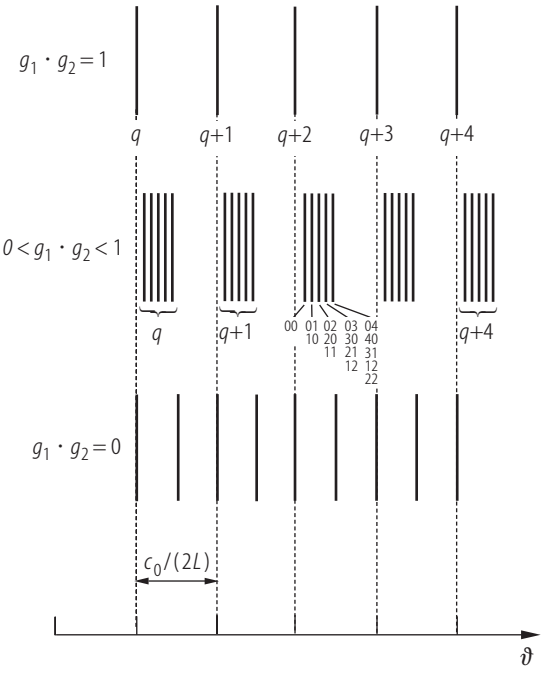

Fig. 8.1.15. Resonance frequencies of the modes of stable resonators with rectangular symmetry for different g-parameter products. The indices mn of some transverse modes are shown for the axial mode of order $q + 2$.

8.1.4 Aperture-limited stable resonators

In addition to selecting the number of oscillating transverse modes, an aperture inside the resonator will also generate diffraction losses which are the result of a changed transverse mode structure. If the aperture radius is decreased so that it becomes smaller than the fundamental-mode beam radius, the angle of divergence will increase resulting in an increased power fraction hitting the aperture after each round trip. The intensity distribution at the mirrors is no longer Gaussian and the beam propagation inside the resonator does not follow the Gaussian beam propagation rules. The losses of the fundamental mode will decrease as the aperture radius is increased and the intensity profile will approach that of a Gaussian beam. However, decreasing the diffraction loss by opening the aperture will also enable higher-order modes to reach laser threshold.

8.1.4.1 Resonators with one aperture

If only one aperture is placed inside the resonator directly in front of mirror 1 (Fig. 8.1.16), the field distributions at mirror 1 are eigensolutions of the Kirchhoff integral equation (8.1.8) for the round trip [61Boy, 61Fox, 63Fox, 65Li, 65Heu, 65Sie, 66Kog1, 66Kog2]. In circular geometry with an aperture radius a, the integral equation for the fields of the transverse eigenmodes reads:

$$\gamma_{pl} E_{pl}(r_2, \Phi_2) = \mathrm{i}\,\frac{\exp[-\mathrm{i}\,kL]}{2L\,g_2\,\lambda_0} \times \int_0^{2\pi}\int_0^{a} E_{pl}(r_1,\phi_1)\cdot\exp\left[\frac{-\mathrm{i}\pi}{2L\,g_j\,\lambda_0}\left(G(r_1^2+r_2^2)-2r_1r_2\cos(\phi_1-\phi_2)\right)\right] r_1\mathrm{d}r_1\mathrm{d}\phi_1 \qquad (8.1.47)$$

with

$G = 2g_1\,g_2 - 1$,
$L = n\,L_0$: optical resonator length (L_0 : geometrical length),
λ_0 : vacuum wavelength, $k = 2\pi/\lambda_0$: wave number.

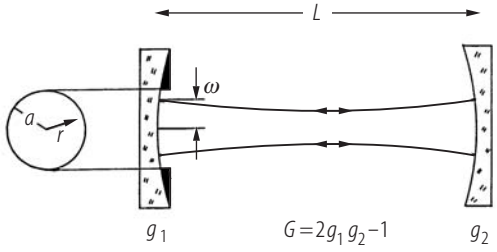

Fig. 8.1.16. Stable resonator with aperture-limited mirror 1 (circular symmetry).

In contrast to the unconfined resonator, the loss factors $V = |\gamma_{pl}|$ are now lower than 1.0 since the eigenmodes exhibit diffraction losses at the aperture. The diffraction loss and the mode structure depend only on two parameters:

1. *the equivalent G-parameter*: $G = 2g_1g_2 - 1$,
2. *the effective Fresnel number*: $N_{\mathrm{eff}} = a^2/(2Lg_2\lambda_0)$.

The effective Fresnel number is proportional to the area of the aperture. Its relationship to the Gaussian beam radius $w_{00}^{(1)}$ at mirror 1 is given by:

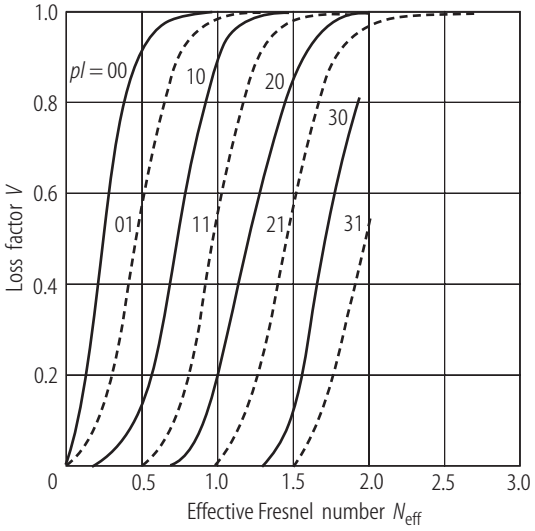

Fig. 8.1.17. Loss factor per round trip of different transverse modes in circular symmetry for $G = 0.0$ as a function of the effective Fresnel number N_{eff}. The aperture radius is equal to the Gaussian beam radius for $N_{\text{eff}} = 1/\pi \approx 0.318$.

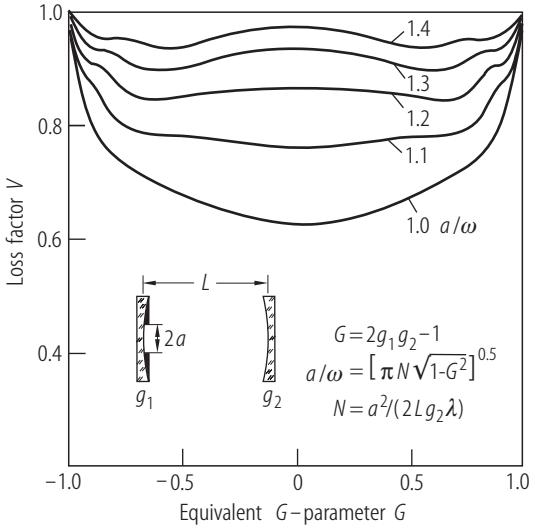

Fig. 8.1.18. Calculated loss factors per round trip of the fundamental mode in stable resonators with a circular aperture of radius a as a function of the equivalent G-parameter $G = 2g_1g_2 - 1$. The aperture radius is shown normalized to the Gaussian beam radius w.

$$\left[\frac{a}{w_{00}^{(1)}}\right]^2 = \pi N_{\text{eff}}\sqrt{1-G^2}\,. \tag{8.1.48}$$

Stable resonators in fundamental-mode operation with an aperture radius that is 1.2 . . . 1.5 times larger than the Gaussian beam radius exhibit an effective Fresnel number around 1.0. All resonators having the same absolute value of the equivalent g-parameter and the same absolute value of the effective Fresnel number exhibit the same eigenmodes and loss factors. These resonators are referred to as equivalent resonators. The integral equation (8.1.47) generally cannot be solved analytically. Figure 8.1.17 presents the numerically calculated loss factors of different low-order transverse modes as a function of the effective Fresnel number for resonators with $G = 0.0$. In most lasers only the loss of the fundamental mode is of practical interest. The loss of the fundamental mode determines both the laser threshold and the efficiency, whereas the losses of higher transverse modes affect only the output power. Figure 8.1.18 shows calculated loss factors per round trip in fundamental-mode operation as a function of the equivalent G-parameter, a comparison with experimental data is shown in Fig. 8.1.19.

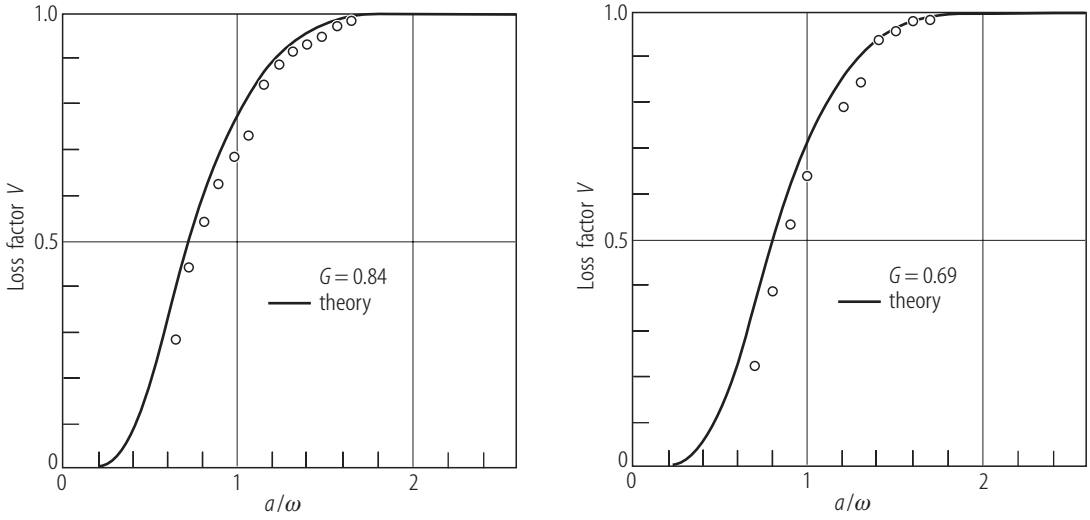

Fig. 8.1.19. Measured loss factors per round trip as a function of the ratio of the aperture radius a to the Gaussian beam radius w for two different G-parameters. The solid line represents the numerically calculated loss factor [88Ozy].

In order to minimize the fundamental-mode loss the aperture radius has to be chosen as large as possible. However, to prevent the next transverse mode from oscillating it is necessary to choose an aperture radius of less than 1.2 ... 1.4 times the Gaussian beam radius. The larger $|G|$ and the higher the gain of the medium, the closer the aperture radius can approach the Gaussian beam radius. The loss per round trip of the fundamental mode can be approximated by using the empirical relation [87Sil, 87Gro]:

$$\Delta V = \exp\left[-\alpha N_{\text{eff}}^{\beta}\right] . \tag{8.1.49}$$

The parameters α and β for the TEM_{00} mode read:

G	0.0	0.2	0.4	0.5	0.6	0.7	0.8	0.85	0.9	0.95	0.99
α	8.4	6.9	4.9	4.4	3.8	3.5	2.9	2.6	2.3	2.0	1.83
β	1.84	1.66	1.38	1.34	1.34	1.27	1.16	1.08	1.01	0.86	0.59

8.1.4.2 Resonators with two apertures

This case is much more complicated to deal with since the mode properties depend on three parameters rather than only on two parameters. In order to calculate the loss factor and the mode structure, the Kirchhoff integral has to be applied to both transits inside the resonator. If the aperture radii at mirror 1 and 2 are a_1 and a_2, respectively (Fig. 8.1.20), the loss per round trip of each transverse mode is a function of the modified g-parameters $g_1 a_1/a_2$, $g_2 a_2/a_1$, and the Fresnel number N with

$$N = \frac{a_1 a_2}{\lambda L} . \tag{8.1.50}$$

It is, therefore, difficult to present a general overview of the mode properties of these resonators. Furthermore, the number of publications dealing with double-aperture resonators is very limited [65Li, 65Str, 83Pic, 83Rig]. The loss per round trip is given by $\Delta V_{\text{R}} = 1 - |\gamma_{p\ell}|^2$. It is common to

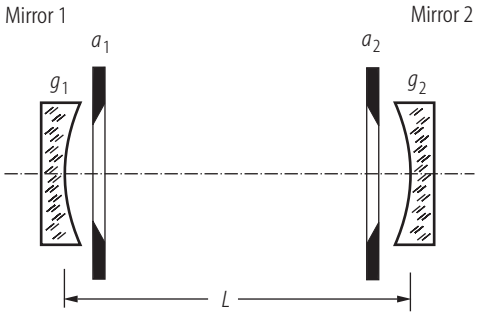

Fig. 8.1.20. Stable resonator with two aperture-limited mirrors.

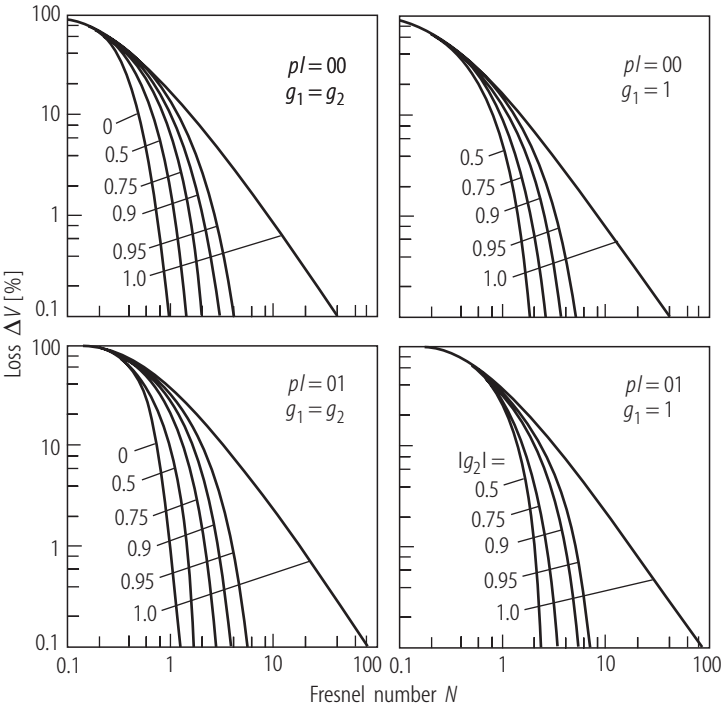

Fig. 8.1.21. Diffraction losses per transit of stable resonators in circular symmetry with both mirrors limited by apertures with radius $a_1 = a_2 = a$ as a function of the Fresnel number $a^2/(\lambda L)$. The losses for the fundamental mode and the next-order transverse mode are shown. The curve parameter is the g-parameter of mirror 2 (after [65Li]).

define the loss per transit via $\Delta V_{\mathrm{T}} = 1 - \sqrt{|\gamma_{p\ell}|^2}$, which represents the average loss per transit since the losses are generally different for the two directions. Diffraction losses per transit of stable resonators in circular symmetry with both mirrors limited by apertures with radius $a_1 = a_2 = a$ as a function of the Fresnel number $a^2/(\lambda L)$ are shown in Fig. 8.1.21.

8.1.5 Misalignment sensitivity

The misalignment sensitivity of a resonator is defined as the sensitivity with which the diffraction losses or the output power are changed due to mirror tilt [77Ber, 80Hau, 86DeS, 86Mag, 88Hau2, 92Hod2]. In this section we will only discuss the influence of the mirror misalignment on the resonator losses. The geometrical effect of a mirror tilt is shown in Fig. 8.1.22 for a resonator with one aperture-limited mirror. Rotation of mirror j by an angle α_j results in a rotation of the optical axis by an angle θ_j with the center of curvature of mirror i being the pivot point. As in the aligned resonator, the optical axis is defined by the line going through the centers of curvature of

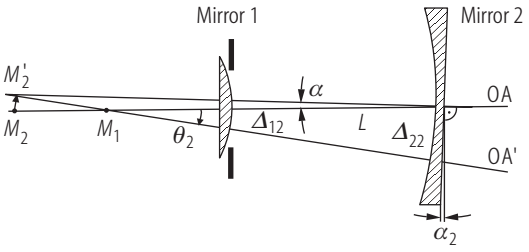

Fig. 8.1.22. Geometry of mirror misalignment in an optical resonator. Rotation of mirror 2 by α_2 results in a shift of the optical axis by Δ_{12} at mirror 1 and by Δ_{22} at mirror 2. The pointing stability θ and the shifts can be calculated by using (8.1.51)–(8.1.53). These equations are also applicable to unstable resonators.

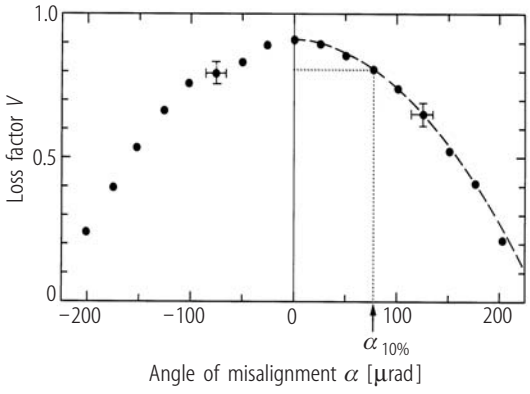

Fig. 8.1.23. Measured loss factors per round trip of a stable resonator as a function of the angle of misalignment of mirror 2. Mirror 1 is limited by an aperture with radius a ($G = 0.34$, $L = 0.7$ m, $a = 0.55$ mm, $\lambda_0 = 1.064$ μm).

the mirrors. The angle of rotation of the optical axis θ_j, also referred to as the pointing stability, and the shifts Δ_{jj}, Δ_{ij} of the intersecting points of the optical axis on mirror j and mirror i, respectively, read [80Hau]:

$$\theta_j = \alpha_j \frac{1 - g_i}{1 - g_1 g_2} , \tag{8.1.51}$$

$$\Delta_{jj} = \alpha_j \frac{L g_i}{1 - g_1 g_2} , \tag{8.1.52}$$

$$\Delta_{ij} = \alpha_j \frac{L}{1 - g_1 g_2} , \tag{8.1.53}$$

where g_i is the g-parameter of mirror i, and $i, j = 1, 2$ with $i \neq j$. The transverse eigenmodes will keep oscillating parallel to the optical axis whether the resonator is aligned or not. Furthermore, as far as stable resonators are concerned, the mode structure also stays almost symmetric to the optical axis. Since the optical axis comes closer to one side of the aperture if one or both mirrors are tilted, additional diffraction losses are generated. The effective aperture radius is decreased by the shift of the optical axis. For all linear resonators, stable as well as unstable ones, the loss factor decreases parabolically with the angle of rotation for small mirror tilts:

$$V(\alpha) = V(0) \left[1 - 0.1 \left(\frac{\alpha}{\alpha_{10\%}} \right)^2 \right] \tag{8.1.54}$$

with $V(0)$ being the loss factor for the aligned resonator (Fig. 8.1.22). Measured loss factors per round trip of a stable resonator as a function of the angle of misalignment of mirror 2 are shown in Fig. 8.1.23.

The angle $\alpha_{10\%}$ denotes the angle of misalignment at which the loss factor has decreased by 10% and consequently the losses have increased by 10%. This angle is used to define the misalignment sensitivity of optical resonators. A low misalignment sensitivity is equivalent to a small 10%-angle $\alpha_{10\%}$. Typical values of $\alpha_{10\%}$ for a stable resonator in fundamental-mode operation are on the order

of 50 μrad. The exact value of the 10%-angle depends on the g-parameters of the mirrors, the Fresnel number, the resonator length, and the aperture radii. All resonators exhibit two 10%-angles, each corresponding to the tilt of one mirror. It is customary to define an average misalignment sensitivity by taking the geometrical mean value of the two 10%-angles:

$$\alpha_{10\%} = \frac{1}{2}\sqrt{\alpha_{10\%,1}^2 + \alpha_{10\%,2}^2} \tag{8.1.55}$$

with the additional indices indicating the corresponding mirror. This mean angle defines the average angle by which both mirrors can be rotated simultaneously before a 10% increase in diffraction losses is generated.

8.1.5.1 Fundamental-mode operation

Let both aperture radii a_1, a_2 be adapted to the Gaussian beam radii $w_{00}^{(1)}$, $w_{00}^{(2)}$ at the mirrors with $a_i = s\, w_{00}^{(i)}$ and $s = 1.2 \ldots 1.6$. If mirror i is misaligned by an angle α_i, a first-order perturbation analysis of the diffraction integral yields for the loss factor per round trip [80Hau]:

$$V(\alpha_i) = V(0)\left[1 - \alpha_i^2 \frac{s^2}{\exp[2s^2] - 1} D_i^2\right] \tag{8.1.56}$$

with

$$D_i^2 = \frac{\pi L^*}{\lambda_0}\sqrt{\left(\frac{g_j}{g_i}\right)} \frac{1 + g_1 g_2}{(1 - g_1 g_2)^{1.5}}\,, \tag{8.1.57}$$

$L^* = L_0 - (n-1)l/n$: effective resonator length,
L_0: geometrical resonator length,
n: index of refraction of active medium,
l: length of active medium.

The misalignment of a resonator with both mirrors aperture-limited is shown in Fig. 8.1.24.

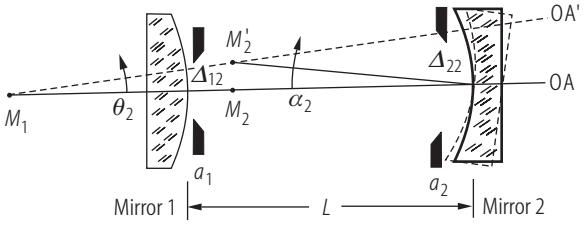

Fig. 8.1.24. Misalignment of a resonator with both mirrors aperture-limited [80Hau] (© OSA 1980).

If both mirrors are misaligned, the mean 10%-angle is given by

$$\alpha_{10\%} = \sqrt{0.1}\,\frac{\sqrt{\exp[2s^2] - 1}}{s\sqrt{D_1^2 + D_2^2}} = \sqrt{0.1}\,\frac{\sqrt{\exp[2s^2] - 1}}{sD} \tag{8.1.58}$$

with

$$D = \sqrt{\left(\frac{\pi L}{\lambda_0}\right)\frac{1 + g_1 g_2}{(1 - g_1 g_2)^{1.5}}\,\frac{|g_1 + g_2|}{\sqrt{g_1 g_2}}}\,. \tag{8.1.59}$$

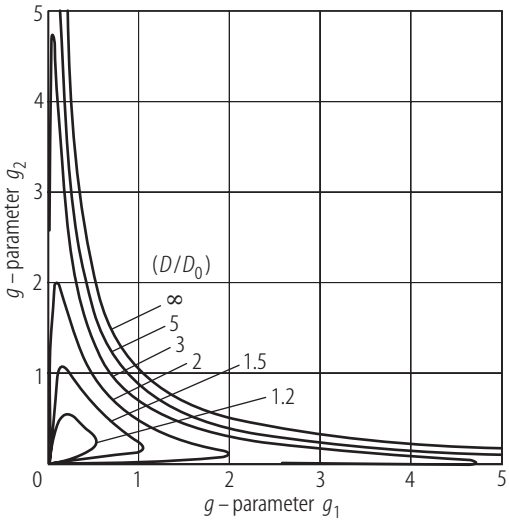

Fig. 8.1.25. Curves of constant misalignment sensitivity D for resonators with both apertures adapted to the Gaussian beam radius. D_0 is the sensitivity of the confocal resonator [80Hau] (© OSA 1980).

We define D as the misalignment sensitivity of the resonator since a small value of D results in a large 10%-angle (Fig. 8.1.25). The misalignment sensitivity in Fig. 8.1.25 is normalized to the sensitivity D_0 of the symmetric confocal resonator with $g_1 = g_2 = 0$, given by

$$D_0 = \sqrt{\frac{2\pi L}{\lambda_0}} \,. \tag{8.1.60}$$

The misalignment sensitivity is only a function of the resonator length and the g-parameters. Lowest misalignment sensitivities again are attained for resonators near the axes of the stability diagram.

8.1.5.2 Multimode operation

With both mirrors aligned the modes fill the entire medium since it represents the only mode-selecting aperture in the resonator. As the optical axis is rotated due to misalignment, the mode structure gets cut at one edge of the medium (lower left corner in Fig. 8.1.26) resulting in a decrease of the mode volume [86DeS, 92Hod2]. However, the optical axis remains the center of gravity of the mode structure which means that the beam gets clipped on both sides although only one side is affected by an edge. For a radius b of the active medium and small angles of misalignment, the cross-sectional area $A_b(\alpha)$ of the beam in the misaligned resonator reads

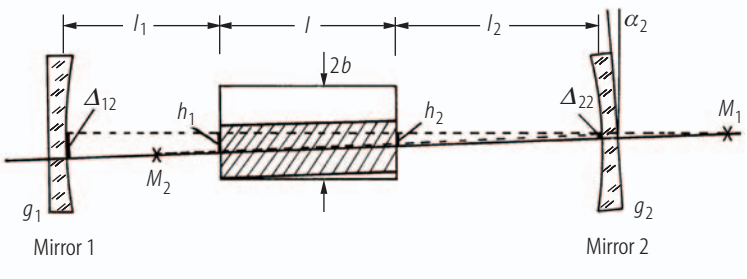

Fig. 8.1.26. A misaligned stable resonator in multimode operation. The hatched area indicates the mode volume [92Hod2] (© Taylor & Francis 1992).

$$A_b(\alpha) = \pi\, b^2 \left[1 - 0.1 \left(\frac{\alpha}{\alpha_{10\%}}\right)\right] , \tag{8.1.61}$$

where $\alpha_{10\%,i}$ is the angle at which the mode cross section and, consequently, the output power have decreased by 10%, when mirror i is tilted (Fig. 8.1.26):

$$\alpha_{10\%,i} = \frac{0.025\,\pi\, b}{L_{\text{eff}}} \, \frac{|1 - g_1 g_2|}{|1 - x_j/\rho_j|} , \quad i, j = 1, 2 , \quad i \neq j \tag{8.1.62}$$

with

$x_j = \ell_j - \ell(n-1)/(2n)$, if $\rho_j > \ell_j + \ell/(2n)$,
$x_j = \ell_j + \ell(n+1)/(2n)$ else,
$L_{\text{eff}} = \ell_1 + \ell_2 + \ell/n$: effective resonator length.

The dependence of the measured 10%-angle $\alpha_{10\%,2}$ on the effective resonator length L_{eff} is shown in Fig. 8.1.27 for four stable resonators.

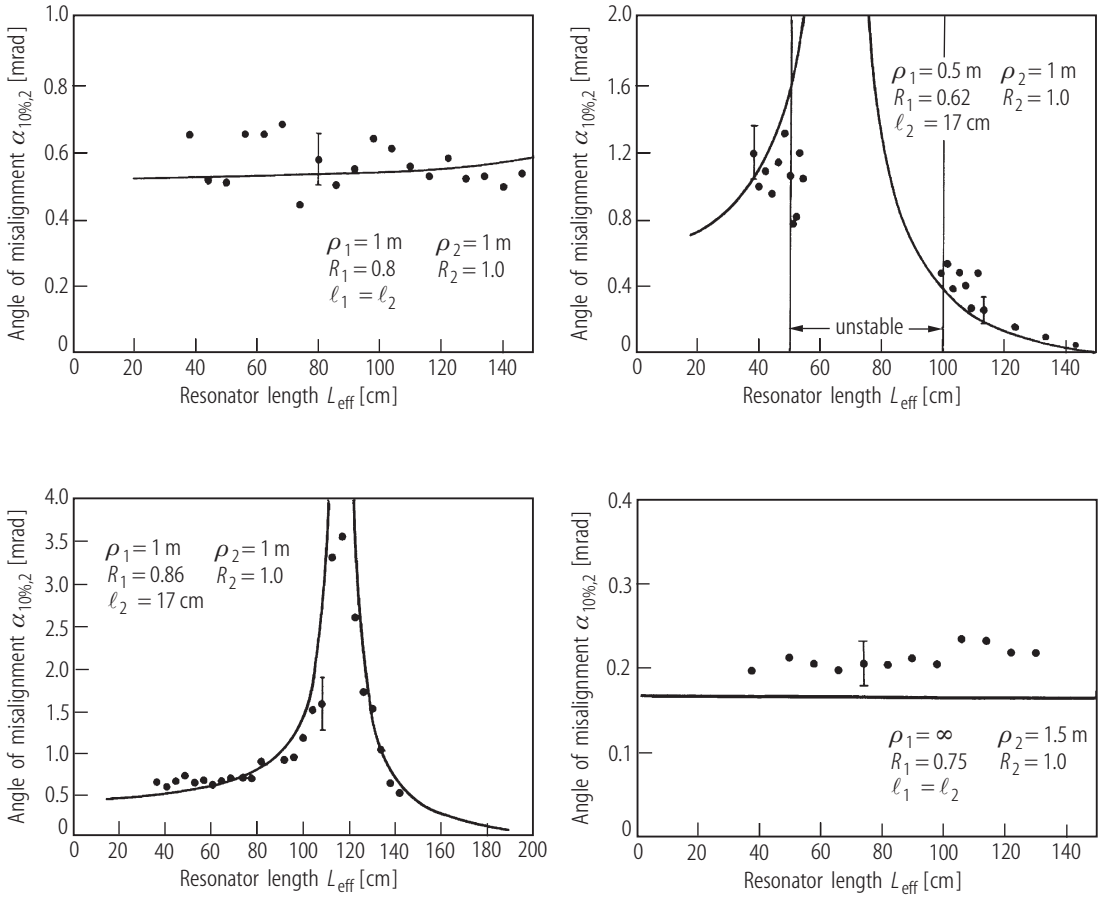

Fig. 8.1.27. Dependence of the measured 10%-angle $\alpha_{10\%,2}$ for four stable resonators on the effective resonator length L_{eff} (pulsed Nd:YAG rod laser in single-shot operation, $b = 3.17$ mm, $l = 75$ mm). The theoretical curves calculated with (8.1.62) are marked by solid lines. Resonator data are presented in each graph. In the unstable region (top right graph), (8.1.62) does not apply [92Hod2] (© Taylor & Francis 1992).

8.1.6 Unstable resonators

If the g-parameters of the resonator mirrors fulfill the relations $g_1 g_2 < 0$ or $g_1 g_2 > 1$, the radiation inside the resonator cannot be characterized by Gauss-Hermite or Gauss-Laguerre polynomials. These resonators are referred to as *unstable resonators* [65Sie, 72Ana], whereby the term "unstable" accounts for the fact that a Gaussian beam launched into the resonator will increase its beam radius after each round trip and, therefore, does not represent a "stable" eigensolution of the resonator (Fig. 8.1.28). By using the equivalent G-parameter $G = 2g_1 g_2 - 1$ we can characterize the different resonator schemes (as already discussed in Sect. 8.1.2):

- *stable resonators*: $0 < |G| < 1$,
- *resonators on the stability limits*: $|G| = 1$,
- *unstable resonators*: $|G| > 1$.

See Fig. 8.1.3 for the stability diagram of optical resonators.

Furthermore, one is able to distinguish *positive-branch* unstable resonators ($G > 1$) and *negative-branch* unstable resonators ($G < -1$). The steady-state field distributions on the mirrors of unstable resonators, similar to stable resonators, are solutions of the Kirchhoff integral equation (see (8.1.8)). However, in contrast to stable resonators, the beam propagation inside unstable resonators, to a good approximation, can be described by the propagation laws of geometrical optics.

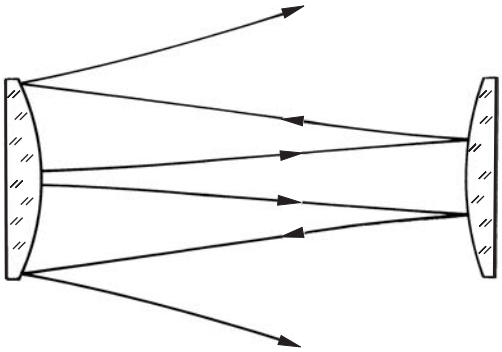

Fig. 8.1.28. No Gaussian beam can reproduce itself in an unstable resonator. The beam radii at the mirrors increase with each round trip.

8.1.6.1 Beam propagation

8.1.6.1.1 Characterization of unstable resonators

Unstable resonators are characterized by the presence of spherical waves inside the resonator that reproduce themselves after each round trip [65Sie, 66Kah, 72Ana]. In every unstable resonator we can find two spherical waves whose radii of curvature at any plane inside the resonator are reproduced after a round trip. If R_+ and R_- denote the radii of curvature at mirror 1 (after being reflected off the mirror) of the two spherical waves (Fig. 8.1.29), the following relation holds:

$$R_\pm = \frac{\pm 2Lg_2}{|G| \pm \sqrt{G^2 - 1} - 2g_2 + 1} \,. \tag{8.1.63}$$

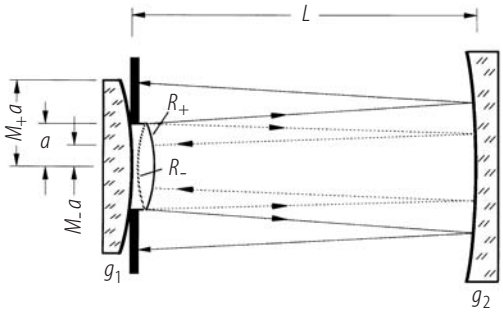

Fig. 8.1.29. The two self-reproducing spherical waves with radii of curvature R_+ and R_- at mirror 1 (after the reflection). After one round trip the beam diameter is changed by a factor $M_+(>1)$ and $|M_-|$ $(M_- < 1)$, respectively.

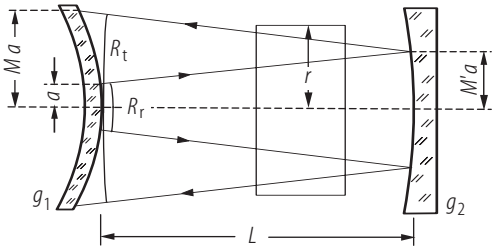

Fig. 8.1.30. Beam propagation inside an unstable resonator (diverging wave).

If mirror 1 is limited by an aperture with radius a, which means that the beam starting at mirror 1 has a diameter of $2a$, the radii of curvature R_+ and R_- reproduce themselves after the round trip, but the beam diameter is magnified by a factor M_+ and M_-, respectively, with

$$M_\pm = |G| \pm \sqrt{G^2 - 1} \quad \text{and} \quad |M_+ M_-| = 1 \,. \tag{8.1.64}$$

The spherical wave with radius R_+ increases the beam radius after each round trip by the factor $|M_+|$, called the *magnification*. Since $|M_+| > 1$ holds, the corresponding spherical wave is referred to as the *diverging wave*. If the power starting at mirror 1 (inside the aperture) is given by P_0, only the power

$$P_1 = \frac{1}{M_+^2} P_0 \tag{8.1.65}$$

hits the mirror inside the aperture after the round trip, provided that the intensity profile is homogeneous. The loss ΔV per round trip and the loss factor V per round trip are thus given by

$$\Delta V = 1 - \frac{1}{M_+^2} \,, \quad V = 1 - \Delta V = \frac{1}{M_+^2} \,. \tag{8.1.66}$$

The loss factor represents the power fraction that stays inside the resonator after each round trip.

In contrast to the diverging wave, the *converging wave* (R_-) decreases the beam diameter after each round trip by a factor $|M_-|$ with $|M_-| < 1$. The power P_0 starting at mirror 1 is conserved, but with every round trip the beam radius at mirror 1 is continuously decreased by $|M_-|$ so that no steady-state beam radius can be established on the mirror. After a few round trips in the resonator, the beam radius of the converging wave reaches its minimum value given by the diffraction limit and will then expand again. The converging wave transforms itself into a diverging wave due to diffraction. It is for this reason that the beam propagation in an unstable resonator is characterized by the divergent wave only. However, the convergent wave may have an influence on the mode properties of unstable resonators, if it is continuously excited by reflection off apertures or the endfaces of the active medium [72Ana, 90Hod2].

Figure 8.1.30 depicts the beam propagation in an unstable resonator. Instead of limiting mirror 1 by an aperture, the size of the highly reflecting area now defines the beam size on the mirror. The

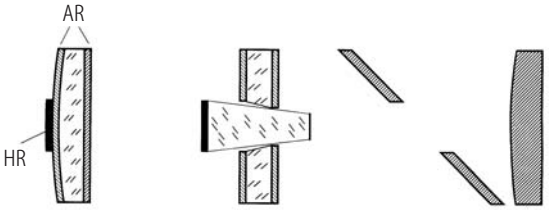

Fig. 8.1.31. Technical realization of the output-coupling mirror of unstable resonators.

laser beam is generated by output coupling around the reflective spot on the mirror. In circular symmetry, the near field exhibits the shape of an annulus with inner radius a and outer radius Ma. The size of mirror 2 is chosen such that no power is coupled out at this side of the resonator. The coatings on both mirrors are highly reflecting for the desired wavelength of laser emission. The following relations hold:

g-parameters:

$$g_i = 1 - \frac{L}{\rho_i} , \quad i = 1, 2 , \tag{8.1.67}$$

equivalent G-parameter:

$$G = 2g_1 g_2 - 1 , \tag{8.1.68}$$

magnification (round trip):

$$M = |G| + \sqrt{G^2 - 1} , \tag{8.1.69}$$

magnification (transit):

$$M' = g_1 + \frac{\sqrt{G^2 - 1}}{2g_2} , \tag{8.1.70}$$

radius of curvature of the spherical wave at mirror 1:

- traveling towards the mirror:

$$R_\mathrm{t} = \frac{L}{M' + 1 - 2g_1} , \tag{8.1.71}$$

- reflected off the mirror:

$$R_\mathrm{r} = \frac{2Lg_2}{M + 1 - 2g_2} , \tag{8.1.72}$$

loss factor per round trip:

$$V = \frac{1}{M^2} . \tag{8.1.73}$$

Three different ways to accomplish this special output-coupling scheme in unstable resonators exist (Fig. 8.1.31): The high-reflecting, confined mirror can be held in place by thin pins or mounted in the bore of a highly transmitting substrate (b). More common is the application of a high-reflecting coating on an AR-coated substrate as depicted in (a). For CO_2 lasers and other lasers emitting in the wavelength range on the order of 10 μm, the output coupling by means of a scraper is a well established technique (c).

8.1.6.1.2 Resonator schemes

Unstable resonators can be subdivided into two different classes:

1. $g_1 g_2 > 1$, *positive branch*
   These resonators exhibit either zero or two focal points inside the resonator. The centers of curvatures of the spherical waves at the mirrors are located either outside ($g_1 > 0$, $g_2 > 0$) or inside ($g_1 < 0$, $g_2 < 0$) the resonator.

2. $g_1 g_2 < 0$, *negative branch*
   One center of curvature of the spherical wave is located inside the resonator. The *negative-branch unstable resonators* therefore exhibit a focal spot in the resonator. Due to possible damage of the active medium by the high intracavity intensities, these resonators are only used in high-gain gas lasers. Compared to positive-branch resonators they exhibit a much lower misalignment sensitivity.

Resonators for which the relation

$$g_1 + g_2 = 2g_1 g_2 \tag{8.1.74}$$

holds, are referred to as *confocal resonators* (Fig. 8.1.32). For confocal resonators, the focal points of the two resonator mirrors are on top of each other, which means that the unstable resonator acts like a telescope. This special mirror arrangement provides a collimated output beam. The mode volume can thus be easily adapted to the volume active medium yielding optimum fill factors.

Figure 8.1.33 shows curves of constant magnification in the stability diagram. The broken lines indicate the confocal resonators. The curves with magnification $|M| = 1$ are the stability limits.

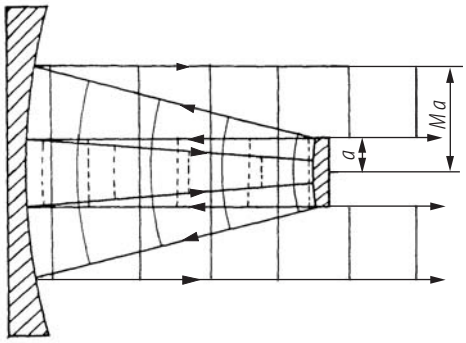

Fig. 8.1.32. Beam propagation in a positive-branch confocal unstable resonator with magnification $|M| = 2$.

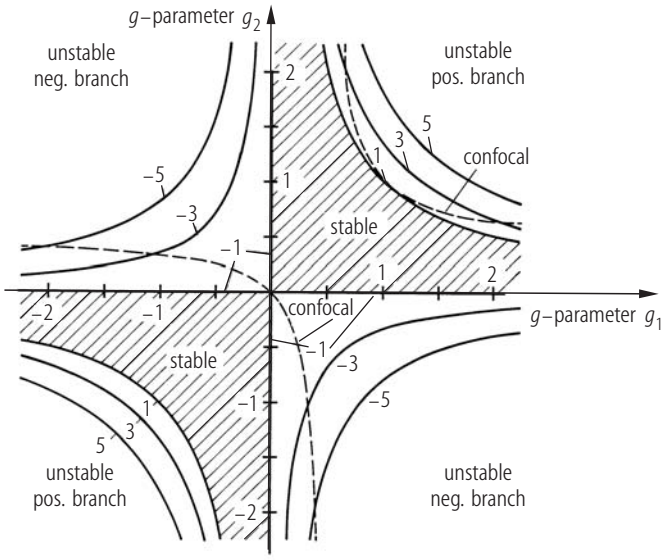

Fig. 8.1.33. Curves of constant magnification in the stability diagram. The broken lines indicate the confocal resonators. The curves with magnification $|M| = 1$ are the stability limits.

8.1.6.2 Mode structures and losses

The steady-state field distributions on the mirrors of unstable resonators can be calculated similarly to those of stable resonators by applying the integral equation (8.1.47) (Fig. 8.1.34) [65Sie, 67Sie, 74Sie, 75Szi, 87Oug, 88Hau1]. For both stable and unstable resonators the same integral equations can be used, the only difference is that the absolute value of the G-parameter is now greater than 1.0. Similar to the treatment of stable resonator modes, the integral equations can be simplified by separating the coordinates. The intensity distributions of the eigenmodes and the loss factor $V = |\gamma|^2$ again depend on the absolute value of the equivalent G-parameter G and the absolute value of the effective Fresnel number $N_{\text{eff}} = a^2/(2Lg_2\lambda)$. Unstable resonators exhibit an infinite set of TEM modes with mode indices pl and mn, but the mode properties are completely different as compared to the modes of stable resonators (Fig. 8.1.35). In contrast to stable-resonator modes, the loss factor does not always increase as the aperture radius is increased, leading to a periodic sequence of loss factor maxima.

Since different transverse modes exhibit their maxima at different Fresnel numbers, the loss factor curves cross, which means that at this point two transverse modes have the same diffraction loss. For transverse modes without azimuthal structure ($l = 0$) the loss factor is higher as compared to other modes and also higher than the geometrical loss factor of $1/M^2$. The reason for the lower loss becomes apparent if we investigate the intensity profiles of the modes at the loss-factor maxima. Since the profiles are more centered as compared to the homogeneous profile assumed in the preceding section, a higher power fraction hits the output coupler again after the round trip resulting in a higher loss factor.

It is important to note that the beam radii of different transverse modes are the same. This property, together with the difference in diffraction loss between transverse modes, determines

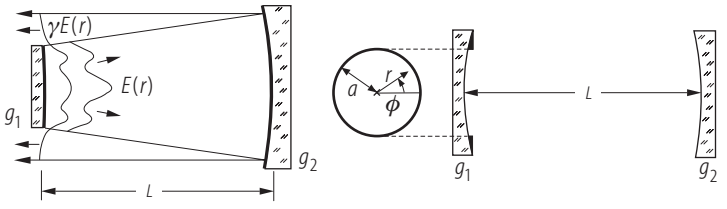

Fig. 8.1.34. Calculation of the field distribution at the plane of the output coupler for unstable resonators in circular symmetry. After the round trip the shape of the field at mirror 1 is still the same.

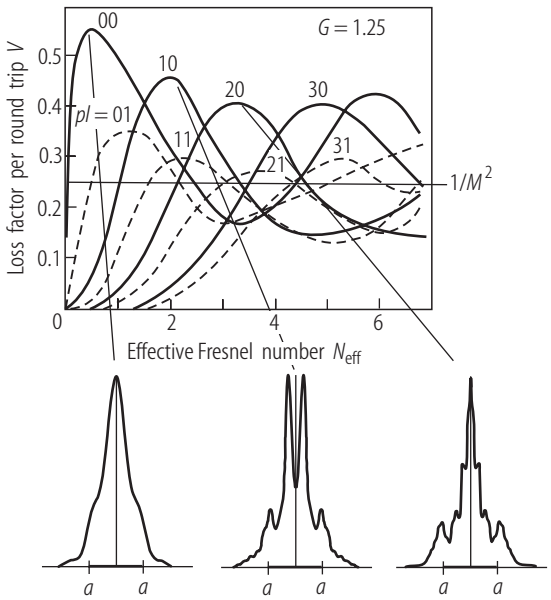

Fig. 8.1.35. Calculated loss factor per round trip as a function of the effective Fresnel number N_{eff} for unstable resonators in circular symmetry with magnification $M = 2$. The radial intensity distributions at the plane of the output coupler are shown for the first three loss-factor maxima.

the special oscillation behavior of unstable resonators. The mode with the lowest loss will start oscillating first and deplete the gain in the same area of the active medium that might be used by other transverse modes. These modes, however, exhibit too high of a loss for the leftover gain to reach the laser threshold. Except for the operation at mode-crossing points, unstable resonators thus oscillate in a single transverse mode with no azimuthal structure ($l = 0$).

For practical applications, therefore, it is sufficient to determine the loss and the mode structure only for the lowest-loss modes. The calculated loss factors per round trip of the lowest-loss mode for unstable resonators in circular and rectangular symmetry are presented in Fig. 8.1.36. In Fig. 8.1.37 measured and calculated loss factors per round trip of unstable resonators in circular symmetry with magnification $M = 4$ are shown. In these graphs, the loss factor is plotted versus the equivalent Fresnel number N_{eq}, which is related to the effective Fresnel number via

$$N_{\mathrm{eq}} = N_{\mathrm{eff}} \sqrt{G^2 - 1}\,. \tag{8.1.75}$$

By using the equivalent Fresnel number as a mode parameter, the mode-crossing points are characterized by integral values of N_{eq}. In order to attain single-transverse-mode operation in an unstable resonator, it, therefore, is recommended to choose half-integral values of the equivalent Fresnel number because the loss difference between modes is a maximum in these areas (Fig. 8.1.38).

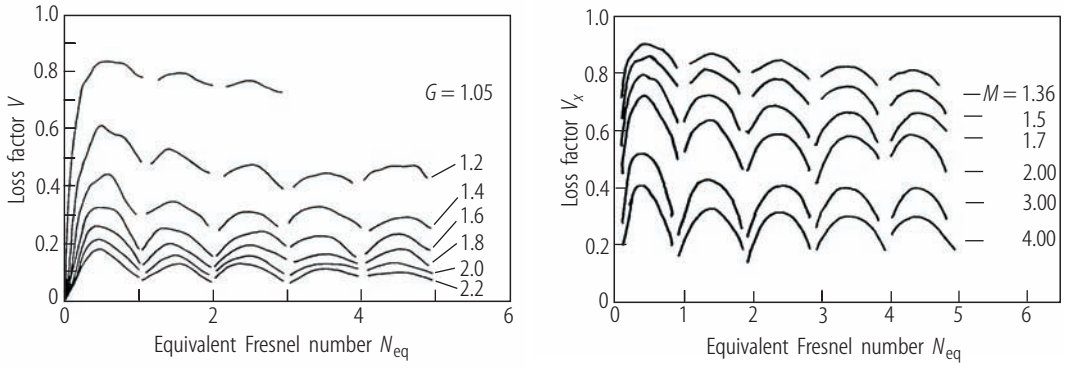

Fig. 8.1.36. Calculated loss factor per round trip of the lowest-loss modes as a function of the equivalent Fresnel number N_{eq}. (**a**) circular symmetry with mirror radius a, (**b**) rectangular symmetry with mirror width $2a$, one-dimensional loss factor V_x, the total loss factor is $V = V_x V_y$ [92Hod1] (Chapman & Hall 1992).

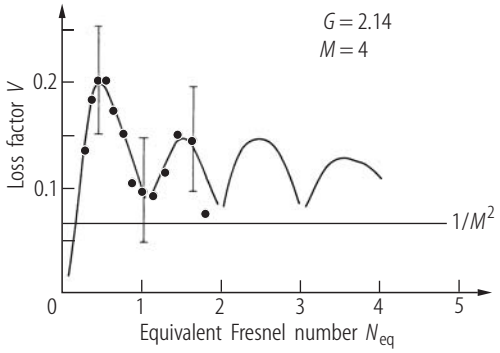

Fig. 8.1.37. Measured and calculated loss factors per round trip of unstable resonators in circular symmetry with magnification $M = 4$ as a function of the equivalent Fresnel number (pulsed Nd:YAG laser) [88Hau1] (© AIP 1988).

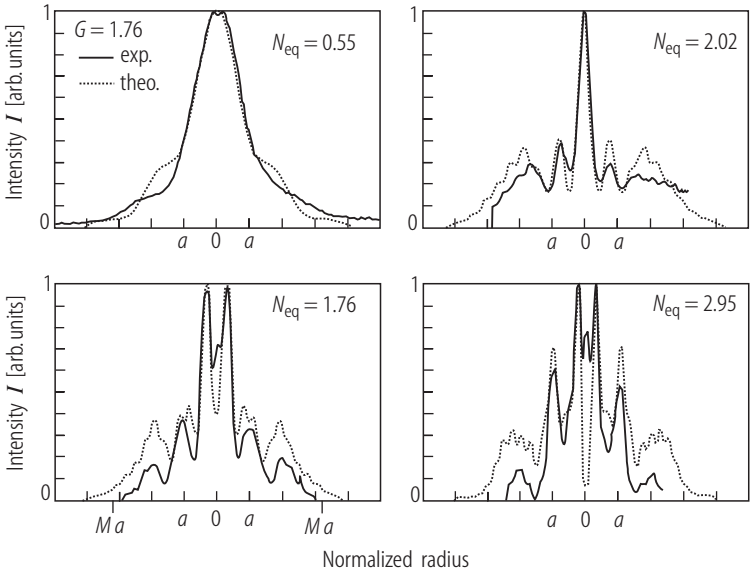

Fig. 8.1.38. Measured radial intensity distributions at the plane of the output coupler of unstable resonators in circular symmetry with $G = 1.76$ ($M = 3.21$) and different equivalent Fresnel numbers. The profile within the radius a is reflected by the mirror, the outer portion of the mode is coupled out. The dotted lines are the numerically calculated distributions (pulsed Nd:YAG laser) [88Hau1] (© AIP 1988).

8.1.6.3 Beam quality

8.1.6.3.1 Circular symmetry

The beam quality of unstable resonators is determined by the diffraction at the confined output-coupling mirror. If we assume that the outcoupled beam exhibits a plane phase front, the intensity distribution in the focal spot is given by the intensity distribution in the far field of a homogeneously illuminated annular ring with inner radius a and outer radius Ma. Application of the diffraction integral in the Fraunhofer approximation yields the far-field intensity distribution (Fig. 8.1.39):

$$I(\theta) = I(0)\,\frac{M^2}{M^2-1}\left[\frac{J_1(2\pi Ma\theta/\lambda)}{\pi Ma\theta/\lambda} - \frac{1}{M^2}\,\frac{J_1(2\pi a\theta/\lambda)}{\pi a\theta/\lambda}\right], \tag{8.1.76}$$

where J_1 is the Bessel function of order 1. For high magnifications ($M \gg 1$), the far-field intensity distribution of a round aperture is obtained with a Full-Width-Half-Maximum (FWHM) diameter of the central peak of

$$\Delta\theta = 0.51\frac{\lambda}{Ma}\,. \tag{8.1.77}$$

The power fraction in the side lobe and the spot radius r decrease as the magnification of the resonator is increased. It is for this reason that the magnification of unstable resonators is generally

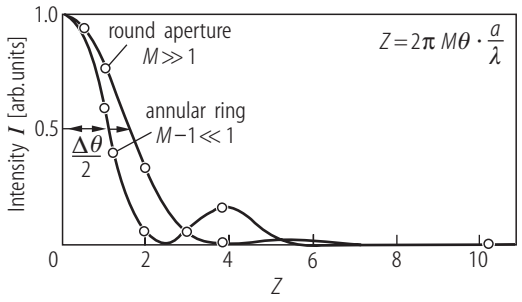

Fig. 8.1.39. Far-field intensity distributions of a homogeneously illuminated ring with inner radius a and outer radius Ma in the limits of low and high magnification M (calculated with (8.1.76)).

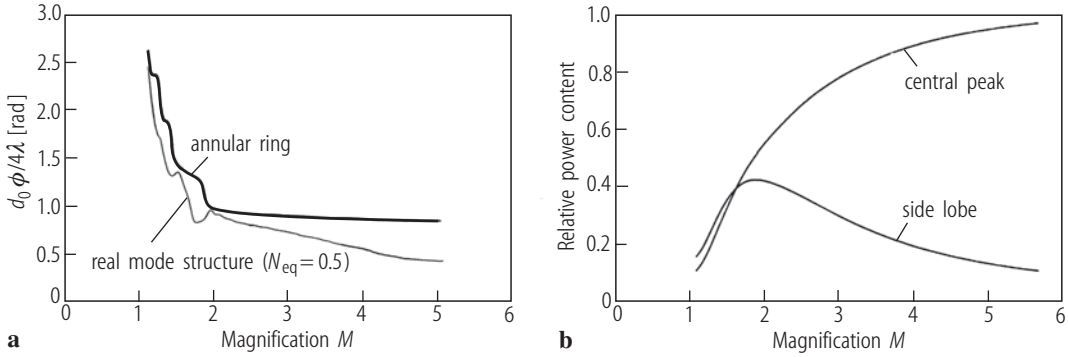

Fig. 8.1.40. Calculated beam parameter products $d_0\Phi/4\lambda$ (d: beam width, Φ: full angle of divergence, both defined via 86.5% power content) and power fractions in the center peak and in the side lobe as a function of the magnification (using the far-field distribution of a homogeneously illuminated ring with inner radius a and outer radius Ma).

chosen as high as possible with an upper limit given by the gain of the medium. Unstable resonators are mostly applied to active media with sufficiently high small-signal gain ($g_0 l > 1.5$). For low-gain media the optimum magnification would be too low to have the major power fraction going into the central peak.

In the limit of high magnifications, the beam parameter product approaches the value for a round beam with a homogeneous intensity distribution (Fig. 8.1.40). Compared to a Gaussian beam, the beam parameter product of unstable resonators is at least 2.5 times higher. For typical magnifications between $M = 2$ and $M = 4$, the beam quality of unstable resonators is about three times worse as compared to a Gaussian beam. The model used to calculate the beam quality assumes that the near field is a perfect annular ring. In reality the mode structure in the near field exhibits variations in both the amplitude and the phase. This diffraction effect leads to a lower power fraction in the side lobe and to slightly lower beam parameter products. This is mainly due to a less steep slope in the outer area of the beam.

8.1.6.3.2 Rectangular symmetry

A similar geometrical treatment can be performed for unstable resonators in rectangular symmetry. The one-dimensional far field is given by the Fourier transform of a double slit with a slit width of $(M-1)a$ and a slit separation (center-to-center) of $(M+1)a$. The angular intensity distribution in one dimension reads

$$I(\theta) = I(0)\left[\frac{\sin[\pi\,\theta(M-1)a/\lambda]\;\cos[\pi\,\theta(M+1)a/\lambda]}{\pi\,\theta(M-1)a/\lambda}\right]^2 . \tag{8.1.78}$$

For the same magnification, the intensity distribution at the focus of unstable resonators in rectangular symmetry exhibits much higher side lobes as compared to circular-symmetric unstable resonators (Fig. 8.1.41).

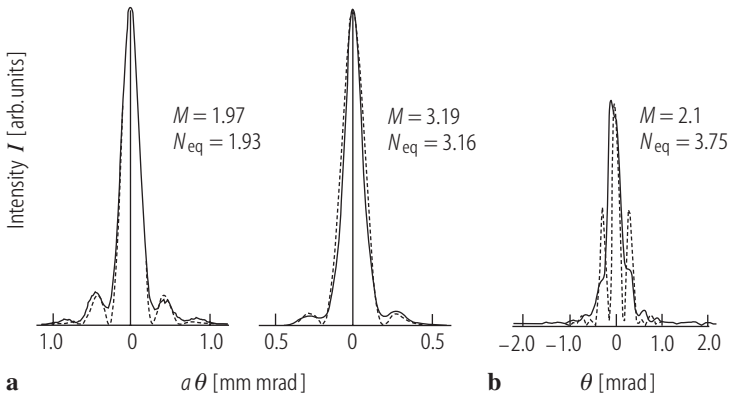

Fig. 8.1.41. Measured (solid lines) and calculated (broken lines) intensity distributions at the focus of unstable resonators for Nd:YAG lasers ($\lambda = 1.064$ μm). (**a**) circular symmetry, $a = 1.5$ mm, (**b**) rectangular symmetry, $a = 2.0$ mm [92Hod1].

8.1.6.4 Unstable resonators with variable-reflectivity mirrors

The power content in the side lobes of the far field of unstable resonators can be decreased by using output-coupling mirrors with a variable reflectivity profile [65Vak, 70Zuc, 84McC, 88Sne, 88DeS2, 88DeS1, 92Mag, 93Hod1, 93Hod2]. The reflectivity profile which generally exhibits a maximum at the center improves the beam quality by two effects: The diffraction of the power into the side lobes is considerably decreased by replacing the hard edge by a continuous transition from high to low reflectance (Fig. 8.1.42). Furthermore, the center reflectivity and the shape of the profile can be varied to generate a specified intensity profile in the near field (e.g. flat-top beams). The specific shape of the reflectivity profile is only of secondary importance, especially if the center

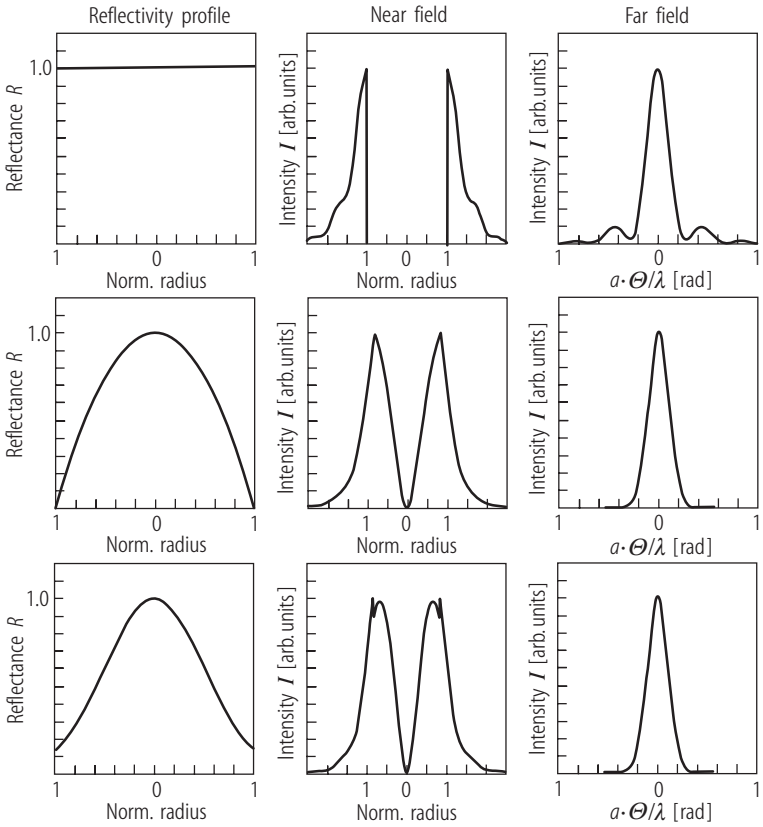

Fig. 8.1.42. Calculated intensity distributions in the near field and the far field of a confocal unstable resonator with $M = 2$ and $N_{eq} = 0.5$ for different reflectivity profiles of the output coupler.

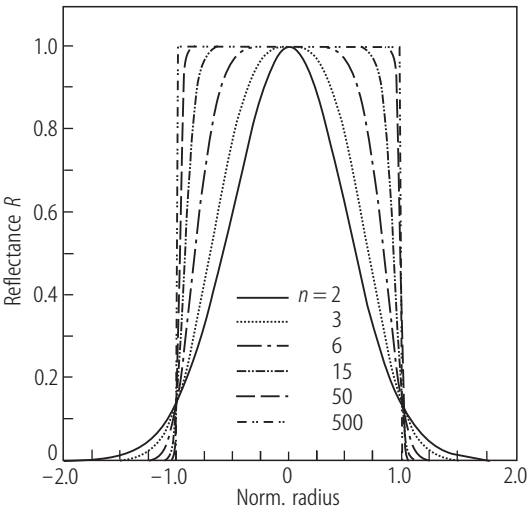

Fig. 8.1.43. Super-Gaussian reflectivity profiles for different indices n as a function of the radius.

reflectivity is chosen lower than 100%. However, in order to maximize the fill factor, steeper profiles are preferred since the mode with its correspondingly steeper slopes can then be better adapted to the active medium. From 1985 to 1994 much effort was spent to develop coating techniques for generating Variable-Reflectivity Mirrors (VRM) exhibiting Gaussian, super-Gaussian (Fig. 8.1.43), and parabolic reflectivity profiles [85Lav, 88DeS1, 89Emi, 90Pie, 93Dup, 93Pie, 94Bos3, 94Bos2, 94Bos1].

The VRMs most commonly used exhibit a *super-Gaussian reflectivity profile* which in circular symmetry reads:

$$R(r) = R_0 \exp\left[-2\left(\frac{r}{w}\right)^n\right] \tag{8.1.79}$$

with

R_0 : center reflectivity,
w : profile radius,
n : super-Gaussian index,
r : radial coordinate.

The super-Gaussian index n determines the shape of the reflectivity profile. For $n = 2$ the profile is Gaussian and with increasing n the slopes become steeper until the hard-edge profile is approached in the limit $n \to \infty$ (Fig. 8.1.43). The mode properties can be evaluated by using the stationary condition for the electric field. The corresponding intensity profile is given by

$$I(r) = I_0 \exp\left[-2\left(\frac{r}{w_M}\right)^n\right] \tag{8.1.80}$$

with

$$w_M = w\,(M^n - 1)^{1/n}\,, \quad M > 1\,. \tag{8.1.81}$$

The total loss factor per round trip reads:

$$V = \gamma\gamma^* = \frac{R_0}{M^2}\,. \tag{8.1.82}$$

Thus, the intensity distribution at the output coupler inside the resonator is also super-Gaussian with a beam radius w_M. The intensity profile of the near field can be obtained by multiplying

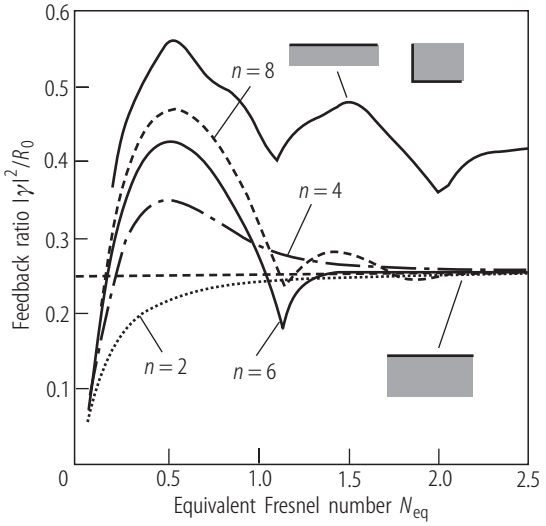

Fig. 8.1.44. Calculated loss factor per round trip of the lowest-loss mode ($l = 0$) as a function of the equivalent Fresnel number for circularly symmetric unstable resonators with magnification $M = 2$ using different super-Gaussian indices n [92Bow].

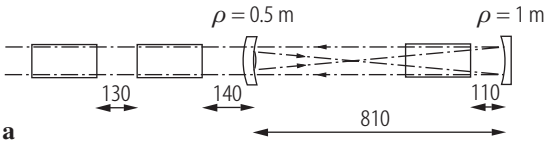

a

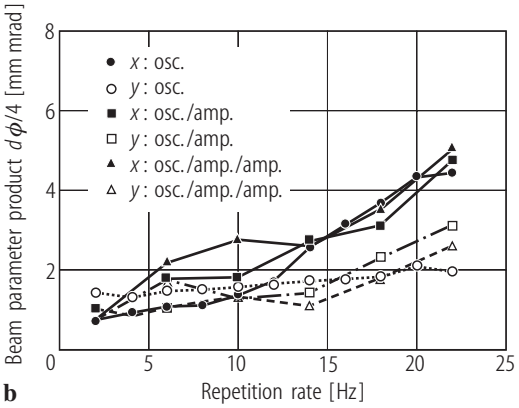

b

Fig. 8.1.45. Measured beam parameter products $d\,\Phi/4$ (d: beam width, Φ: full angle of divergence, both defined via 86.5% power content) in the x- (width) and the y-direction (height) for a 2.3 kW Nd:YAG slab laser system with one oscillator slab and two amplifier slabs of dimensions $7 \times 26 \times 179$ mm^3. The unstable resonator comprises a VRM with profile radii of 2 mm and 7 mm in the x- and y-direction, respectively. Total pump energy: 3,400 J; pulse length: 4 ms. Data are shown for one (osc.), two (osc./amp.) and three slabs (osc./amp./amp.) [93Hod3] (© OSA 1993).

(8.1.80) with the intensity transmission $1 - R(r)$ of the VRM. In this approach the loss factor per round trip is the same for all super-Gaussian indices and equal to the geometrical loss factor! This result can be verified if diffraction integrals are used to propagate the field inside the resonator (Fig. 8.1.44). Only for low equivalent Fresnel numbers can the beam propagation not be described by geometrical optics.

Owing to their excellent beam qualities, unstable resonators with variable-reflectivity mirrors have found application in both gas and solid-state lasers. VRMs are commercially available for a variety of laser wavelengths ranging from the visible to the infrared at 10.6 μm. In solid-state lasers, these resonators are mostly applied to low to medium power Q-switch systems [88Sne, 88Lav], but successful operation in free-running lasers with output powers in the kW range has also been reported [92Mag, 93Hod1, 93Hod2, 93Hod3, 94Bos2] (Fig. 8.1.45). If a flat-topped intensity distribution in the near field is required (e.g. for efficient filling of amplifier stages), the center reflectivity and the reflectivity profile can be used as design parameters. In order to attain optimum filling of the active medium by the laser mode an optimization of the reflectivity profile is required.

Since the adaptation of the beam width to the width of the active medium is easier to accomplish if the mode exhibits steep slopes, super-Gaussian profiles with high index n provide better means to maximize the output power. For an unstable resonator with a Gaussian VRM, a complete filling of the active medium will generate side lobes in the far field. However, for super-Gaussian profiles with $n > 2$, the super-Gaussian field distributions at the output coupler are not eigensolutions of the paraxial wave-equation. The intensity distributions inside the resonator, therefore, will change when the field propagates inside the resonator. This may result in ripples and hot spots. The same statement holds for the field transmitted through the VRM.

8.1.6.5 Applications of unstable resonators

The main advantage of unstable resonators is the adaptation of the beam radius inside the resonator by changing the mirror radius a. Since single-transverse-mode operation is not linked to the size of the mirror, as is the case for stable resonators, beam qualities close to the diffraction limit can be attained even for gain media with very large cross sections. In contrast to stable resonators, a high mode volume and a high beam quality can be realized simultaneously. Unfortunately, there are several drawbacks which limit the application of unstable resonators.

First of all, the power content in the side lobes of the far field might cause problems in specific applications. In order to minimize the power content in the side lobes the magnification has to be chosen as high as possible. This, however, requires an active medium with a high gain. It therefore makes no sense to use an unstable resonator in a HeNe laser, since the gain is too low to obtain a good laser efficiency. Secondly, the output power of unstable resonators generally is 20% ... 30% lower as compared to a stable resonator in multimode operation (Fig. 8.1.46). This is due to a lower fill factor in combination with additional diffraction losses induced by the rim of the active medium. If one is more interested in the output power than in attaining an excellent beam quality, it is therefore more advantageous to use a stable resonator in multimode operation. This preference of multimode stable resonators is also due to their easier alignment and their lower sensitivity to mirror misalignment.

Unstable resonators have found application in high-power CO_2 lasers [69Kru, 71Loc, 72Fre, 73Wis, 77Isa, 88Coo] and excimer lasers [79Rea, 85Iza, 88Lit], both of which generally exhibit a high gain and a large cross section of the active medium. Unstable resonators are also used in pulsed solid-state rod lasers [76Ewa, 77Her, 80Giu, 86Har, 86Upp1, 87Apa, 88Sne, 89Par, 90Hod1, 90Hod2, 90Hod3, 90Yas, 92Hod1, 91Mag, 92Mag, 93Hod1, 93Hod2, 94Bos2, 94Bur]. Unfortunately, the thermal lensing of the solid-state laser materials deteriorates the beam quality and makes beam handling quite difficult. In addition, unstable resonators are sensitive to aberrations of the thermal

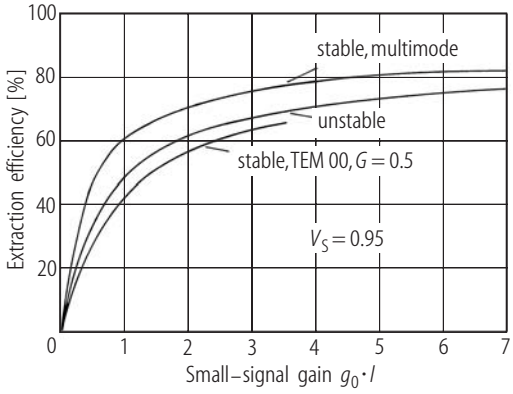

Fig. 8.1.46. Maximum extraction efficiency as a function of the small-signal gain for different resonators. Calculation based on diffraction integrals in combination with rate equations [97Hod].

lens resulting in a deterioration of the beam quality in high-power solid-state lasers. It is for these reasons that most applications of unstable resonators for solid-state rod lasers are limited to low-power Q-switch systems and free-running systems with less than 100 W average power. Higher power and good beam quality can be realized with zig-zag lasers due to the first-order compensation of the thermal lens. Unfortunately, the zig-zag slab geometry is too complicated to be considered a reasonable choice for a commercial product. The utilization of unstable resonators in diode lasers [89Ruf], dye lasers [95Cha], and free-electron lasers [84Moo, 86Skl, 87Skl] has also been reported.

8.1.7 Output power of stable resonators

8.1.7.1 Calculation of the output power of stable resonators

In the resonator model used (Fig. 8.1.47) it is assumed that both the forward-traveling beam with intensity $I^+(z)$ and the backward-traveling beam with intensity $I^-(z)$ cover the same area of the active medium. The complete overlap of the two counterpropagating beams is characteristic for stable resonators. During a round trip the intensity is decreased due to diffraction losses (loss factors $V_1 \ldots V_4$), scattering, and absorption inside the medium (loss factor V_S), and by output coupling. In steady-state operation, these losses are compensated by the amplification process characterized by the small-signal gain coefficient g_0.

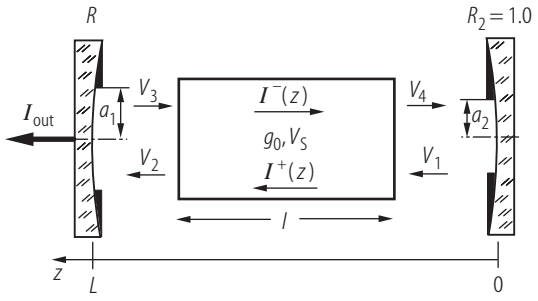

Fig. 8.1.47. Resonator model used for the calculation of the output power.

The next assumption we make is that no spatial hole burning is present meaning that at any plane inside the medium the intensity $I(z)$ is given by the sum of the two intensities $I^+(z)$ and $I^-(z)$. This is a reasonable approach for most lasers since the effect of spatial hole burning on the output power is smoothed out by atomic motion (gas lasers), energy migration, or axial multimode operation (solid-state lasers). However, in single-axial-mode solid-state or liquid dye lasers, spatial hole burning has an impact on the output power (it is lower by up to 30%). In these cases a realistic model for the output power requires the incorporation of the interference between the two counterpropagating fields resulting in the intensity profile

$$I(z) = I^+(z) + I^-(z) - 2\sqrt{I^+(z)I^-(z)}\,\cos[2kz] \tag{8.1.83}$$

with k being the wave number inside the medium. Without spatial hole burning, the differential equations for the intensities read [86Sie, 88Mil, 78Rig]:

$$\frac{\mathrm{d}I^{\pm}(z)}{\mathrm{d}z} = \pm\left[\frac{g_0}{\left(1+\frac{I^+(z)+I^-(z)}{I_S}\right)^X} - \alpha_0\right] I^{\pm}(z)\,, \tag{8.1.84}$$

where g_0 is the small-signal gain coefficient, I_S is the saturation intensity, α_0 is the loss coefficient, and X is equal to 1.0 (0.5) for homogeneous (inhomogeneous) broadening.

Equation (8.1.84) can be solved analytically if we assume that the intensity sum is constant with $I^+(z) + I^-(z) = 2I$. The mean intensity I now represents the intensity of the beam traveling towards the output coupling mirror. Equation (8.1.84) then yields for the factor GV_S by which the intensity is amplified in a transit through the medium

$$GV_S = \exp\left[\frac{g_0\ell}{(1+\frac{2I}{I_S})^X}\right]\exp\left[-\alpha_0\ell\right] \ . \tag{8.1.85}$$

By using the steady-state condition

$$G^2 R V_S^2 V_1 V_2 V_3 V_4 = 1 \tag{8.1.86}$$

the intensity I is found to be

$$I = \frac{I_S}{2}\left[\left(\frac{g_0\ell}{\left|\ln\sqrt{RV_S^2V_1V_2V_3V_4}\right|}\right)^{1/X} - 1\right] \ . \tag{8.1.87}$$

If the cross-sectional area of the beam is A_b ($= \pi\, a_1^2$ in Fig. 8.1.47), the output power is given by

$$P_{out} = A_b I(1-R)V_2 = A_b I_S \frac{(1-R)V_2}{2\left(\left|\ln\sqrt{RV_S^2V}\right|\right)^{1/X}}\left[(g_0\ell)^{1/X} - \left(\left|\ln\sqrt{RV_S^2V}\right|\right)^{1/X}\right] \tag{8.1.88}$$

with the round trip diffraction loss factor $V = V_1V_2V_3V_4$.

This expression for the output power of stable resonators can be used to a very good approximation, if the output coupling is low (high reflectance R). In this case the sum of the two intensities inside the medium is almost constant as a numerically calculated example in Fig. 8.1.48 indicates. For lower reflectances, the z-dependence of the intensities has to be taken into account by solving the differential equation (8.1.84) using the boundary conditions at the mirrors. Unfortunately, the solution can only be found numerically due to the homogeneously distributed loss (loss coefficient α_0) inside the medium [78Rig, 80Eim, 80Sch]. However, for homogeneously broadened lasers ($X = 1$) it is possible to derive an analytical solution by setting α_0 equal to zero in (8.1.84) and taking into account the loss by multiplying the intensity at the high-reflecting mirror with the loss factor $V_S^2 = \exp[-2\alpha_0 l]$. This method provides an analytical expression for the output power that is very close to the numerical solution (the difference is less than 0.5%). After a lengthy calculation the final expression reads [88Hod]:

$$P_{out} = A_b I_S \ \frac{(1-R)V_2}{1 - RV_2V_3 + \sqrt{RV}\,(1/(V_1V_2V_S) - V_S)}\left[g_0\ell - \left|\ln\sqrt{RV_S^2V}\right|\right] \tag{8.1.89}$$

with

$$V = V_1V_2V_3V_4 \ .$$

A comparison with (8.1.88) indicates that the z-dependence of the gain leads to a change in the fraction. For high reflectances R both equations provide similar output powers. Without lack of generality, we combine all losses into one and consider a resonator that exhibits a loss factor per transit V_S. Equation (8.1.89) then reads:

$$P_{out} = A_b I_S \ \frac{1-R}{1-R+\sqrt{R}\,(1/V_S - V_S)}\left[g_0\ell - \left|\ln\sqrt{RV_S^2}\right|\right] \ . \tag{8.1.90}$$

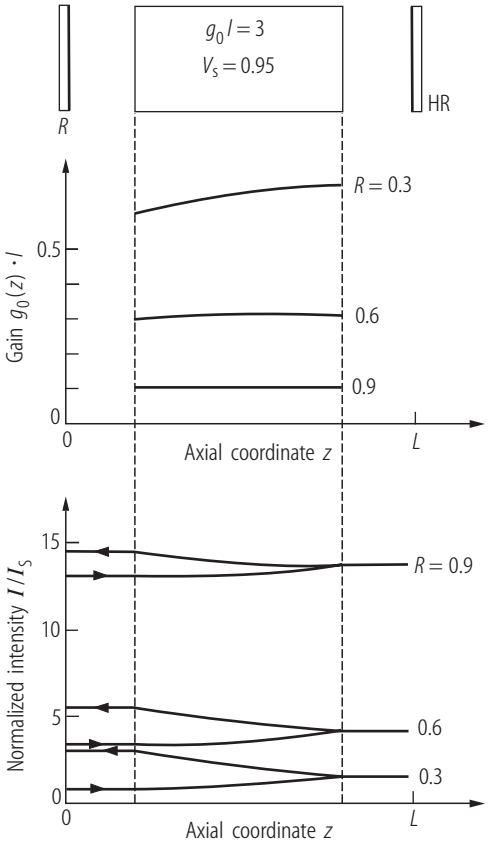

Fig. 8.1.48. Gain coefficient g_0 and normalized intensity I/I_S as a function of the axial coordinate z for different reflectances R of the output coupler, calculated with (8.1.84) ($g_0 l = 1.5$, $\alpha_0 l = 0.053$, no diffraction losses).

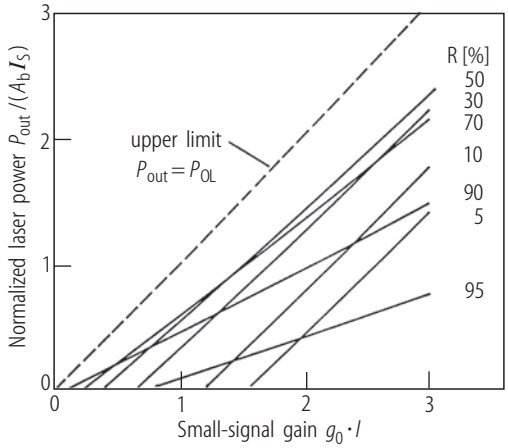

Fig. 8.1.49. Normalized laser power $P_{\text{out}}/(A_{\text{b}} I_{\text{S}})$ as a function of the small-signal gain $g_0 l$ for different reflectances of the output coupler according to (8.1.90) assuming a loss per transit of 5% ($V_{\text{S}} = 0.95$).

Figure 8.1.49 presents the normalized output power $P_{\text{out}}/(A_{\text{b}} I_{\text{S}})$ as a function of the small-signal gain $g_0 l$ which for most laser materials is proportional to the pump power. Starting at the threshold small-signal gain $(g_0 \ell)_{\text{th}} = |\ln(\sqrt{R} V_{\text{S}})|$ the power increases linearly with the small-signal gain and the slope of the curve becomes steeper as the reflectance R of the output coupler is decreased. The output power cannot exceed the power P_{OL} that is available in the medium in the form of inversion, with

$$P_{\text{OL}} = A I_{\text{S}} g_0 \ell = \eta_{\text{excit}} P_{\text{electr}} \tag{8.1.91}$$

with

A : cross-sectional area of the medium,
η_{excit} : excitation efficiency,
P_{electr} : electrical pump power.

Only if the laser resonator exhibits no losses ($V_{\mathrm{S}} = 1.0$ and $R \to 1.0$ in (8.1.90)) and the laser beam fills the whole medium ($A_{\mathrm{b}} = A$) can all the available power P_{OL} be extracted from the active medium (broken line in Fig. 8.1.49). Note that (8.1.91) holds only for homogeneously broadened lasers. For inhomogeneous line broadening, the available power is a function of the laser intensity due to the broadening of the homogeneous line width.

The slope of the output power with respect to the electrical pump power is referred to as the slope efficiency η_{slope} with

$$\eta_{\mathrm{slope}} = \frac{\mathrm{d}P_{\mathrm{out}}}{\mathrm{d}P_{\mathrm{electr}}} = \frac{\eta_{\mathrm{excit}}}{AI_{\mathrm{S}}} \frac{\mathrm{d}P_{\mathrm{out}}}{\mathrm{d}(g_0\ell)} = \eta_{\mathrm{excit}}\, \gamma\, \frac{1-R}{1-R+\sqrt{R}\,(1/V_{\mathrm{S}} - V_{\mathrm{S}})}\ , \tag{8.1.92}$$

where $\gamma = A_{\mathrm{b}}/A$ is the fill factor.

The slope efficiency is a function of the loss, the output coupling, and the ratio of the mode volume to the volume of the active medium. This ratio, called the fill factor, can be calculated in a first approach by using the beam diameter of the highest-order mode inside the active medium. If the active medium represents the only aperture inside the stable resonator and a high enough number of transverse modes are able to oscillate (let us say more than 10), the maximum fill factor of 1.0 is obtained. In fundamental-mode operation with the Gaussian beam radius w being adapted to the radius b of the active medium ($b \approx 1.3\, w$), the fill factor typically is around 0.9.

Unless the resonator exhibits no losses, only a fraction of the maximally available power P_{OL} can be extracted in the form of a laser beam. This fraction is referred to as the extraction efficiency η_{extr} of the resonator:

$$\eta_{\mathrm{extr}} = \frac{P_{\mathrm{out}}}{P_{\mathrm{OL}}} = \frac{1}{\eta_{\mathrm{excit}}} \frac{P_{\mathrm{out}}}{P_{\mathrm{electr}}}\ . \tag{8.1.93}$$

The total efficiency of the laser resonator is given by:

$$\eta_{\mathrm{tot}} = \frac{P_{\mathrm{out}}}{P_{\mathrm{electr}}} = \eta_{\mathrm{excit}}\eta_{\mathrm{extr}}\ . \tag{8.1.94}$$

8.1.7.2 Optimum output coupling and maximum output power

If the reflectance of the output coupler is varied at a given small-signal gain or pump power, the output power exhibits a maximum at the optimum output coupling. This behavior is easy to understand considering the fact that the output power is zero at low reflectances (laser threshold is not reached) and at a reflectance of 100% (no power is coupled out of the resonator). Therefore, a maximum of the output power and the extraction efficiency must exist for a certain value of the output coupling. Going back to the approximate power formula (8.1.88) we can find the optimum reflectance R_{opt} and the maximum output power $P_{\mathrm{out,max}}$ by setting the derivative $\delta P_{\mathrm{out}}/\delta(\ln R)$ equal to zero. Again, we assume that the losses per transit are represented by the loss factor $V_{\mathrm{S}} = \exp[-\alpha_0 l]$, and we consequently set the diffraction loss factor V equal to 1.0. By using the approximation $1 - R \approx |\ln R|$, the following expressions are obtained [82Sve]:

8.1.7.2.1 Homogeneous line broadening

Maximum output power:

$$P_{\mathrm{out,max}} = A_{\mathrm{b}} I_{\mathrm{S}} \alpha_0 \ell \left[\sqrt{\frac{g_0 \ell}{\alpha_0 \ell}} - 1 \right]^2 = \left[\sqrt{\eta_{\mathrm{excit}} P_{\mathrm{electr}} A_{\mathrm{b}} / A} - \sqrt{A_{\mathrm{b}} I_{\mathrm{S}} \alpha_0 \ell} \right]^2 . \tag{8.1.95}$$

Maximum extraction efficiency:

$$\eta_{\mathrm{extr,max}} = \frac{\alpha_0 \ell}{g_0 \ell} \left[\sqrt{\frac{g_0 \ell}{\alpha_0 \ell}} - 1 \right]^2 . \tag{8.1.96}$$

Optimum output coupling:

$$\ln R_{\mathrm{opt}} = -2 \alpha_0 \ell \left[\sqrt{\frac{g_0 \ell}{\alpha_0 \ell}} - 1 \right] . \tag{8.1.97}$$

Although (8.1.88) is only an approximate expression for the output power, the extreme values given by (8.1.95)–(8.1.97) can, to a very good approximation, be used to optimize the power performance of a laser system. This can be easily verified in Fig. 8.1.50 in which the correct extreme values (found by solving numerically the differential equation (8.1.84)) are shown [80Sch]. Even for lasers with high small-signal gain ($g_0 l > 3$) and high loss ($\alpha_0 l > 0.1$), which require a low reflectance for optimum performance, the difference between the exact extreme values and the ones given by (8.1.96) and (8.1.97) is negligible. Note that the graph presented in Fig. 8.1.50 assumes a fill factor of $\gamma = A_{\mathrm{b}}/A = 1.0$. The optimum parameters for a given laser are represented by the intersecting point of the two curves with constant small-signal gain and constant loss. Again, we find that an extraction efficiency of 100% is only attainable if the laser exhibits no loss ($\alpha_0 l = 0$) and the output coupling is close to zero.

The losses have a less dramatic impact on the output power if the small-signal gain of the laser is high. This is why at the same average pump power, lasers provide a higher average output power in pulsed operation than in cw operation. For a repetition rate f and a pulse width Δt, the small-signal gain is higher by the factor $1/(f\Delta t)$ as compared to cw operation at the same average pump power. According to Fig. 8.1.50, the extraction efficiency is increased leading to a higher average output power. Furthermore, the extraction efficiency becomes less sensitive to changes in output coupling as Fig. 8.1.51 indicates. The realization of the optimum output coupling is thus much less critical than in a low-gain laser. Figure 8.1.52 presents experimental examples for output power and output energies as a function of the output coupling.

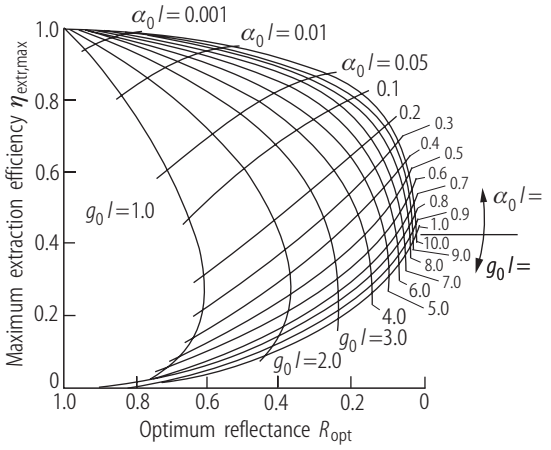

Fig. 8.1.50. Diagram for the determination of the optimum reflectance R_{opt} and the maximum extraction efficiency $\eta_{\mathrm{extr,max}}$ of homogeneously broadened lasers using the small-signal gain $g_0 l$ and the loss per transit $\alpha_0 l = -\ln V_{\mathrm{S}}$ (fill factor $\gamma = 1.0$) (after [80Sch]).

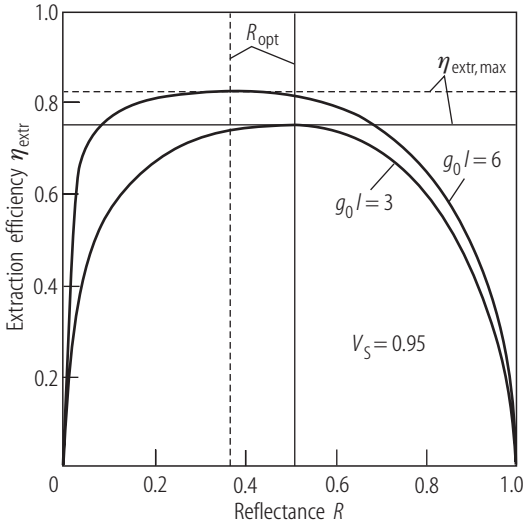

Fig. 8.1.51. Numerically calculated extraction efficiency as a function of the mirror reflectance R for high small-signal gains. The horizontal and vertical lines mark the analytical values given by (8.1.96) and (8.1.97). Loss factor per transit: $V_S = 0.95$.

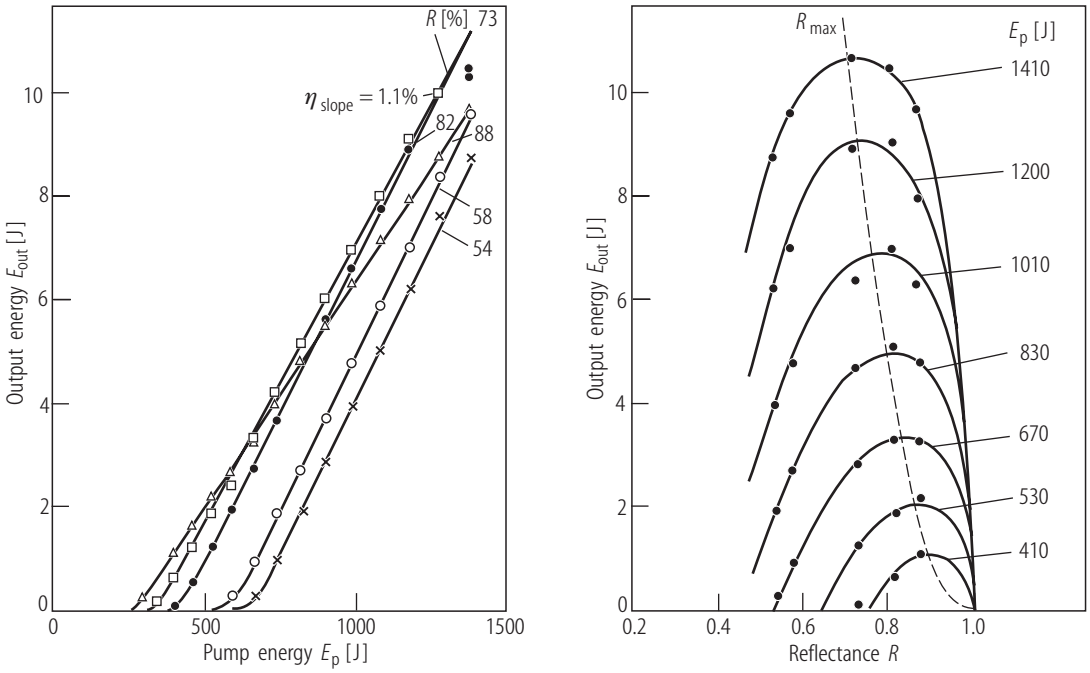

Fig. 8.1.52. Measured output energy per pulse of Nd:YAG lasers as a function of the pump energy E_p and the output-coupling reflectance R [97Hod]. The lines represent interpolations.

Expression (8.1.89) can be used to calculate the output power of a stable resonator if the small-signal gain, the losses, and the fill factor of the resonator are known. The experimental determination of the gain and the loss is easy to accomplish (e.g. Findlay-Clay analysis). The determination of the fill factor, however, is more difficult if only a small number of transverse modes is considered. In multimode operation the fill factor can, to a good approximation, be calculated by using the cross-sectional area of the aperture. If the aperture with radius a is located at the active medium with radius b, the fill factor is given by

$$\gamma = \frac{\pi a^2}{\pi b^2} \,. \tag{8.1.98}$$

If the aperture is not close to the medium, the beam propagation inside the resonator can be used to determine the equivalent aperture radius inside the medium. In order to obtain the correct output power with (8.1.89), the diffraction loss per transit in multimode operation has to be incorporated into the loss factors $V_1 \ldots V_4$.

8.1.7.2.2 Inhomogeneous line broadening

Maximum output power:

$$P_{\text{out,max}} = A_\text{b} I_\text{S} \, \frac{|\ln R|^2}{\alpha_0 \ell + \ln \sqrt{R}} \, . \tag{8.1.99}$$

Optimum output coupling:

$$\left[\alpha_0 \ell - \ln \sqrt{R_\text{opt}}\right]^3 = (g_0 \ell)^2 \left[\alpha_0 \ell + \ln \sqrt{R_\text{opt}}\right] \, . \tag{8.1.100}$$

Note that the output power (8.1.99) is always positive since (8.1.100) implies that $\alpha_0 \ell + \ln \sqrt{R}$ is greater than zero. The output power refers to the power of one single axial mode, and the small-signal gain is generated only by those inverted atoms whose resonance frequencies lie within the homogeneous linewidth around the axial-mode frequency. In order to obtain the total output power the contributions of the other axial modes have to be added. Again, these expressions are only valid for high mirror reflectances.

8.1.8 Thermal lensing in solid-state lasers

In solid-state lasers the active medium exhibits the properties of a thermally induced lens when the material is pumped. The refractive power is brought about by a combination of heat generation due to absorption of pump and laser radiation and the flow of heat to the outer periphery due to cooling [70Koe, 70Fos, 87Met]. For a laser rod this leads to a temperature distribution which is parabolic with respect to the radial position r if the thermal conductivity is constant and the medium is illuminated homogeneously by the excitation source. This results in a similar radial dependence of the index of refraction:

$$n(r) = n_0 (1 - \gamma r^2) \, , \tag{8.1.101}$$

where n_0 is the index of refraction at the center. To a first approximation, the refractive power D of a rod of length l is given by

$$D = 2 \gamma n_0 \ell \, . \tag{8.1.102}$$

The refractive power is proportional to the pump power and inversely proportional to the pumped area A:

$$D = \frac{\alpha}{A} \, P_\text{pump} \, . \tag{8.1.103}$$

The proportionality constant α, referred to as the thermal lensing coefficient, is a figure of merit for the thermal properties of a laser material (Table 8.1.1).

Table 8.1.1. Thermal-lensing coefficients of solid-state laser rods and the corresponding refractive powers at 1 kW of pump power for a rod diameter of 10 mm. For flashlamp-pumped lasers, the pump power refers to the electrical power into the flashlamps. In the case of diode-pumping, the pump power is the optical pump power absorbed by the laser medium. The range of the thermal-lensing coefficient is generated by different pump conditions and variations in crystal quality and doping concentration.

Material	α [mm/kW]	D [m^{-1}]
Flashlamp-pumped:		
Nd:YAG	0.021 ... 0.030	0.27 ... 0.38
Nd:glass	0.15 ... 0.19	1.91 ... 2.42
Nd:YAP	0.037 ... 0.069	0.47 ... 0.88
Nd:YLF	-0.003[a]; 0.0014[b]	-0.048; 0.018
Diode-pumped at 808 nm:		
Nd:YAG	0.1 ... 0.15	1.27 ... 1.91
Nd:YVO_4	0.09 ... 0.14	1.14 ... 1.78
Nd:YLF	-0.015[a]; 0.008[b]	-0.24; 0.09

[a] σ-polarized at $\lambda = 1053$ nm.
[b] π-polarized at $\lambda = 1047$ nm.

8.1.8.1 Fundamental-mode operation

In order to determine the propagation of the Gaussian beam (fundamental mode) inside the resonator, the concept of the equivalent g-parameters is applied [65Kog, 75Loe, 79Iff, 81Kor, 86Mag, 86Web, 87Mag, 93Hod4]. An optical resonator with an internal thermal lens (lens resonator) exhibits the same Gaussian beam radii at the mirrors as the equivalent empty resonator with the equivalent g-parameters g_i^* and the equivalent resonator length L^* (Fig. 8.1.53) with

$$g_i^* = g_i - Dd_j(1 - d_i/\rho_i) \; , \quad i, j = 1, 2 \; ; \quad i \neq j \; , \tag{8.1.104}$$

$$g_i = 1 - (d_1 + d_2)/\rho_i \; , \tag{8.1.105}$$

$$L^* = d_1 + d_2 - Dd_1d_2 \; . \tag{8.1.106}$$

Note that the term $d_1 + d_2$ is the effective resonator length L_{eff} of the resonator, which means that we could replace the thick lens by a thin lens with d_1, d_2 being the distances to the two mirrors. The resulting ray-transfer matrix for a transit between the mirrors would be identical. By using the equivalent resonator parameters, the Gaussian beam propagation inside the resonator can be calculated by making use of the fact that the mirror surfaces are surfaces of constant phase for the beam.

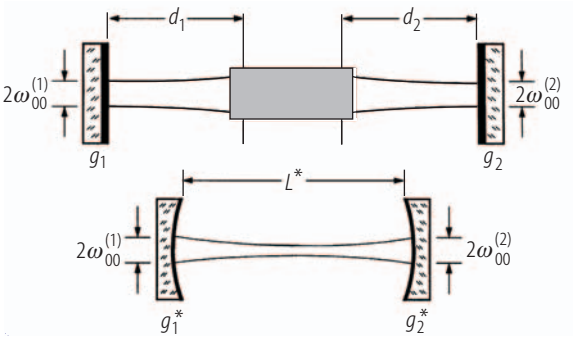

Fig. 8.1.53. The lens resonator and its equivalent resonator. Both resonators exhibit identical Gaussian beam radii at the mirrors, but the beam propagation is different.

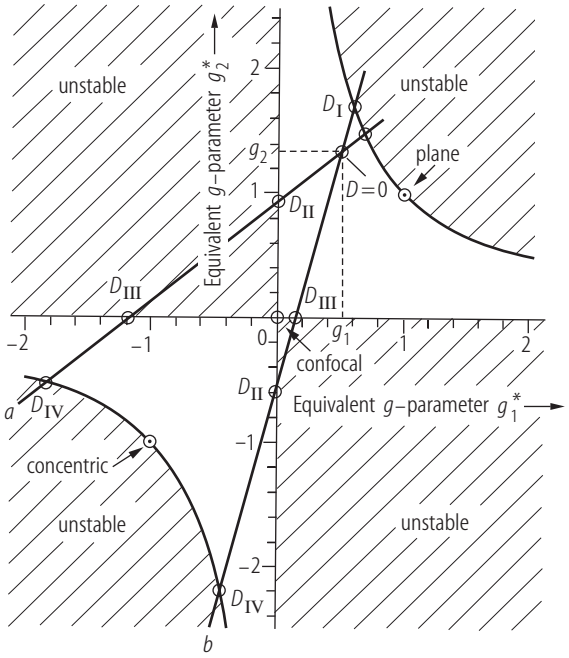

Fig. 8.1.54. Lens resonators with one internal lens move along straight lines through the equivalent g-diagram as the refractive power D is increased. The slope of the lines depends on the position of the medium and on the mirror curvatures.

The properties of a lens resonator can be visualized in the equivalent g-diagram (Fig. 8.1.54). The resonator starts at the point (g_1, g_2) and moves along a straight line through the diagram with increasing refractive power. In general, the lens resonator passes through stable zones and unstable zones. A lens resonator is called stable for $0 < g_1^* g_2^* < 1$ and unstable for $|g_1^* g_2^*| > 1$. Four characteristic refractive powers exist at which the resonator intersects stability limits (see Fig. 8.1.54):

(a) $g_1^* g_2^* = 1$ and $g_1^* > 0$:
$$D_{\mathrm{I}} = -\frac{1}{\rho_1 - d_1} - \frac{1}{\rho_2 - d_2} , \tag{8.1.107}$$

(b) $g_1^* = 0$:
$$D_{\mathrm{II}} = -\frac{1}{\rho_1 - d_1} + \frac{1}{d_2} , \tag{8.1.108}$$

(c) $g_2^* = 0$:
$$D_{\mathrm{III}} = \frac{1}{d_1} - \frac{1}{\rho_2 - d_2} , \tag{8.1.109}$$

(d) $g_1^* g_2^* = 1$ and $g_1^* < 0$:
$$D_{\mathrm{IV}} = \frac{1}{d_1} + \frac{1}{d_2} . \tag{8.1.110}$$

If $|D_{\mathrm{II}}| < |D_{\mathrm{III}}|$ holds, the lens resonator passes through the upper left unstable region in Fig. 8.1.54. Resonators with the property $D_{\mathrm{II}} = D_{\mathrm{III}}$ can reach the origin of the diagram (confocal resonator). These resonators are characterized by the condition

$$\frac{d_2}{d_1} = \sqrt{\frac{g_1}{g_2}} , \tag{8.1.111}$$

which for a resonator with two identical mirrors means that the lens is located in the center. By using the equivalent resonator parameters, the beam propagation of the Gaussian beam with wavelength λ inside the lens resonator can be derived from the known beam radii at the resonator mirrors. The Gaussian beam exhibits two waists whose position and radius are a function of the refractive power. The following relations hold for the resonator shown in Fig. 8.1.55:

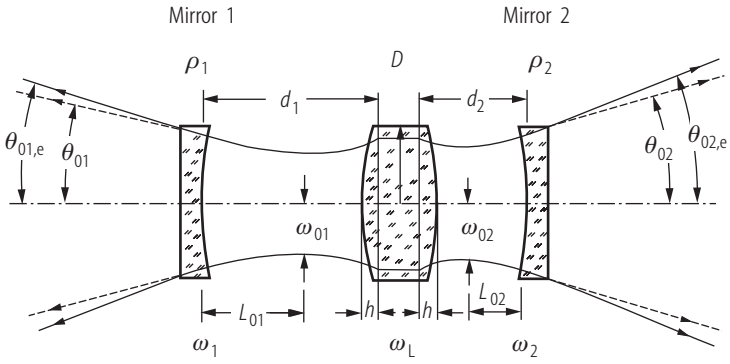

Fig. 8.1.55. Propagation of the Gaussian beam in a lens resonator.

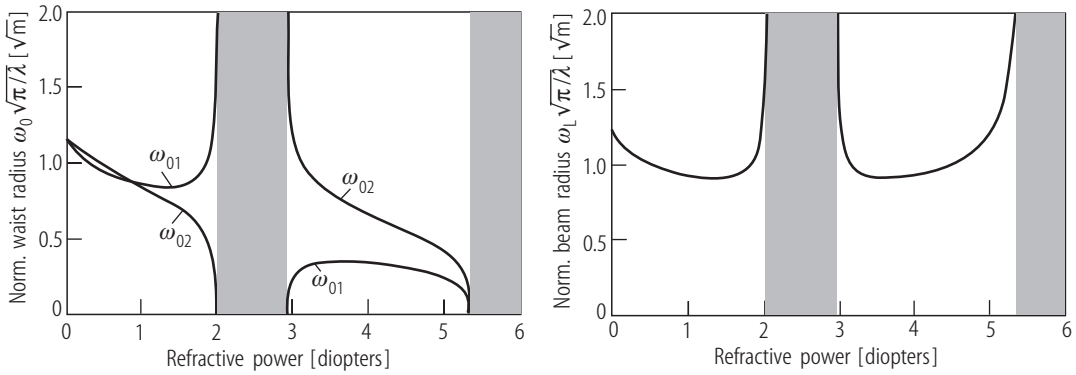

Fig. 8.1.56. Gaussian beam radius in the active medium w_L, waist radii w_{0i}, and half angles of divergence θ_{0i} as a function of the refractive power of the thermal lens ($\rho_1 = \infty$, $\rho_2 = 3$ m, $d_1 = 0.3$ m, $d_2 = 0.5$ m).

Beam radius at mirror i:
$$w_i^2 = \frac{\lambda L^*}{\pi}\sqrt{\frac{g_j^*}{g_i^*(1-g_1^*g_2^*)}}\,. \tag{8.1.112}$$

Waist radii:
$$w_{0i}^2 = \frac{\lambda L^*}{\pi}\frac{\sqrt{g_1^*g_2^*(1-g_1^*g_2^*)}}{g_j^*(L^*/\rho_i)^2 + g_i^*(1-g_1^*g_2^*)}\,. \tag{8.1.113}$$

Beam radius at the principal planes:
$$w_L^2 = w_1^2\left[\left(1-\frac{d_1}{\rho_1}\right)^2 + \left(\frac{d_1}{L^*}\right)^2\frac{g_1^*(1-g_1^*g_2^*)}{g_2^*}\right]\,. \tag{8.1.114}$$

Location of beam waist i:
$$L_{0i} = L^*\frac{g_j^*L^*/\rho_i}{g_j^*(L^*/\rho_i)^2 + g_i^*(1-g_1^*g_2^*)}\,. \tag{8.1.115}$$

Half angle of divergence:
$$\theta_{0i} = \frac{\lambda}{\pi\, w_{0i}}\,. \tag{8.1.116}$$

The beam waist i is located to the left of mirror i for $L_{0i} < 0$ and to the right for $L_{0i} > 0$. In Fig. 8.1.55 L_{01} is positive and L_{02} is negative. Due to the thermal lens, the two angles of divergence are different because the two waist radii are not equal. The beam parameter product is the same on both sides of the resonator and is given by:

$$w_{01}\theta_{01} = w_{02}\theta_{02} = \frac{\lambda}{\pi}\,. \tag{8.1.117}$$

Unfortunately, the above shown expressions are too complicated to discuss in general; therefore, it is necessary to calculate the beam parameters to get a feeling for the beam characteristics. Figure 8.1.56 presents the beam radius in the medium w_L and the waist radii w_{0i} as a function of the refractive power. The stability limits are characterized by infinite or zero waist radii whereby

the divergence exhibits a reciprocal behavior since the beam parameter product has to remain constant.

Typically, the Gaussian beam radius inside the medium exhibits a minimum which is approximately located in the middle of each stable zone. If ΔD denotes the range of the refractive power within which the resonator is stable, the minimum Gaussian beam radius in the medium reads:

$$w_{\mathrm{L,min}}^2 = \frac{4\lambda}{k\pi\,\Delta D}\,. \tag{8.1.118}$$

with $k = 1$ if the confocal point $g_1^* = g_2^* = 0$ is passed and $k = 2$ elsewhere. For the resonator in Fig. 8.1.56 and a wavelength of $\lambda = 1.064$ μm, we get a minimum beam radius of 0.531 mm in both stable zones. The Gaussian beam radius in the medium stays relatively constant over a range of the refractive power that covers about 90% of the stable zone. Within this range fundamental-mode operation can be attained if an aperture is placed in front of the medium whereby the aperture radius a needs to be adapted to the Gaussian beam radius:

$$a = 1.3\,w_{\mathrm{L,min}}\,. \tag{8.1.119}$$

8.1.8.2 Transverse multimode operation

If no aperture is used inside the resonator, all transverse modes will oscillate whose beam radii are smaller than the radius b of the active medium [81Kor]. The number of oscillating modes is equivalent to the beam quality factor M^2 and can, to a good approximation, be calculated with

$$M^2 = \left(\frac{b}{w_{\mathrm{L}}}\right)^2, \tag{8.1.120}$$

where w_{L} is the Gaussian beam radius at the principal planes of the thermal lens. Since the Gaussian beam radius changes with increasing thermal lens power, the beam quality of multimode lasers is a function of the pump power. Insertion of (8.1.114) into (8.1.120) yields for the beam propagation factor:

$$M^2 = \frac{\pi\,b^2}{\lambda L^*}\sqrt{\frac{g_1^*(1-g_1^*g_2^*)}{g_2^*}}\left[\left(1-\frac{d_1}{\rho_1}\right)^2 + \left(\frac{d_1}{L^*}\right)^2\frac{g_1^*(1-g_1^*g_2^*)}{g_2^*}\right]^{-1}. \tag{8.1.121}$$

This expression is only valid for $M^2 > 1$ since lower beam quality factors make no physical sense. At the stability limits the beam quality factor approaches $M^2 = 1$. For rectangular active media, the radius b has to be replaced with half the side length. In general, the beam quality factors in the x- and the y-direction are different. With the knowledge of the beam quality factor (8.1.121), the waist radii w_{mi} and the half angles of divergence θ_{mi} can be calculated using (8.1.113) and (8.1.116):

$$w_{mi} = \sqrt{M^2}\,w_{0i}\,, \quad \theta_{mi} = \sqrt{M^2}\,\theta_{0i} \tag{8.1.122}$$

with the beam parameter product

$$w\theta = w_{m1}\theta_{m1} = w_{m2}\theta_{m2} = M^2\,\frac{\lambda}{\pi}\,. \tag{8.1.123}$$

The locations of the waist radii are the same as for the Gaussian beam. It is interesting to note that the beam parameter product in multimode operation does not depend on the laser wavelength λ, since the beam quality factor scales with $1/\lambda$. We thus cannot improve the focusability by using

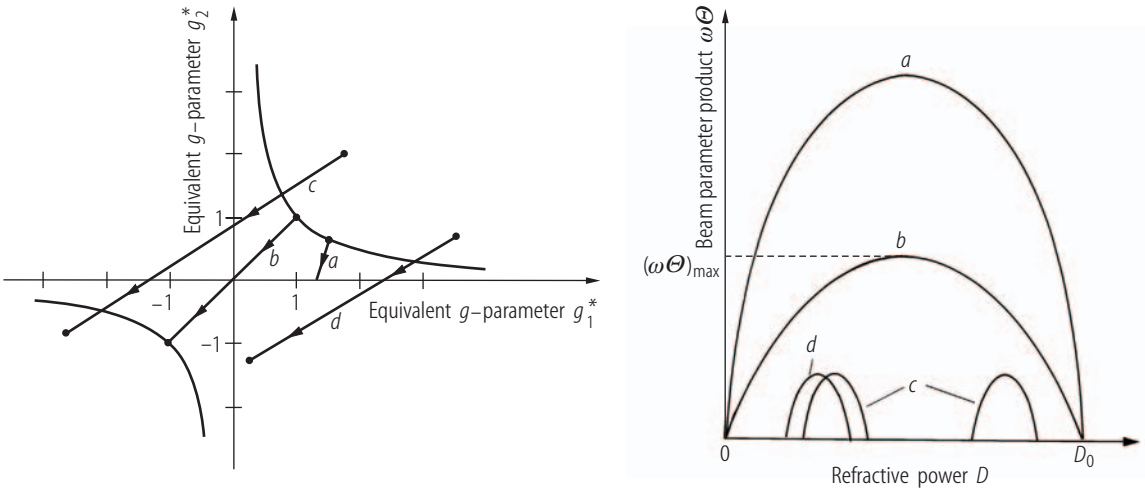

Fig. 8.1.57. Qualitative dependence of the beam parameter product $w\theta$ on the refractive power D for four resonators. In all resonators the thermal-lens power is varied from 0 to D_0. Due to the different resonator geometries, the resonators pass through differently sized stable zones in the equivalent stability diagram [93Hod4].

a smaller wavelength. The beam parameter product of the Gaussian beam becomes lower with a smaller wavelength but the smaller Gaussian beam radius also leads to the oscillation of a higher number of transverse modes. Therefore, the beam parameter product remains constant. As previously discussed, the Gaussian beam radius in the medium exhibits a minimum near the center of a stable zone. Therefore, the multimode beam parameter product has a maximum at this point and decreases towards both stability limits. The maximum beam parameter product can be calculated by inserting (8.1.118) into (8.1.120):

$$(w\theta)_{\max} = k\,\frac{b^2\Delta D}{4} \tag{8.1.124}$$

with

$k = 1$, if the origin of the equivalent stability diagram is passed,
$k = 2$, otherwise,
ΔD: refractive power range within which the lens resonator is stable.

Figure 8.1.57 presents the qualitative dependence of the beam parameter product on the refractive power for four different resonators with different refractive power ranges ΔD and their different paths in the equivalent g-diagram. For stable resonators, the output power drops drastically as the resonators penetrate into unstable zones due to increasing diffraction losses at the active medium. The impetus of (8.1.124) is a relationship between maximum beam parameter product and range of pump power ΔP_{pump} within which the resonator is stable:

$$(w\theta)_{\max} = \frac{k}{4\pi}\,\alpha\,\Delta P_{\text{pump}}\,. \tag{8.1.125}$$

Since the output power is proportional to the pump power, the maximum beam parameter product is proportional to the maximum output power (provided that the resonator is stable at all pump powers). For diode-pumped Nd:YAG lasers, the maximum TEM_{00}-mode output power is about 30 W, higher output powers can only be achieved in multimode operation, with a typical increase in M^2 of 10 per 50 W of output power.

8.1.9 Ring resonators

8.1.9.1 General properties of ring resonators

In linear resonators, the interference of the two counterpropagating waves generates a modulation of the intensity along the optical axis. The intracavity intensity distribution of an axial mode of order q outside the active medium reads:

$$I(z) = I_0 \left[1 - \frac{2R}{1+R^2} \cos(2\pi q z/L)\right] , \tag{8.1.126}$$

where L is the resonator length, R is the reflectance of the output-coupling mirror, and z is the coordinate along the optical axis, starting at a mirror surface. The intensity minima exhibit a periodicity of half the wavelength of the axial mode $\lambda_q = 2L/q$. Due to gain saturation this results in a modulated axial gain distribution, referred to as *spatial hole burning*. The modulation frequency depends on the axial mode order.

In homogeneously broadened lasers, only one axial mode should theoretically be observed since the axial mode with the highest small-signal gain has access to the whole gain and will suppress the oscillation of adjacent modes. However, the spatial hole burning induces an axial mode competition because different modes are amplified in different areas of the gain medium. This may lead to multimode oscillation with random jumping between axial modes. Furthermore, the lower extraction efficiency at the intensity minima results in a decreased output power unless a high number of axial modes can coexist. In order to attain single-axial-mode operation with a high output power it is necessary to prevent spatial hole burning. In the twisted-mode resonator, this is accomplished by using orthogonal polarization states for the back- and the forth-traveling wave [65Evt]. Another way to generate a homogeneous intensity profile along the optical axis is unidirectional beam propagation in a ring resonator [63Tan, 65Her, 69Ana, 71Sch, 72Clo, 72Kog, 79Jar] (Fig. 8.1.58). By using an optical diode inside the resonator the axial modes are forced to propagate in one direction only. The optical diode can be realized with a retardation plate, a Faraday rotator, or a combination of both such that the losses generated at polarizers are higher for one propagation direction (Fig. 8.1.59). In asymmetric unstable ring resonators, the different propagation characteristics associated with the oppositely traveling waves can be used to generate unidirectional beam propagation [73Fre, 73Poz, 74Fre] (e.g. by inserting apertures). Unidirectionality can also be attained by means of an external feedback mirror which reflects the reverse oscillation [65Her]. However, with an external mirror, the ratio of the forward to the reverse power is only on the order of 1000:1 because a fraction of the power always has to propagate in the reverse direction to make this scheme work [74Fre]. A twisted-mode technique has to be applied in addition to suppress the residual hole burning.

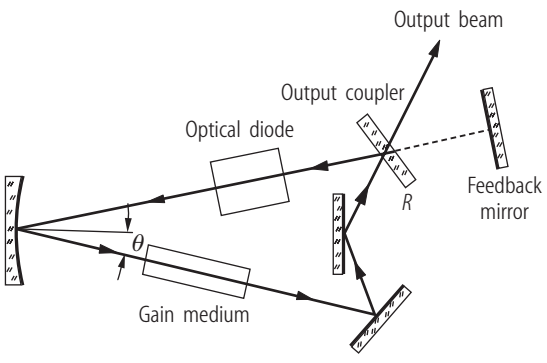

Fig. 8.1.58. Concept of a stable ring resonator. Unidirectionality can be achieved with an intracavity optical diode or an external mirror that feeds back the wave having the wrong propagation direction.

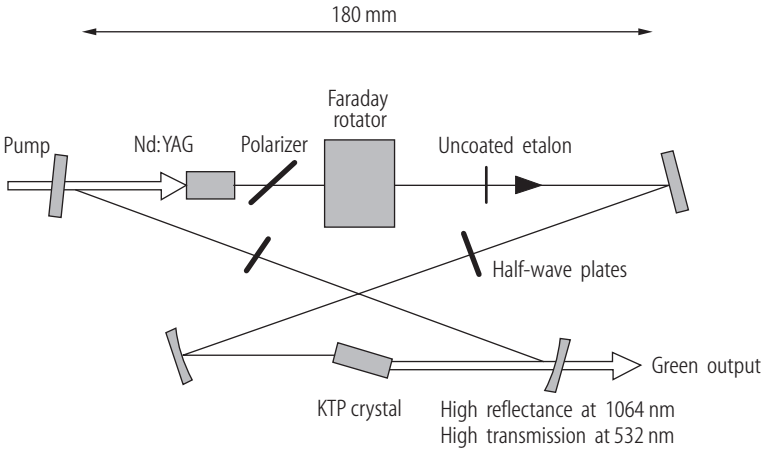

Fig. 8.1.59. A cw diode-laser-pumped Nd:YAG laser with intracavity second harmonic generation. The Faraday rotator produces a polarization rotation by 7.5° at 1.064 μm. The same rotation is provided by the two half-wave plates. The two rotations add in one direction generating losses at the polarizer. In the intended propagation direction, the two rotations cancel. The laser provides an output power of 3.1 W at 532 nm in single-mode operation for a pump power of 14 W at 808 nm [96Mar] (© OSA 1996).

In general, ring resonators are set up with more than three mirrors to decrease the astigmatism induced by the mirror tilt. For an angle of incidence of θ, a curved mirror exhibits a focal length of $f \cos\theta$ in the tangential plane (paper plane in Fig. 8.1.58) and a focal length of $f/\cos\theta$ in the sagittal plane, where f is the focal length at normal incidence. By using more mirrors or a z-fold geometry (Fig. 8.1.59) the angles of incidence can be kept small. It is also possible to compensate the astigmatism by using special resonator designs [72Kog].

Similar to linear stable resonators, the Gaussian beam propagation in stable ring resonators can be evaluated by means of the Gaussian ABCD law. In order to include the astigmatism, four-dimensional ray-transfer matrices have to be used. Starting at an arbitrary plane, the ray-transfer matrix for a round trip is calculated. The Q^{-1}-matrix of the elliptical Gaussian beam is a solution of the generalized ABCD law:

$$\mathsf{Q}^{-1} = (\mathsf{C} + \mathsf{D}\mathsf{Q}^{-1})(\mathsf{A} + \mathsf{B}\mathsf{Q}^{-1})^{-1} , \tag{8.1.127}$$

where A, B, C, D are the 2×2 submatrices of the 4×4 ray-transfer matrix, and the superscript -1 denotes the inverse matrix. The matrix Q^{-1} contains the q-parameters of the Gaussian beam at the reference plane:

$$\mathsf{Q}^{-1} = \begin{pmatrix} 1/q_{xx} & 1/q_{xy} \\ 1/q_{yx} & 1/q_{yy} \end{pmatrix} . \tag{8.1.128}$$

For planar ring resonators, the Gaussian beam is simple astigmatic, which means that the nondiagonal elements of Q^{-1} are zero. In this case, the beam propagation can be calculated separately for the sagittal plane and the tangential plane by using the common 2×2 round-trip matrices. The ring resonator is stable in one plane if the following relation holds for the elements of the corresponding ray-transfer matrix:

$$|\mathsf{A} + \mathsf{D}| < 2 . \tag{8.1.129}$$

In contrast to a linear resonator, the mirror surfaces of a ring resonator generally do not match the phasefronts of the Gaussian beam. The Gaussian beam waist is always located at that plane at which the round-trip matrix exhibits equal diagonal elements ($A = D$).

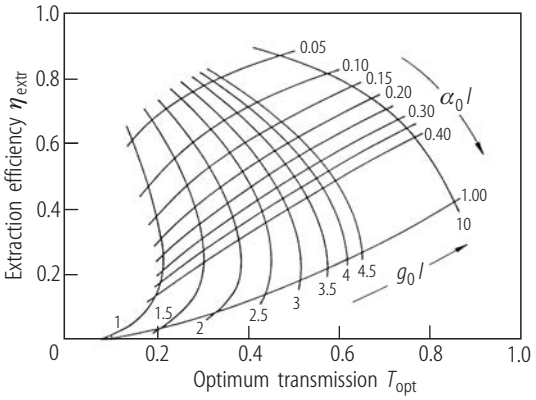

Fig. 8.1.60. Calculated maximum extraction efficiency of ring resonators with a homogeneously broadened active medium as a function of the optimum transmission of the output-coupling mirror. The curve parameters are the small-signal gain $g_0 l$ and the loss per transit $\alpha_0 l$.

The unidirectionality in ring resonators generates different beam properties as compared to those of linear resonators. First, the electric-field distribution is reproduced after one transit. Therefore, the frequency separation of the axial modes is twice that of linear resonators with length L:

$$\Delta\nu = \frac{c}{L} \,. \tag{8.1.130}$$

Secondly, light amplification takes place only once per round trip. The steady-state condition for ring oscillators, therefore, reads:

$$GRV_S = 1 \,, \tag{8.1.131}$$

where G is the gain factor, R is the reflectance of the output coupler, and V_S is the loss factor ($= 1 - \text{loss}$) per transit. For a linear resonator, the corresponding steady-state condition is given by $G\sqrt{R}\,V_S = 1$. In order to reach laser threshold for the same output coupling, the pump power in a ring resonator has to be higher than in a linear resonator by a factor γ, with

$$\gamma = \frac{\ln(RV_S)}{\ln(\sqrt{R}\,V_S)} \,. \tag{8.1.132}$$

This implies that at identical pump powers, the output power of a ring oscillator is lower. However, this is only due to the fact that the ring resonator is overcoupled when the linear resonator exhibits optimum output coupling. If the output coupling is adjusted, the ring resonator provides the same maximum output power as the linear resonator. Maximum extraction efficiencies of ring resonators and the corresponding optimum output-coupling transmission are visualized in Fig. 8.1.60 for different values of the small-signal gain and the loss per transit. The maximum extraction efficiencies of ring resonators are identical to those attainable with linear resonators (see Fig. 8.1.50).

8.1.9.2 Unstable ring resonators

The ring geometry can also be applied to unstable resonator schemes as shown in Fig. 8.1.61 [69Ana, 73Poz, 73Fre, 74Fre]. Preferably, an asymmetric confocal resonator set-up is chosen which means that the transfer matrix for one round trip, starting at the output coupler, is different for the two propagation directions. The main advantage associated with the asymmetric design is a greater design flexibility. The flat mirrors in the collimated-beam path can be placed arbitrarily

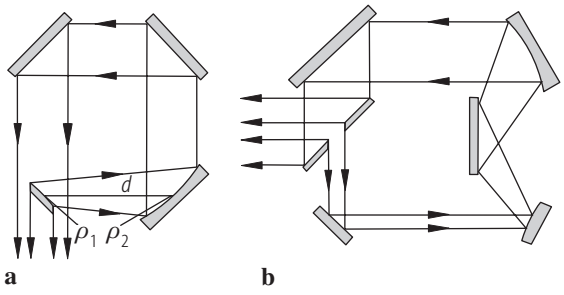

Fig. 8.1.61. Asymmetric confocal unstable ring resonators. (**a**) confined output coupler, (**b**) scraper.

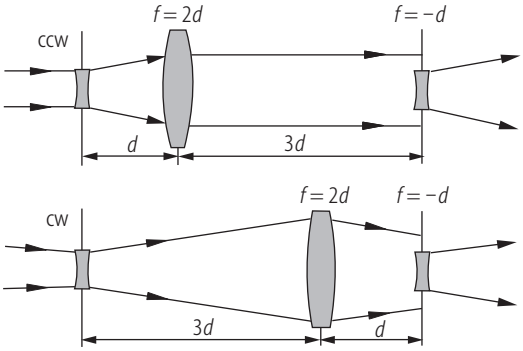

Fig. 8.1.62. Beam propagation of the diverging waves in a confocal unstable ring resonator with magnification $M = 2$. The resonator shown in Fig. 8.1.61a is represented as a lens waveguide. A mirror with radius of curvature ρ is replaced by a lens with focal length $f = \rho/2$. In the counterclockwise direction (ccw), the output beam (beam portion missing the biconcave lens) is collimated.

without changing the magnification of the resonator. This enables one to incorporate several active media or to increase the round-trip time. Unfortunately, there is no discrimination against one propagation direction since the forward and the reverse wave exhibit the same output-coupling losses. However, the different propagation characteristics of the two waves can be used to suppress one of the waves. The round trips in the resonator of Fig. 8.1.61a in the clockwise (cw) and the counterclockwise (ccw) directions are equivalent to the transits in the lens waveguides depicted in Fig. 8.1.62. In both directions, we can find two self-reproducing spherical wavefronts, referred to as the diverging wave and the converging wave. The converging wave in unstable resonators is generally not observed since it will transform itself into a diverging wave after a few round trips. Therefore, the asymmetric unstable ring resonator supports two diverging waves having opposite propagation directions. Although the asymmetry generates different propagation characteristics for these counterpropagating waves they exhibit the same magnification. The different propagation characteristics can be used to discriminate against one direction.

Unstable ring resonators have been realized in CO_2 lasers [69Ana, 73Fre, 73Poz, 74Fre, 88Cal], dye lasers [76Mar, 80Tes], and solid-state lasers [86Upp1]. The effect of thermal lensing on the performance of unstable solid-state ring lasers is discussed in [86Upp2]. A discrimination against the reverse-traveling wave can be achieved by locating the active medium where the forward-traveling mode exhibits the larger mode volume [73Fre, 74Fre]. By using this technique, power ratios of 20:1 have been observed. Unidirectional operation, however, requires intracavity apertures to discriminate against the reverse oscillation. Alternatively, an optical feedback of the reverse-traveling wave can be applied such that the radius of curvature and the propagation direction of the forward-traveling wave is matched. In [74Fre], the use of a feedback mirror increased the ratio of the forward to the reverse power of a CO_2 laser from 16:1 to 1,600:1.

The suppression of the reverse-traveling wave by means of intracavity apertures is very effective in negative-branch unstable ring resonators [78Pax, 83Oug, 84Skl, 86Upp1]. Both the forward and the reverse wave exhibit an intracavity focus at different locations in the resonator (Fig. 8.1.63a). By placing an aperture in the focus plane of the forward-traveling wave, a high loss is generated for the reverse-traveling wave. The aperture can also serve as a spatial filter to filter out phase distortions

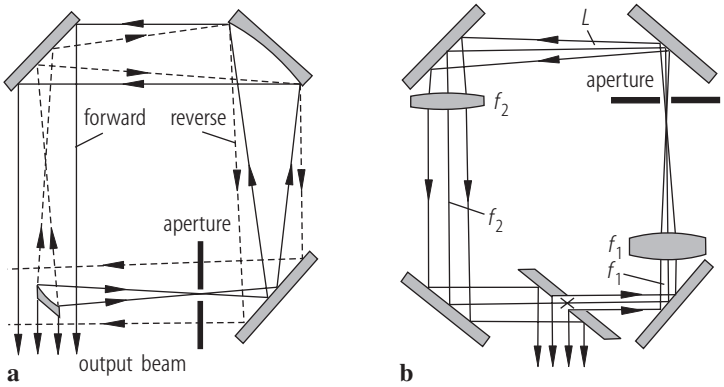

Fig. 8.1.63. Beam propagation in negative-branch unstable ring resonators. (**a**) Fourier-transform resonator with the forward wave (solid line) and the reverse wave (broken line), (**b**) Forward-traveling wave in a self-imaging unstable resonator with $L = f_1 + f_2$. The reverse-traveling wave (not shown) is collimated in the upper section and it exhibits a focus at the scraper.

and smooth out the spatial intensity distribution. A special negative-branch ring resonator is the self-imaging unstable resonator as depicted in Fig. 8.1.63b [78Pax, 84Skl].

8.1.9.3 Nonplanar ring resonators

In planar ring resonators with the mirrors tilted around the same axis, s-polarized and p-polarized light represent the polarization eigenstates for a resonator round trip. The phase shifts induced at the mirror generally are different for the two polarizations, but no mixing between s- and p-polarization can occur. This is different in the nonplanar geometry in which the mirrors are tilted around different axes. The polarization properties of nonplanar rings can be evaluated by using the Jones matrix formalism [86Sie, 89Kin, 89Nil]. It can be shown that nonplanar ring resonators act as polarization rotators having left-circularly and right-circularly polarized light as the eigenstates. When combined with a Faraday rotator and a polarizing element, the rotation of the polarization plane at the mirrors can be used to discriminate against one propagation direction.

A widely used laser employing this technique is the diode-laser-pumped monolithic nonplanar Nd:YAG ring oscillator [85Kan, 87Kan, 88Nil, 88Sch, 89Nil, 91Che] (Fig. 8.1.64). A dc magnetic field is used to generate a polarization rotation via the Faraday effect (Verdet constant of YAG: 103°/(Tm)). In the clockwise direction, the rotation of the polarization plane caused by the internal reflections at the surfaces B, C, and D and the Faraday rotation cancel, giving an s-polarized eigenmode at the front surface. In the opposite direction, the two rotations add, resulting in an elliptically polarized eigenmode. The reflectance R of the front surface (Fresnel-reflection) is slightly higher for the s-polarization than for the p-polarization. The wave in the ccw direction, therefore, has a higher laser threshold and is suppressed. The suppression also works if the two polarization rotations do not cancel in the clockwise direction. In [88Sch], the 17° rotation caused by the internal

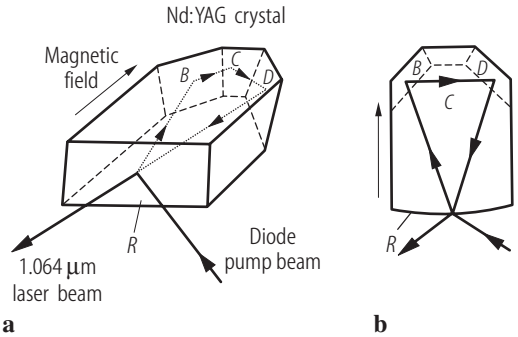

Fig. 8.1.64. Beam propagation in a diode-pumped monolithic non-planar Nd:YAG ring oscillator. The size of the crystal is $11 \times 7 \times 3$ mm^3. (**a**) side view, (**b**) top view [88Sch] (© AT Fachverlag 1988).

reflections was superimposed by a 0.6° Faraday rotation. At the coated front surface of the crystal, the resulting difference in polarization for the two propagation directions generated a loss difference of 0.6%. This small difference was sufficient to realize unidirectional single-mode operation with an output power of 100 mW (400 mW optical pump power).

Due to the mechanical stability and the highly stable pump source, the monolithic Nd:YAG ring resonator has the capability of providing single-mode operation with narrow linewidths and high output stability. Commercial lasers provide output powers in the 100 mW range with linewidths of less than 3 kHz and an rms stability of better than 0.05%. With active frequency stabilization, very narrow linewidths down to the sub-Hertz range have been achieved [88Nil, 89Day, 92Day].

8.1.10 Waveguide resonators

8.1.10.1 Motivation

In all high-power laser systems, the removal of the heat generated by the pump process is crucial for efficient operation. In sealed-off gas lasers, the gas is mainly cooled through heat conduction to the walls of the tube, a process which is not very efficient if cylindrical discharge tubes are used. The cooling can be approved by at least one order of magnitude if a discharge geometry is used that exhibits a larger ratio of the cooling surface to the discharge volume. Besides the annular geometry, the most promising concept pursued in the last decade is the slab waveguide laser, as depicted in Fig. 8.1.65. Heat removal in a slab laser scales inversely with the electrode separation d. Typical electrode distances for CO_2 slab waveguide lasers are between 1.5 mm and 2.5 mm. The discharge volume can be controlled via the cross-sectional area of the electrodes. This means that the output power of slab lasers is scaled by area rather than length as in conventional geometries.

Assuming a constant laser efficiency η_{tot} of 10%, the scaling law for the maximum achievable output power of a waveguide CO_2 laser per area of one electrode can be approximated by [91Now]:

$$P_{\mathrm{out,max}} = \frac{3}{d}\,\frac{W}{\mathrm{cm}^2}\,, \tag{8.1.133}$$

where the electrode distance d is given in mm. This expression holds only for distances d greater than 1.5 mm since smaller electrode gaps will decrease the laser efficiency due to an increase in diffraction losses and a decrease of the excitation efficiency. The small electrode separation puts a severe constraint on the resonator design. In the larger dimension an unstable resonator can

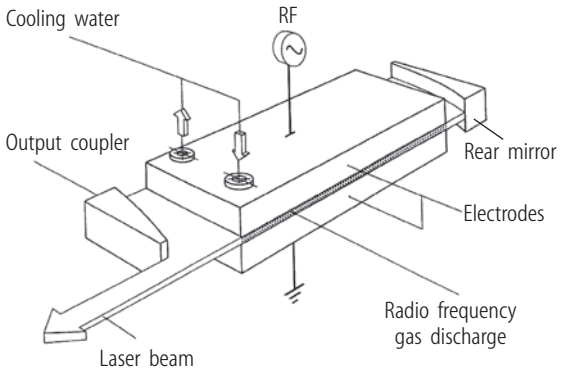

Fig. 8.1.65. CO_2 slab waveguide laser with unstable waveguide resonator and a RF excited gas discharge (RF frequencies between 50 and 100 MHz) [91Now] (© AT Fachverlag 1991). Electrode separations between 1.5 and 2.5 mm are used. The width and the length of the discharge regions typically are 4 ... 7 cm and 60 ... 100 cm, respectively. Electrode materials commonly used are aluminum and copper.

be utilized to achieve near-diffraction-limited beam quality. Unfortunately, in the perpendicular direction the small gap width in combination with the length of the electrodes makes it virtually impossible to propagate a Gaussian beam through the discharge region without touching the electrodes. A stable resonator used in this direction, therefore, will exhibit modes that are guided by the electrodes rather than modes that follow the laws of free-space propagation as in conventional open resonators. This resonator concept using guided-mode propagation is referred to as a waveguide resonator [64Mar, 76Laa, 87Hal]. Guided-mode propagation occurs if the Fresnel number of the waveguide $a^2/(\lambda L)$ is much lower than 1, where L is the length of the waveguide and $2a$ its diameter. Waveguide resonators comprise two external mirrors and the mode properties result from a combination of the mode properties of the waveguide itself and the mode discrimination that occurs due to the free-space propagation between the waveguide's ends and the resonator mirrors.

8.1.10.2 Eigenmodes of hollow rectangular waveguides

In waveguide lasers, the cross section of the waveguide is very large compared to the wavelength λ. It is thus justified to neglect terms of first order or higher order in λ/a and λ/b. With this approximation, the fields in the walls and at the wall surface vanish and the internal fields become transverse. The following electric fields $\boldsymbol{E}(x,y,z,t) = (E_x, E_y, E_z)$ and magnetic fields $\boldsymbol{H}(x,y,z,t) = (H_x, H_y, H_z)$ are obtained for the rectangular waveguide shown in Fig. 8.1.66, provided that the waveguide length is large compared to its width and its height [76Laa]. The y-polarized hybrid modes $E^y H^x_{mn}$ read:

$$E_x = E_z = 0\,, \quad H_y = H_z = 0\,,$$

$$E_y = \frac{1}{\sqrt{ab}}\,\exp[\mathrm{i}(\beta_{mn} z - \omega t)]\exp[-\alpha_{mn} z] \begin{bmatrix} \cos\left[\frac{m\pi x}{2a}\right] & \cos\left[\frac{n\pi y}{2b}\right] & m,n \text{ odd}, \\ \cos\left[\frac{m\pi x}{2a}\right] & \sin\left[\frac{n\pi y}{2b}\right] & m \text{ odd}, n \text{ even}, \\ \sin\left[\frac{m\pi x}{2a}\right] & \cos\left[\frac{n\pi y}{2b}\right] & m \text{ even}, n \text{ odd}, \\ \sin\left[\frac{m\pi x}{2a}\right] & \sin\left[\frac{n\pi y}{2b}\right] & m,n \text{ even}, \end{bmatrix},$$

$$H_x = -\sqrt{\frac{\varepsilon_0}{\mu_0}}\,E_y \tag{8.1.134}$$

where $\omega = 2\pi c_0/\lambda$ is the angular light frequency, ε_0 is the permittivity of free space, μ_0 is the permeability of free space, and m, n are integer numbers with $m, n \geq 1$. For $\lambda \ll a$ and $\lambda \ll b$, the propagation constants are given by:

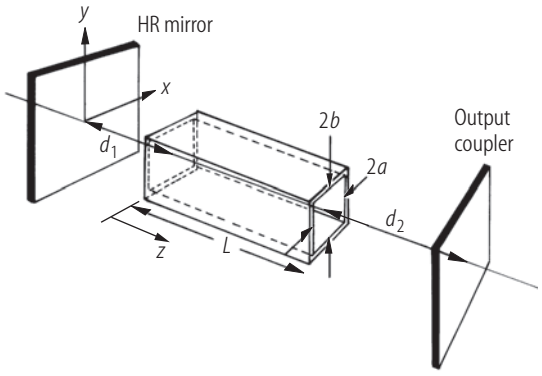

Fig. 8.1.66. A waveguide resonator with a hollow, rectangular waveguide.

$$\alpha_{mn} = \frac{\pi^2}{4k^2}\left[\frac{m^2}{a^3}\mathrm{Re}\left(\frac{1}{\sqrt{\varepsilon-1}}\right) + \frac{n^2}{b^3}\mathrm{Re}\left(\frac{\varepsilon}{\sqrt{\varepsilon-1}}\right)\right] , \tag{8.1.135}$$

$$\beta_{mn} = k\left[1 - \frac{\pi^2}{8k^2}\frac{m^2}{a^2}\left(1 - \frac{2}{ak}\mathrm{Im}\left(\frac{1}{\sqrt{\varepsilon-1}}\right)\right) - \frac{\pi^2}{8k^2}\frac{n^2}{b^2}\left(1 - \frac{2}{bk}\mathrm{Im}\left(\frac{\varepsilon}{\sqrt{\varepsilon-1}}\right)\right)\right] , \tag{8.1.136}$$

where $k = 2\pi/\lambda$ is the wave number and Re, Im denote the real part and the imaginary part of the expression in the bracket, respectively. These field distributions represent the eigenmodes if the following relations hold:

$$\frac{m\lambda}{4a} \ll 1 , \quad \frac{n\lambda}{4b} \ll 1 , \tag{8.1.137}$$

$$\frac{m\lambda}{4a} \ll \left|\sqrt{\varepsilon-1}\right| , \quad \frac{n\lambda}{4b} \ll \left|\frac{\sqrt{\varepsilon-1}}{\varepsilon}\right| . \tag{8.1.138}$$

Similar expressions are obtained for x-polarized hybrid modes $E^x H^y_{mn}$ [76Laa].

Both sets of hybrid modes (x- and y-polarized) are orthonormal:

$$\int_{-b}^{+b}\int_{-a}^{+a} E_{mn}E^*_{m'n'}\,\mathrm{d}x\,\mathrm{d}y = \delta_{mm'}\delta_{nn'}\exp[-2\alpha_{mn}z] , \tag{8.1.139}$$

where E_{mn} stands for E_y, E_x for y-polarized modes and x-polarized modes, respectively. The eigenmodes form a complete set and can thus be used as a basis set for a mode expansion. Any continuous field distribution $E(x, y)$ launched into the waveguide can be expanded in a linear combination of the waveguide eigenmodes. Each eigenmode can be described as a superposition of two plane waves being reflected off the waveguide walls at an angle θ_m:

$$\theta_m = \frac{m\lambda}{4a} . \tag{8.1.140}$$

For all waveguide modes, the intensity maxima can be understood as a result of constructive interference of the two plane waves (Fig. 8.1.67). Waves propagating at any other angles than the ones given by (8.1.140) do not generate a constant intensity distribution in the z-direction due to a varying phase shift between the waves. The waveguide eigenmodes are determined by the fact that each of the plane waves has to interfere constructively with the other wave after being reflected by the wall. The propagation angles for the fundamental waveguide mode ($m = 1$) of CO_2 lasers typically are between 1 and 3 mrad. We are thus dealing with reflection at grazing incidence.

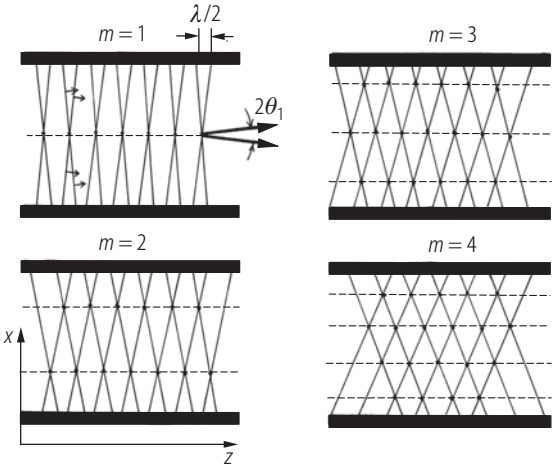

Fig. 8.1.67. The eigenmodes of a rectangular waveguide can be considered a superposition of two plane waves propagating at angles $\pm\theta_m$ to the z-axis. The horizontal, broken lines indicate the location of the intensity maxima. Note the phase difference of $\lambda/2$ between the two waves at the wall.

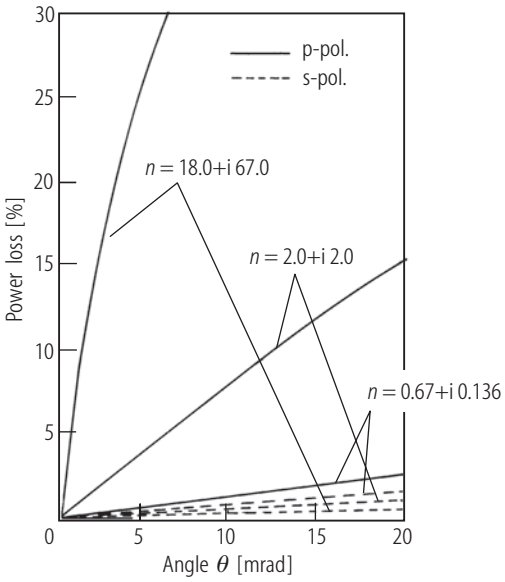

Fig. 8.1.68. Reflection of a plane wave at the interface of an absorbing medium. The power loss of p-polarized and s-polarized waves as a function of the angle θ between the wave vector and the surface is shown for different refractive indices n of the medium (calculation using Fresnel equations).

Table 8.1.2. Refractive indices and calculated absorption coefficients of the x-polarized (α_1^x) and the y-polarized (α_1^y) fundamental mode for different waveguide materials (one-dimensional waveguide in the x-direction with $a = 1$ mm and $\lambda = 10.6$ µm, using (8.1.135) and the corresponding equation for the x-polarized mode). The refractive indices $n = n_1 + \mathrm{i}\, n_2$ of the metals are from [95Paq] (extrapolated data). The refractive indices of the dielectrics are from [92Khe].

Material	n_1	n_2	α_1^x [1/mm]	α_1^y [1/mm]
Cu	15	63	1.054×10^{-4}	2.51×10^{-8}
Au	18	67	1.264×10^{-4}	2.63×10^{-8}
Al	28	95	1.966×10^{-4}	2.00×10^{-8}
Al_2O_3	0.67	0.136	2.238×10^{-6}	1.40×10^{-6}
BeO	0.64	0.59	4.688×10^{-6}	2.13×10^{-6}
SiO_2	1.9	0.73	1.506×10^{-5}	3.37×10^{-6}

An accurate treatment of the reflection at the interface of an absorbing medium reveals that at grazing incidence both p- and s-polarized waves experience a phase shift of π. Taking this phase shift into account, a zero phase shift between incoming wave 1 and the reflected wave 2 can only be realized at the angles θ_m. The absorption loss of waveguide modes can now be simply explained by applying the Fresnel equations for the reflection and absorption of light at the interface of an absorbing medium. For grazing incidence, the power loss due to absorption increases proportionally to the angle between the wave vector and the surface (Fig. 8.1.68).

In Table 8.1.2 refractive indices and calculated absorption coefficients of the x-polarized (α_1^x) and the y-polarized (α_1^y) fundamental mode for different waveguide materials are given.

Waveguide modes exhibit features that support high-power operation of a waveguide laser with diffraction-limited beam quality. The beam diameters of the transverse modes scale with the waveguide cross section. Therefore, all modes have access to the same gain region, generating a strong mode competition. In addition, due to the reflection losses, the active medium (waveguide) provides a transverse-mode discrimination proportional to m^2/a^3. Since higher-order modes exhibit higher absorption losses, only a limited number of transverse waveguide modes (let us say not more than 10) will oscillate in a waveguide laser. Since waveguide modes are not eigensolutions of free-space propagation, the mode of the waveguide resonator is a combination of several

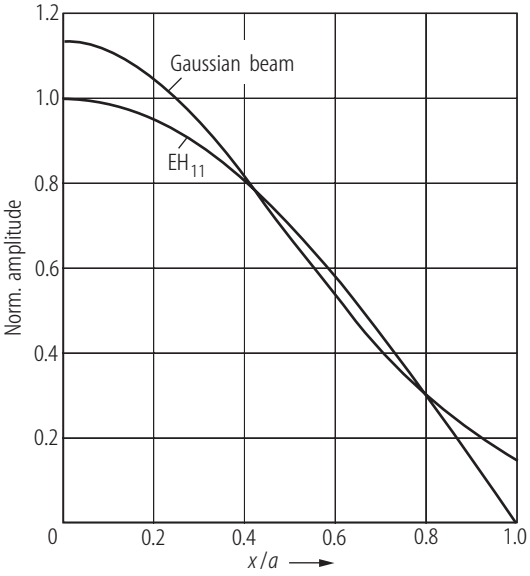

Fig. 8.1.69. Approximation of the field of the fundamental waveguide mode EH_{11} by a Gaussian beam with beam radius $w_0 = 0.703\ a$.

waveguide modes. In order to attain a diffraction-limited laser beam, the lowest-loss mode of the waveguide resonator should closely resemble the fundamental waveguide mode. The goal of waveguide resonator design, of course, is to attain a near-diffraction-limited output beam, preferably with properties similar to those of a Gaussian beam. Since the field distributions of the waveguide modes form a complete orthogonal set, the one-dimensional field distribution $E_m(x)$ of the m-th resonator mode at the end of the waveguide can be written as a linear combination of waveguide-mode field distributions $\Phi_n(x)$:

$$E_m(x) = \sum_{n=1}^{\infty} c_{mn} \Phi_n(x) \ , \tag{8.1.141}$$

where the c_{mn} are complex constants. The propagation of this field distribution to the mirror and back to the waveguide will generate higher losses for the high-order waveguide modes since they propagate at higher angles of divergence. The free-space propagation thus provides an additional waveguide-mode discrimination. By using appropriate mirror curvatures and mirror distances, it should, therefore, be possible to generate a lowest-loss resonator mode exhibiting most of its power in the fundamental waveguide mode. The fundamental waveguide mode EH_{11} can be approximated by a Gaussian beam with beam radius $w_0 = 0.703\ a$ resulting in a power overlap of about 98% (Fig. 8.1.69). This Gaussian beam could be similar to the fundamental resonator mode, for instance, if the waveguide end was imaged onto itself by means of the resonator mirror. Higher-order waveguide modes would be suppressed because they are coupled back into the waveguide less efficiently. The same statement holds for circular, hollow waveguides, whose mode properties can be found in [61Sni, 64Mar, 74Mar, 76Deg, 79Abr]. The eigenmodes of coaxial waveguides can be found in [93Ehr].

8.1.10.3 Properties of waveguide resonators

With the knowledge of the waveguide eigenmodes and their propagation constants, it is possible to evaluate the mode properties of the waveguide resonator itself. The general waveguide resonator consists of two mirrors with radii of curvature ρ_1 and ρ_2 positioned at a distance d_1 and d_2 from the waveguide ends (Fig. 8.1.70). The free-space propagation from the waveguide to the mirrors

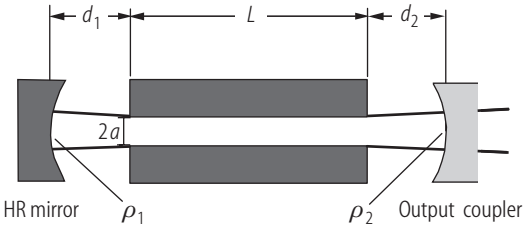

Fig. 8.1.70. Schematic of a waveguide resonator.

and back generates coupling losses for the waveguide modes. The goal of the waveguide resonator design is to find configurations that provide a fundamental resonator mode with low coupling losses and a good mode discrimination against higher-order modes.

8.1.10.3.1 Waveguide resonator configurations

Three different configurations can be distinguished: Case I, Case II, and Case III resonators.

8.1.10.3.1.1 Case I resonators

The resonator mirrors are placed close to the waveguide ends, at a distance of typically less than 10 times the waveguide dimension. The resonator modes can be closely approximated by the waveguide eigenmodes. All resonator modes experience a round-trip loss that is determined by the absorption loss $2\alpha L$. The mode discrimination is rather low and, depending on the small-signal gain, the output coupling, the type of line broadening, and the dimensions of the waveguide, the output beam will be a combination of several transverse waveguide modes. Assuming a refractive index of $n = 1$ of the gas, the resonance frequencies of the modes are determined by:

$$2\beta_{nm}L = q\ 2\pi\ , \tag{8.1.142}$$

where q is the axial mode order, L is the waveguide length, and β_{nm} is the propagation constant according to (8.1.136). In order to achieve fundamental-mode operation, it is necessary to choose the waveguide cross section a small so that higher-order modes cannot reach the laser threshold. Unfortunately, the coupling losses of the fundamental waveguide mode will increase too, resulting in a decrease in laser efficiency.

8.1.10.3.1.2 Case II resonators

The waveguide ends are imaged onto themselves by the resonator mirrors. Imaging requires a distance d_i of each mirror equal to its radius of curvature ρ_i. Each waveguide mode is imaged back onto itself and no coupling losses occur for infinite mirrors. However, the transverse mode discrimination is as poor as in true Case I resonators.

8.1.10.3.1.3 Case III resonators

In both, rectangular and cylindrical waveguides, the fundamental waveguide mode can be approximated by a Gaussian beam with 98% power overlap (Fig. 8.1.71). Propagation of the fundamental waveguide mode can be described by Gaussian beam propagation of a Gaussian beam with waist radius $w_0 = 0.703\ a$ (rectangular symmetry) or $w_0 = 0.6345\ a$ (circular waveguide). Given this assumption, the wavefront curvature of the mode at a distance z from the waveguide reads:

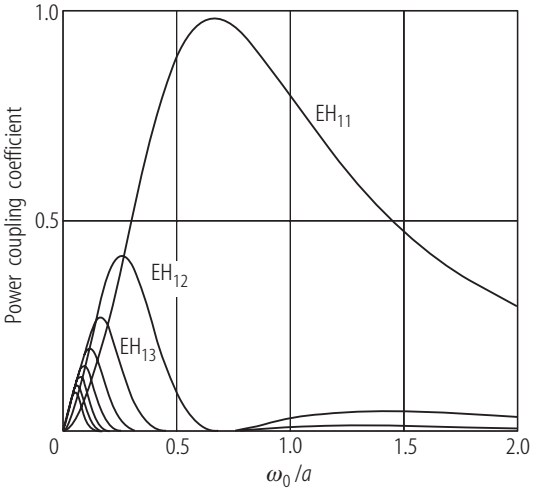

Fig. 8.1.71. Power coupling coefficients for the EH_{1m} modes of circular waveguides as a function of the ratio of the beam waist radius w_0 of the Gaussian beam to the guide radius a [92Jen] (© OSA 1992).

$$R(z) = 2z_0 \left[\frac{z}{z_0} + \frac{z_0}{z} \right] , \tag{8.1.143}$$

where $z_0 = \pi\, w_0^2/\lambda$ is the Rayleigh range. By choosing the mirror curvature ρ equal to $R(z)$ at the mirror position $d = z$, the beam propagation is reversed and the EH_{11} mode will be coupled back into the waveguide with low losses. This configuration combines low fundamental-mode loss and excellent transverse-mode discrimination since higher-order modes will not couple back efficiently. It is for this reason that most waveguide resonators investigated in the past were based on this principle. Numerical calculation of the coupling losses of the EH_{11} mode indicated that positioning the mirrors at $d = z_0$ with $\rho = 2z_0$ yields the lowest loss.

8.1.10.3.2 Calculated round-trip losses of the lowest-loss resonator mode

Calculated round-trip losses of the lowest-loss resonator mode as a function of d/ρ are presented in Fig. 8.1.72 for symmetric resonators and circular waveguides. The parameter of the curves is $\alpha = 2\pi\, a^2/(\lambda\rho)$. The meaning of this parameter and others shown in the graph shall be explained in the next paragraph. Case I and Case II resonators are given by $d/\rho = 0$ and $d/\rho = 1$, respectively.

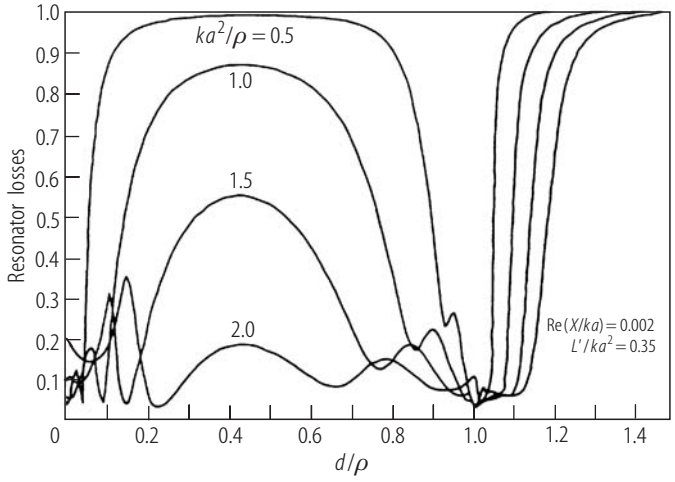

Fig. 8.1.72. Calculated round-trip loss (lowest-loss mode) for symmetric waveguide resonators with a circular waveguide of radius a and effective length L' as a function of the mirror distance-to-radius-of-curvature ratio d/ρ. The curve parameter is the inverse of the normalized mirror curvature $\rho/(ka^2)$; K is the wave number; the function X is explained in the text below. Both mirrors have a radius of curvature ρ and are located at a distance d from the adjacent waveguide end [90Alv] (© IEEE 1990).

Case III coupling with $d = z_0$ is equivalent to $\alpha = 2.41$ and $d/\rho = 0.5$. Although the curve with $\alpha = 2.41$ is not shown, it is obvious that Case III resonators provide similar low losses as the other two resonators. However, this graph indicates that low losses can also be realized with resonators that do not belong to one of the three resonator classes. These additional loss minima are a result of the interference between different waveguide modes. A realistic description of waveguide resonator properties generally requires the incorporation of multiple waveguide modes.

8.1.10.3.3 Mode properties of a general waveguide resonator

The mode properties of a general waveguide resonator are determined by seven independent parameters. For the free-space propagations, four independent parameters can be found in the phase term of the two Collins integrals. Those parameters are: ka^2/d_1, ka^2/d_2, d_1/ρ_1, and d_2/ρ_2. The independent parameters governing the waveguide propagation are contained in the propagation constant (8.1.135)/(8.1.136): L'/ka^2, L/ka^2, and Re $(1/\sqrt{\varepsilon - 1})/ka$. A generalized presentation of waveguide resonator properties, therefore, is a seven-dimensional problem. However, in most cases the effective length L' differs from the geometrical length L by no more than a few percent and we may skip L as a parameter. In both circular waveguides and one-dimensional rectangular waveguides, we are dealing with the following six independent, dimensionless parameters:

- the *effective length parameter*: $\dfrac{L'}{ka^2}$,
- the *distance parameters*: $\dfrac{d_1}{ka^2}$, $\dfrac{d_2}{ka^2}$,
- the *distance-curvature ratios*: $\dfrac{d_1}{\rho_1}$, $\dfrac{d_2}{\rho_2}$,
- the *waveguide loss parameter*: $\dfrac{\mathrm{Re}(X)}{ka}$ with $X = \begin{bmatrix} \varepsilon/\sqrt{\varepsilon - 1} \\ 1/\sqrt{\varepsilon - 1} \\ (\varepsilon + 1)/\sqrt{2(\varepsilon - 1)} \end{bmatrix}$ $\begin{matrix} \text{rect., } x\text{-pol. ,} \\ \text{rect., } y\text{-pol. ,} \\ \text{circular .} \end{matrix}$

In order to simplify the discussion, we focus on resonators with two flat mirrors. This restriction leaves us with four independent parameters. The properties of waveguide resonators with curved mirrors can be found in [72Abr, 73Deg, 85Hil].

8.1.10.4 Waveguide resonator mode and loss calculations

Since the waveguide modes and the free-space modes (Gauss-Laguerre polynomials in circular symmetry and Gauss-Hermite polynomials in rectangular symmetry) both form complete sets, they can be used as basis sets for the resonator modes [84Ger, 88Hil, 89Jac2]. In general, a limited number of functions (on the order of 10 waveguide modes and 50 free-space modes) from both sets are taken into account. This is mathematically not correct, but the truncation errors can be kept in the sub-percent range if only the first three lowest-loss resonator modes are considered. For simplicity we restrict the discussion to one-dimensional rectangular waveguides [88Hil, 89Jac2]. A similar treatment for circular waveguides can be found in [84Ger]. The field distribution $E_p(x)$ of the p-th resonator mode at the end of the waveguide is written as a linear combination of N waveguide eigenmode field distributions $\Phi_n(x)$ and as a linear combination of M free-space modes $\Psi_m(x)$. For the free-space modes we use Gauss-Hermite polynomials with the beam waist with radius w_0 located at the waveguide end. The Gaussian beam waist radius w_0 is preferably chosen in the range $0.6a < w_0 < 0.8a$.

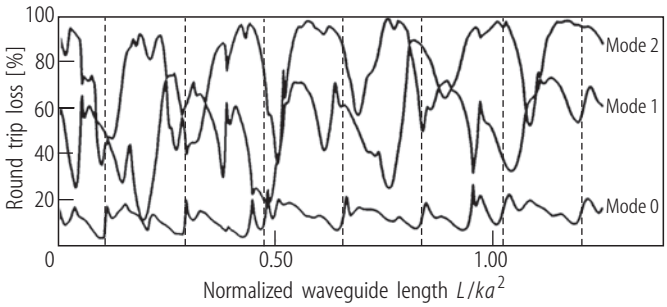

Fig. 8.1.73. Calculated resonator losses versus the effective-length parameter for the three lowest-loss modes of a symmetric waveguide resonator with flat mirrors (circular waveguide, $a = 1$ mm, $\lambda = 10.6$ μm, refractive index of the wall material: $n = 0.67 + \mathrm{i}\ 0.136$ (alumina), mirror distances: $d_1 = d_2 = 20$ mm, $d/(ka^2) = 0.0337$. Six hybrid modes EH_{1m} and 12 free-space modes TEM_{0m} were used as basis sets. An effective-length parameter L/ka^2 of 1.0 corresponds to a waveguide length of $L = 593$ mm. See text for an explanation of the vertical lines [94Pet] (© SPIE 1994).

Calculated round-trip losses of a symmetric, circular waveguide resonator with flat mirrors using the matrix method are presented in Fig. 8.1.73 for $\lambda = 10.6$ μm. The length of the 2 mm-cross-section aluminum waveguide is varied, but the distance from the waveguide ends to the mirrors remains fixed at $d = 20$ mm. Over several relatively wide ranges of the waveguide length, low losses of the fundamental mode and an excellent discrimination against the next-order mode can be simultaneously realized. In these length ranges the lowest-loss mode is predominantly EH_{11} with small amounts of higher-order waveguide modes. Operation near points of degeneracy, like at $L/ka^2 = 0.25$ or 0.5, has to be avoided since the output beam may switch between EH_{11}- and EH_{12}-like intensity distributions. The most surprising behavior in this graph is the periodic oscillation of the loss curves. This structure can be attributed to interference among two or more waveguide eigenmodes.

At the loss minima, two or more waveguide modes emerge from the guide with relative amplitudes and phases such that the spot size of the beam coupled back into the waveguide assumes a minimum. The coupling loss at that point is lower than the coupling loss of the EH_{11} mode discussed earlier. These resonances were investigated in detail in [84Ger] (circular guide) and [88Hil] (rectangular guide) using two waveguide modes.

The periodicity of the resonances in $L/(ka^2)$ can be attributed to the periodic regeneration of the relative phase between the modes at the waveguide ends. Although the resonator modes in Fig. 8.1.73 represent combinations of more than two waveguide modes, most loss minima of the lowest-loss mode can be assigned to a resonance between two of the three waveguide modes EH_{11}, EH_{12}, and EH_{13}. The broken vertical lines indicate resonances that can be attributed to a mixing of EH_{11} and EH_{13}.

The waveguide resonator mode calculations rely on the exact knowledge of the refractive index of the guide material, a requirement that can be hardly met, especially for metals. Furthermore, the finish of the waveguide walls and heat-induced variations in the waveguide dimensions also have a strong influence on the mode properties. In addition, the mode calculations hold only for the passive resonator. The gain saturation and inhomogeneous gain profiles may considerably change the mode properties. Therefore, the numerical evaluation of the resonator properties can only be considered a starting point of the laser design, and the optimization of the laser properties have to be accomplished experimentally. Furthermore, in gas lasers with relatively large gain bandwidths (like CO_2 lasers), wavelengths other than the desired one may exhibit lower round trip losses resulting in the oscillation at the unwanted wavelength or a switching between wavelengths. This

stems from the dependence of the refractive index on the wavelength, which is particularly strong for metallic waveguides.

The dimensions of the waveguide are usually determined by constraints on output power and heat removal which means that the waveguide cross section can only be varied within a small range. With the dimensions of the gain medium being more or less fixed, a first step in the resonator design would be to place the resonator mirrors as close as possible top the waveguide ends. Preferably, the resonator parameters should be chosen such that the resonator is working between two resonances of the EH_{12} and EH_{13} modes since the second-order resonator mode is most likely to exhibit a loss minimum near these resonances. For small distances d_1, d_2 between the mirrors and the rectangular waveguide, the absolute locations of the mode-mixing points between mode EH_{mn} and $EH_{m'n'}$, to a good approximation, are given by [88Hil]:

$$\frac{L + d_1 + d_2}{ka^2} = \frac{16\,p}{\pi\,|m^2 - m'^2 + n^2 - n'^2|}\,, \quad p = 1, 2, \ldots \tag{8.1.144}$$

The experimental set-up can then be optimized experimentally by varying the mirror distances, the mirror curvatures, and, to some extent, the waveguide cross section. In general, waveguide lasers provide excellent beam properties, combining a high fill factor, good mode control, and beam qualities near the diffraction limit. In the first two decades since the first reported implementation of a waveguide laser in 1971 [71Smi], mostly circular waveguides were used. In the late 80s and early 90s the interest shifted to slab waveguides due to the area scaling of the output power and the realization of near-diffraction-limited beam quality using off-axis unstable resonator schemes [89Jac1, 90Nis, 90Now, 91Now, 92Col, 94Pet, 95Eis, 96Lap]. Several commercial CO_2 slab waveguide lasers are used in medical applications (100 W) and in material processing with output powers in the kW range [88Tul, 90Nis, 92Hob, 92Dal, 92Yar, 92Mef1, 92Mef2, 94Pet, 96Lap]. In order to achieve high output power with a compact laser head, folded waveguide designs are often used. Popular folding schemes are the U-fold, the V-fold, and the Z-fold, all three using plane or curved folding mirrors. The theoretical modeling of folded waveguide resonators is more complicated especially if curved mirrors are used [88Hil, 89Jac2, 90Hil].

8.1.10.5 Properties of slab waveguide lasers

One possible set-up of a slab waveguide resonator is depicted in Fig. 8.1.74. The positive-branch confocal unstable resonator in off-axis geometry with magnification M provides near-diffraction-limited beam quality along the wide dimension of the waveguide. The high-reflecting cylindrical mirrors form a one-dimensional Case I waveguide resonator with flat mirrors in the perpendicular direction. Typical dimensions for CO_2 lasers are: $b = 30 \ldots 50$ mm; $L = 60 \ldots 120$ cm; d_1, $d_2 = 15 \ldots 30$ mm; $2a = 1.5 \ldots 2.5$ mm. Mirror distances of less than 15 mm are not feasible due

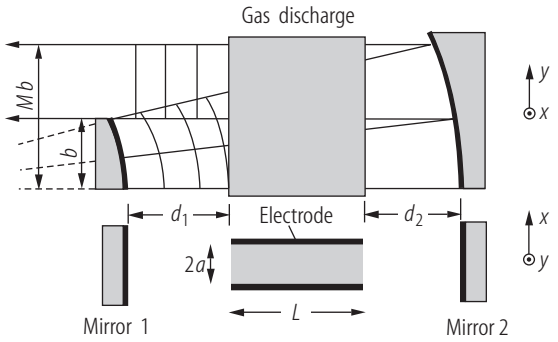

Fig. 8.1.74. Slab waveguide laser utilizing a positive-branch, confocal, off-axis unstable resonator with magnification M in the y-direction.

to possible damage by the discharge plasma. In commercial systems, negative-branch confocal unstable resonators are preferred due to their lower misalignment sensitivity even though the efficiency is about 20% lower. In the negative branch, with both mirrors being concave in the unstable direction, spherical mirrors can also be used resulting in lower coupling losses for the waveguide modes.

The design of the unstable resonator can be performed geometrically since the equivalent Fresnel numbers are relatively high. The output-coupling loss is almost identical to the geometrical loss of $1 - 1/M$ for equivalent Fresnel numbers higher than 10. Typical equivalent Fresnel numbers are between 20 and 60, and magnifications in the range from 1.15 to 1.4 are used. The mirror curvatures needed to set up a confocal unstable resonator with magnification M are given by:

$$\rho_1 = \frac{2(L + d_1 + d_2)}{1 - M} \,, \tag{8.1.145}$$

$$\rho_2 = \frac{-2M(L + d_1 + d_2)}{1 - M} \,, \tag{8.1.146}$$

where $M = -\rho_2/\rho_1$ is positive for positive-branch resonators and negative for negative-branch resonators. The equivalent Fresnel number reads:

$$N_{\mathrm{eq}} = \frac{b^2}{2L\lambda}(M - 1) \,. \tag{8.1.147}$$

The electric field coupled out of the confocal unstable resonator exhibits a phase variation of less than $\lambda/5$ over the entire cross section of the beam (Fig. 8.1.75) resulting in a near-diffraction-limited beam quality. However, due to the different beam dimensions in the x- and the y-directions, the beam is highly astigmatic. The angle of divergence in the waveguide direction is about $(|M| - 1)\, b/(2a)$ higher than in the perpendicular direction. In order to generate a near-circular focus, the astigmatism has to be compensated by means of cylindrical lenses. Typically the far-field intensity profiles of the transformed, stigmatic beams are close to Gaussian in the waveguide direction ($M^2 \sim 1.1$) and exhibit small side lobes in the unstable direction with a 10 ... 20% higher beam propagation factor.

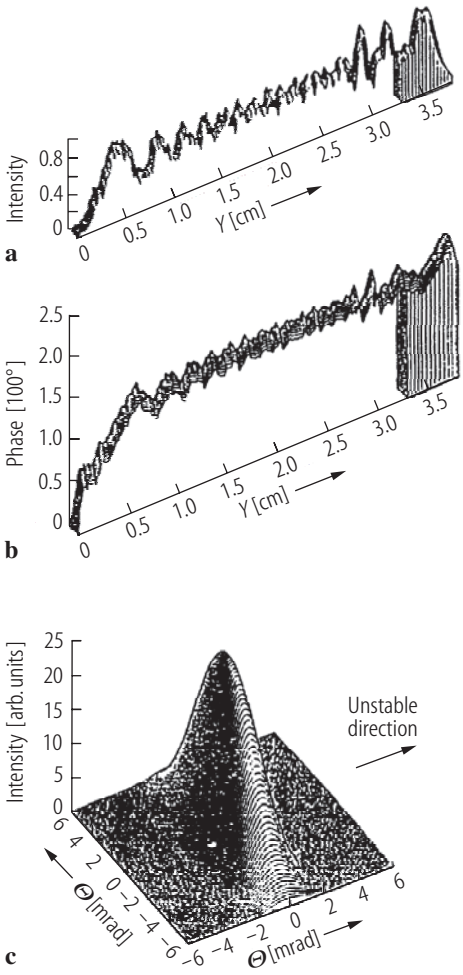

Fig. 8.1.75. Calculated intensity and phase distributions in the near field and in the far field for an off-axis confocal unstable resonator with equivalent Fresnel number $N_{eq} = 20.8$ and magnification $M = 1.15$ ($\lambda = 10.6$ μm). The intracavity near-field intensity distribution at the output coupling mirror is shown in (**a**) and the corresponding phase distribution is given in (**b**). The shaded area indicates the portion being coupled out of the resonator. In the waveguide direction a homogeneous phase and amplitude profile of width 1.5 mm is assumed. Graph (**c**) shows the intensity distribution in the far field. The beam is astigmatic due to a higher divergence in the waveguide direction [91Now] (© AT Fachverlag 1991).

References for 8.1

61Boy Boyd, G.D., Gordon, J.P.: Bell Syst. Tech. J. **40** (1961) 489.
61Fox Fox, A.G., Li, T.: Bell. Syst. Tech. J. **40** (1961) 453.
61Sni Snitzer, E.: J. Opt. Soc. Am. **51** (1961) 491.

62Boy Boyd, G.D., Kogelnik, H.: Bell. Syst. Tech. J. **41** (1962) 1347.

63Fox Fox, A.G., Li, T.: Proc. IEEE **51** (1963) 80.
63Rig Rigrod, W.: J. Appl. Phys. **34** (1963) 62.
63Tan Tang, C.L., Statz, H., deMars jr., G.: J. Appl. Phys. **34** (1963) 2289.

64Abr Abramowitz, M., Stegun, A.: Handbook of mathematical functions, New York: Dover Publ., 1964.
64Gor Gordon, J.P., Kogelnik, H.: Bell Syst. Tech. J. **43** (1964) 2873.
64Mar Marctili, E.A.J., Schmeltzer, R.A.: Bell. Syst. Tech. J. **43** (1964) 1783.

65Evt Evtuhov, E., Siegman, A.E.: Appl. Opt. **4** (1965) 142.
65Her Hercher, M., Young, M., Smoyer, C.B.: J. Appl. Phys. **36** (1965) 3351.
65Heu Heurtley, J.C., Streifer, W.: J. Opt. Soc. Am. **55** (1965) 1472.
65Kog Kogelnik, H.: Bell Syst. Tech. J. **44** (1965) 455.
65Li Li, T.: Bell Syst. Tech. J. **44** (1965) 917.
65Sie Siegman, A.E.: Proc. IEEE **53** (1965) 277.
65Str Streifer, W.: J. Opt. Soc. Am. **55** (1965) 10.
65Vak Vakhimov, N.G.: Radio Eng. Electron. Phys. (English Transl.) **10** (1965) 1439.

66Kah Kahn, K.W.: Appl. Opt. **5** (1966) 407.
66Kog1 Kogelnik, H., Li, T.: Appl. Opt. **5** (1966) 1550.
66Kog2 Kogelnik, H., Li, T.: Proc. IEEE **54** (1966) 1312.
66Mag Magnus, W., Oberhettinger, F., Soni, R.P.: Formulas and theories for special functions of mathematical physics, Berlin–Heidelberg–New York–London–Paris–Tokyo: Springer-Verlag, 1966.

67Bar Barone, S.R.: Appl. Opt. **6** (1967) 861.
67Sie Siegman, A.E., Arrathoon, R.: IEEE J. Quantum Electron. **3** (1967) 156.

68Ber Bergstein, L.: Appl. Opt. **7** (1968) 495.
68Str Streifer, W.: IEEE J. Quantum Electron. **4** (1968) 156.

69Ana Anan'ev, Y.A., Sventsitskaya, N.A., Sherstobitov, V.E.: Sov. Phys. JETP (English Transl.) **28** (1969) 69.
69Bau Baues, P.: Opto-electronics (London) **1** (1969) 37.
69Kru Krupke, W.F., Sooy, W.R.: IEEE J. Quantum Electron. **5** (1969) 575.
69San1 Sanderson, R.L., Streifer, W.: Appl. Opt. **8** (1969) 2129.
69San2 Sanderson, R.L., Streifer, W.: Appl. Opt. **8** (1969) 2241.

70Arn Arnaud, J.A.: Bell. Syst. Tech. J. **49** (1970) 2311.
70Col Collins, S.A.: J. Opt. Soc. Am. **60** (1970) 1168.
70Fos Foster, J.D., Osterink, L.M.: J. Appl. Phys. **41** (1970) 3656.
70Koe Koechner, W.: Appl. Opt. **9** (1970) 2548.

70Sie Siegman, A.E., Miller, H.Y.: Appl. Opt. **9** (1970) 2729.
70Zuc Zucker, H.: Bell Syst. Tech. J. **49** (1970) 2349.

71Loc Locke, E.V., Hella, R., Westra, L.: IEEE J. Quantum Electron. **7** (1971) 581.
71Sch Schäfer, F.P., Müller, H.: Opt. Commun. **2** (1971) 407.
71Smi Smith, P.W.: Appl. Phys. Lett. **19** (1971) 132.

72Abr Abrams, R.L.: IEEE J. Quantum Electron. **8** (1972) 838.
72Ana Anan'ev, Y.A.: Sov. J. Quant. Electron. **1** (1972) 565.
72Clo Clobes, A.R., Brienza, M.J.: Appl. Phys. Lett. **21** (1972) 265.
72Fre Freiberg, R.J., Chenausky, P.P., Buczek, C.J.: IEEE J. Quantum Electron. **8** (1972) 372.
72Kog Kogelnik, H.W., Ippen, E.P., Dienes, A., Shank, C.V.: IEEE J. Quantum Electron. **8** (1972) 373.

73Deg Degnan, J.J., Hall, D.R.: IEEE J. Quantum Electron. **9** (1973) 901.
73Fre Freiberg, R.J., Chenausky, P.P., Buczek, C.J.: Appl. Opt. **12** (1973) 1140.
73Hor Horwitz, P.: J. Opt. Soc. Am. **63** (1973) 1528.
73Poz Pozzo, P.D., Polloni, R., Svelto, O., Zaraga, F.: IEEE J. Quantum Electron. **9** (1973) 1061.
73Wis Wisner, G.R., Foster, M.C., Blaszuk, P.R.: Appl. Phys. Lett. **22** (1973) 14.

74Fre Freiberg, R.J., Chenausky, P.P., Buczek, C.J.: IEEE J. Quantum Electron. **10** (1974) 279.
74Mar Marcuse, D.: Theory of dielectric optical waveguides, in: Theory of dielectric optical waveguides, Pau, Y.H. (ed.), New York: Academic Press, 1974.
74Sie Siegman, A.E.: Appl. Opt. **13** (1974) 353.

75Loe Lörtschner, J.P., Steffen, J., Herziger, G.: Opt. Quantum Electron. **7** (1975) 505.
75Szi Sziklas, E.A., Siegman, A.E.: Appl. Opt. **14** (1975) 1874.

76Deg Degnan, J.J.: Appl. Phys. **11** (1976) 1.
76Ewa Ewanitzky, T.F., Craig, J.M.: Appl. Opt. **15** (1976) 1465.
76Laa Laakmann, K.D., Steier, W.H.: Appl. Opt. **15** (1976) 1334.
76Mar Marowsky, G., Kaufman, K.: IEEE J. Quantum Electron. **12** (1976) 207.

77Ber Berger, N.K., Deryugin, N.A., Lukyanov, Y.N., Studenikin, Y.E.: Opt. Spectrosc. (USSR) **43** (1977) 176.
77Her Herbst, R.L., Komine, H., Byer, R.L.: Opt. Commun. **21** (1977) 5.
77Isa Isaev, A.A., Kazaryan, M.A., Petrash, G.G., Rautian, S.G., Shalagin, A.M.: Sov. J. Quantum Electron. (English Transl.) **7** (1977) 746.

78Pax Paxton, A.H., Salvi, T.C.: Opt. Commun. **26** (1978) 305.
78Rig Rigrod, W.: IEEE J. Quantum Electron. **14** (1978) 377.

79Abr Abrams, R.W.: Waveguide gas lasers, in: Laser Handbook, Vol. 3, Amsterdam: North-Holland, 1979.
79Iff Iffländer, R., Kortz, H.P., Weber, H.: Opt. Commun. **29** (1979) 223.
79Jar Jarrett, S.M., Young, J.F.: Opt. Lett. **4** (1979) 176.
79Nem Nemoto, S., Makimoto, T.: J. Opt. Soc. Am. **69** (1979) 578.

79Rea Reading, S., Sze, R.C., Tallman, C.: Proc. Soc. Photo-Opt. Instrum. Eng. **190** (1979) 311.
79Sie Siegman, A.E.: Opt. Commun. **31** (1979) 369.

80Car Carter, W.H.: Appl. Opt. **19** (1980) 1027.
80Eim Eimerl, D.: J. Appl. Phys. **51** (1980) 3008.
80Giu Giuliani, G., Park, Y.K., Byer, R.L.: Opt. Lett. **5** (1980) 491.
80Hau Hauck, R., Kortz, H.P., Weber, H.: Appl. Opt. **19** (1980) 598.
80Sch Schindler, G.M.: IEEE J. Quantum Electron. **16** (1980) 546.
80Tes Teschke, O., Teixeira, S.R.: Opt. Commun. **32** (1980) 287.

81Kor Kortz, H.P., Iffländer, R., Weber, H.: Appl. Opt. **20** (1981) 4124.

82Sve Svelto, O.: Principles of lasers, New York: Plenum Press, 1982.

83Oug Oughstun, K.E., Slaymaker, P.A., Bush, K.A.: IEEE J. Quantum Electron. **19** (1983) 1558.
83Pic Piché, M., Lavigne, P., Martin, F., Belanger, P.A.: Appl. Opt. **22** (1983) 1999.
83Rig Rigrod, W.W.: IEEE J. Quantum Electron. **19** (1983) 1679.

84Ger Gerlach, R., Wei, D., Amer, N.M.: IEEE J. Quantum Electron. **20** (1984) 948.
84Her Herziger, G., Weber, H.: Appl. Opt. **23** (1984) 1450.
84McC McCarthy, N., Lavigne, P.: Appl. Opt. **23** (1984) 3845.
84Moo Moore, G.T.: Proc. Soc. Photo-Opt. Instrum. Eng. **453** (1984) 255.
84Rip Ripper, G., Herziger, G.: Feinwerktech. Messtech. **92** (1984) 301.
84Skl Sklar, E.: J. Opt. Soc. Am. A **1** (1984) 537.

85Hil Hill, C.A., Hall, D.R.: Appl. Opt. **24** (1985) 1283.
85Iza Izawa, S., Suda, A., Obara, M.: J. Appl. Phys. **58** (1985) 3987.
85Kan Kane, T.J., Byer, R.L.: Opt. Lett. **10** (1985) 65.
85Lav Lavigne, P., McCarthy, N., Demers, J.G.: Appl. Opt. **24** (1985) 2581.
85McC McCarthy, N., Lavigne, P.: Opt. Lett. **10** (1985) 553.
85Tac Taché, J.P.: Opt. Commun. **55** (1985) 419.

86DeS DeSilvestri, S., Laporta, P., Magni, V.: Opt. Commun. **59** (1986) 43.
86Har Harter, D.J., Walling, J.C.: Opt. Lett. **11** (1986) 706.
86Mag Magni, V.: Appl. Opt. **25** (1986) 2039.
86Sie Siegman, A.E.: Lasers, Mill Valley: University Science Books, 1986.
86Skl Sklar, E.: IEEE J. Quantum Electron. **22** (1986) 1088.
86Upp1 Uppal, J.S., Monga, J.C., Bhawalkar, D.D.: Appl. Opt. **25** (1986) 97.
86Upp2 Uppal, J.S., Monga, J.C., Bhawalkar, D.D.: Appl. Opt. **25** (1986) 389.
86Web Weber, H., Iffländer, R., Seiler, P.: Proc. Soc. Photo-Opt. Instrum. Eng. **650** (1986) 92.

87Apa Apanasevich, P.A., Kvach, V.V., Koptev, V.G., Orlovich, V.A.: Sov. J. Quantum Electron. (English Transl.) **17** (1987) 160.
87Gro Gromov, A.N., Trashkeev, S.I.: Opt. Spectrosc. (USSR) **62** (1987) 369.
87Hal Hall, D.R., Hill, C.A.: Radiofrequency-discharge-excited CO_2 lasers, in: Handbook of molecular lasers, New York, Basel: Marcel Dekker, Inc., 1987, p. 165–198.
87Kan Kane, T.J., Nilsson, A.C., Byer, R.L.: Opt. Lett. **12** (1987) 175.
87Mag Magni, V.: J. Opt. Soc. Am. A **4** (1987) 1962.
87Met Metcalf, D., de Giovanni, P., Zachorowski, J., Leduc, M.: Appl. Opt. **26** (1987) 4508.

87Oug Oughstun, K.E.: Unstable resonator modes, in: Wolf, E. (ed.): Progress in optics XXIV, New York: Elsevier Science Publishers B.V., 1987, p. 165–387.
87Ru Ru, P., Narducci, L.M., Tredicce, J.R., Bandy, D.K., Lugiato, L.A.: Opt. Commun. **63** (1987) 310.
87Sil Silichev, O.O.: Sov. J. Quantum Electron. (English Transl.) **17** (1987) 530.
87Skl Sklar, E.: IEEE J. Quantum Electron. **23** (1987) 229.

88Bro Brorsen, S.D.: IEEE J. Quantum Electron. **23** (1988) 512.
88Cal Calahan, K.R., Clayton, C.M., Paxton, A.H.: Appl. Opt. **27** (1988) 2694.
88Coo Cooper, D., Tankersley, L.L., Reintjes, J.: Opt. Lett. **13** (1988) 568.
88DeS1 DeSilvestri, S., Laporta, P., Magni, V., Svelto, O.: Opt. Commun. **67** (1988) 229.
88DeS2 DeSilvestri, S., Laporta, P., Magni, V., Svelto, O., Majocchi, B.: Opt. Lett. **13** (1988) 201.
88Hau1 Hauck, R., Hodgson, N., Weber, H.: J. Appl. Phys. **63** (1988) 628.
88Hau2 Hauck, R., Hodgson, N., Weber, H.: J. Mod. Opt. **35** (1988) 165.
88Hil Hill, C.A.: IEEE J. Quantum Electron. **24** (1988) 1936.
88Hod Hodgson, N.: Proc. Soc. Photo-Opt. Instrum. Eng. **1021** (1988) 89.
88Lav Lavigne, P., McCarthy, N., Parent, A., Snell, K.: Can. J. Phys. **66** (1988) 888.
88Lit Litzenberger, L.N., Smith, M.J.: IEEE J. Quantum Electron. **24** (1988) 2270.
88Mil Miloni, P.W., Eberly, J.H.: Lasers, New York, Chichester, Brisbane, Toronto, Singapore: John Wiley & Sons, 1988.
88Nil Nilsson, A.C., Day, T., Farinas, A.D., Gustafson, E.K., Byer, R.L.: Narrow linewidth operation of diode-laser-pumped nonplanar ring oscillators, Topics in physics: Proceedings of the fourth symposium on frequency and metrology, Ancona, Italy, 1988, Berlin–Heidelberg–New York: Springer-Verlag, 1988.
88Ozy Ozygus, B.: Losses and modestructures of optical resonators, Technical University Berlin, Germany: Internal Report, 1988.
88Sch Schütz, I., Wiegand, S., Wallenstein, R.: Laser Optoelektron. **20** (1988) 39.
88Sne Snell, K.H., McCarthy, N., Piché, M.: Opt. Commun. **65** (1988) 377.
88Tul Tulip, J.: Carbon dioxide slab laser, United States Patent 4,719,639, January 1988.

89Day Day, T., Nilsson, A.C., Fejer, M.M., Farinas, A.D., Gustafson, E.K., Nabors, C.D., Byer, R.L.: Electron. Lett. **25** (1989) 810.
89Eic Eicher, J., Hodgson, N., Weber, H.: J. Appl. Phys. **66** (1989) 4608.
89Egg Eggleston, J.M., Frantz, L.M., Injeyan, H.: IEEE J. Quantum Electron. **25** (1989) 1855.
89Emi Emiliani, G., Piegori, A., DeSilvestri, S., Laporta, P., Magni, V.: Appl. Opt. **28** (1989) 2832.
89Jac1 Jackson, P.E., Baker, H.J., Hall, D.R.: Appl. Phys. Lett. **54** (1989) 1950.
89Jac2 Jackson, P.E., Hall, D.R., Hill, C.A.: Appl. Opt. **28** (1989) 935.
89Kin King, T.A.: Ring laser resonators, in: Hall, D.R., Jackson, P.E. (eds.): Physics and technology of laser resonators, London: Adam Hilger, 1989, p. 62–79.
89Nil Nilsson, A.C., Gustafson, E.K., Byer, R.L.: IEEE J. Quantum Electron. **25** (1989) 767.
89Par Parent, A., Lavigne, P.: Opt. Lett. **14** (1989) 399.
89Ruf Ruff, J.A., Siegman, A.E.: Technical Digest CLEO 89, 296. Washington, D.C.: Optical Society of America, 1989, p. 296.

90Alv Alvarez-Chust, R., Jimenez-Lidon, J.J.: IEEE Photon. Technol. Lett. **2** (1990) 24.
90DeS DeSilvestri, S., Magni, V., Svelto, O., Valentini, G.L.: IEEE J. Quantum Electron. **26** (1990) 1500.
90Hil Hill, C.A., Jackson, P.E., Hall, D.R.: Appl. Opt. **29** (1990) 2240.
90Hod1 Hodgson, N., Haase, T., Weber, H.: Proc. Soc. Photo-Opt. Instrum. Eng. **1277** (1990) 70.

90Hod2 Hodgson, N., Weber, H.: IEEE J. Quantum Electron. **26** (1990) 731.
90Hod3 Hodgson, N., Weber, H.: Opt. Quantum Electron. **22** (1990) 39.
90Nis Nishima, J., Yoshizawa, K.: Proc. Soc. Photo-Opt. Instrum. Eng. **1226** (1990) 340.
90Now Nowack, R., Opower, H., Schaefer, U., Wessel, K., Hall, T., Krüger, H., Weber, H.: Proc. Soc. Photo-Opt. Instrum. Eng. **1276** (1990) 18.
90Pie Piegari, A., Tirabassi, A., Emiliani, G.: Proc. SPIE (Int. Soc. Opt. Eng.) **1125** (1990) 68.
90Yas Yasui, K., Yagi, S., Tanaka, M.: Appl. Opt. **29** (1990) 1277.

91Che Cheng, E.A.P., Kane, T.J.: Opt. Lett. **16** (1991) 478.
91Mag Magni, V., DeSilvestri, S., Svelto, O., Valentini, G.L.: Hundred-watts diffraction limited Nd: YAG laser with super-Gaussian resonator, Technical Digest CLEO 91, Optical Society of America, Washington, D.C., 1991.
91Now Nowack, R., Opower, H., Wessel, K., Krüger, H., Haas, W., Wenzel, N.: Laser und Optoelektronik **3** (1991) 68.

92Bow Bowers, M.S.: Opt. Lett. **17** (1992) 1319.
92Col Colley, A.D., Baker, H.J., Hall, D.R.: Appl. Phys. Lett. **61** (1992) 136.
92Dal Dallarosa, J., Gardner, P.: RF excited CO_2 slab waveguide laser, United States Patent 5,131,004, July 1992.
92Day Day, T., Gustafson, E.K., Byer, R.L.: IEEE J. Quantum Electron. **28** (1992) 1106.
92Hob Hobart, J.L., Yarborough, J.M., Dallarosa, J., Gardner, P.: RF excited CO_2 slab waveguide laser, United States Patent 5,123,028, June 1992.
92Hod1 Hodgson, N., Haase, T.: Opt. Quantum Electron. **24** (1992) 903.
92Hod2 Hodgson, N., Weber, H.: J. Mod. Opt. **39** (1992) 1873.
92Jen Jenkins, R.M., Devereux, R.J.: Appl. Opt. **31** (1992) 5086.
92Khe Khelkal, M., Herlemont, F.: Appl. Opt. **31** (1992) 4175.
92Mag Magni, V., DeSilvestri, S., Qian, L.-J., Svelto, O.: Opt. Commun. **94** (1992) 87.
92Mef1 Mefferd, W.S.: RF excited CO_2 slab waveguide laser, United States Patent 5,131,003, July 1992.
92Mef2 Mefferd, W.S.: RF excited CO_2 slab waveguide laser, United States Patent 5,155,739, October 1992.
92Oug Oughstun, K.E. (ed.): Selected papers on scalar wave diffraction, SPIE Milestone Series Vol. MS**51** , Bellingham, WA: The Society of Photo-Optical Instrumentation Engineers 1992.
92Ren Reng, N., Eppich, B.: Opt. Quantum Electron. **24** (1992) 973.
92Web Weber, H.: Opt. Quantum Electron. **24** (1992) 1027.
92Yar Yarborough, J.M., Hobart, J.L., Dallarosa, J.: RF excited CO_2 slab waveguide laser, United States Patent 5,140,606, August 1992.

93Doc Document ISO/TC 172/SC 9/WG 1 N 56, ISO/CD 11 146, Optics and optical instruments – Lasers and laser related equipment – Test methods for laser beam parameters: Beam width, divergence angle and beam propagation factor, Nov. 26, 1993.
93Dup Duplain, G., Verlyu, P.G., Dobrowolski, J.A., Waldorf, A., Buissiere, S.: Appl. Opt. **32** (1993) 1145.
93Ehr Ehrlichmann, D., Habich, U., Plum, H.-D.: IEEE J. Quantum Electron. **29** (1993) 2211.
93Hod1 Hodgson, N., Bostanjoglo, G., Weber, H.: Appl. Opt. **32** (1993) 5902.
93Hod2 Hodgson, N., Bostanjoglo, G., Weber, H.: Opt. Commun. **99** (1993) 75.
93Hod3 Hodgson, N., Dong, S., Lü, Q.: Opt. Lett. **18** (1993) 1727.
93Hod4 Hodgson, N., Weber, H.: IEEE J. Quantum Electron. **29** (1993) 2497.
93Pie Piegari, A., Emiliani, G.: Appl. Opt. **32** (1993) 5454.

94Bos1 Bostanjoglo, G., Bernhardt, A.: Proc. Soc. Photo-Opt. Instrum. Eng. **2253** (1994) 791.
94Bos2 Bostanjoglo, G., Hodgson, N.: Proc. Soc. Photo-Opt. Instrum. Eng. **2206** (1994) 459.
94Bos3 Bostanjoglo, G., Hodgson, N., Weber, H.: Pure Appl. Opt. **3** (1994) 497.
94Bur Burnham, R., Witt, G., DiBiase, D., Koechner, W.: Proc. Soc. Photo-Opt. Instrum. Eng. **2206** (1994) 489.
94Pet Petersen, C.L., Eisel, D., Brzezinski, J.J., Gross, H.: Proc. Soc. Photo-Opt. Instrum. Eng. **2206** (1994) 91.

95Paq Paquin, R.A.: Properties of Metals; in: Bass, M., Stryland, E.W. Van, Williams, D.R., Wolfe, W.L. (eds.): Handbook of Optics, Vol. II, Washington: Optical Society of America, 1995, Chap. 35.
95Cha Chandra, S., Allik, T.H., Hutchinson, J.A.: Opt. Lett. **20** (1995) 2387.
95Eis Eisel, D., Gross, H., Petersen, C.L.: Slab-waveguide CO_2 laser, United States Patent 5,412,681, May 1995.

96Lap Lapucci, A., Labate, A., Rossetti, F., Mascalchi, S.: Appl. Opt. **35** (1996) 3185.
96Mar Martin, K.I., Clarkson, W.A., Hanna, D.C.: Opt. Lett. **21** (1996) 875.

97Hod Hodgson, N., Weber, H.: Optical resonators, Berlin–Heidelberg–London–New York: Springer-Verlag, 1997.